MSU ENGR-001-01

NON-METALLIC REINFORCEMENT OF CONCRETE BRIDGE DECKS

Final Report

Parviz Soroushian
Siavosh Ravanbakhsh
Lawrence T. Drzal

January 2001

RESEARCH
M.D.O.T.
CONSTRUCTION & TECHNOLOGY
DIVISION

COLLEGE OF ENGINEERING

MICHIGAN STATE UNIVERSITY

EAST LANSING, MICHIGAN 48824

MICHIGAN STATE UNIVERSITY
1855

MSU IS AN AFFIRMATIVE ACTION/EQUAL OPPORTUNITY INSTITUTION

NON-METALLIC REINFORCEMENT OF CONCRETE BRIDGE DECKS

Final Report

Parviz Soroushian
Siavosh Ravanbakhsh
Lawrence T. Drzal

January 2001

COLLEGE OF ENGINEERING

MICHIGAN STATE UNIVERSITY

EAST LANSING, MICHIGAN 48824

1. Report No. RC 1392	2. Government Accession No.	Recipient's Catalog No.
4. Title and Subtitle: Non-Metallic Reinforcement of concrete Bridge Decks		5. Report Date January 2001
7. Author(s): Soroushian, P., Ravanbakhsh, S., Drzal, L.		6. Performing Organization Code
9. Performing Organization Name and Address Michigan State University Civil Engineering Department East Lansing, MI 48824		8. Performing Org. Report No. MSU-ENGR-001-01
12. Sponsoring Agency Name and Address Michigan Departtment of Transportation Construction and Technology Division P.O.Box 30049 Lansing, MI 48909		10. Work Unit No.
		11. Contract/Grant No.
15. Supplementary Notes		13. Type of Report & Period Covered Final Report
		14. Sponsoring Agency Code

16. Abstract.

A comprehensive durability investigation of glass and aramid (Technora®) fiber composite bars was conducted. Major adverse effects on tensile strength of glass fiber composites were covered by extended immersion in warm alkali solution which is representative of concrete environment. Aramid fiber composites performed satisfactorily under accelerated aging effects and were thus selected for further consideration. Bonding of aramid fiber composite bars to concrete was investigated, and criteria for their development in concrete were established. Laboratory studies on aramid fiber composite and steel bar reinforced slabs simulating bridge deck conditions revealed the predominance of punching shear in failure of such slabs. Design criteria for bridge decks reinforced with composite and steel bars were developed to reflected on their actual failure conditions. There design were verified through static and fatigue testing of scaled models of bridge decks reinforced with aramid fiber (Technora®) composite and steel bars. A field demonstration project comprising a concrete bridge deck reinforced with aramid fiber composite bars was implemented and is subjected of long-term monitoring.

17. Key Words composite bars; durability; concrete reinforcement; glass fibers; aramid (Technora®) fibers;bridge decks; steel corrosion		18. Distribution Statement	
19. Security Classification Unclassified	20. Security Classification Unclassified	21. No. of Pages 152	22. Price

Form DOT F 1700.7 (8-72)

NON-METALLIC REINFORCEMENT OF CONCRETE BRIDGE DECKS

Final Report

Parviz Soroushian

Siavosh Ravanbakhsh

Lawrenct T. Drzal

College of Engineering

Michigan State University

E. Lansing, MI 48824

January 2001

ACKNOWLEDGMENT

TABLE OF CONTENT

EXECUTIVE SUMMARY

Fiber reinforced polymer matrix composite bars with glass and aramid (Technora®) reinforcing fibers were subjected to mechanical, physical and durability tests in order to evaluate their performance as reinforcement in concrete bridge decks. Design methodologies were developed for concrete bridge decks reinforced with composite bars, and were verified through laboratory investigations. A field project comprising a concrete bridge deck reinforced with aramid (Technora®) was implemented.

Fiber reinforced composites, when compared with steel bars, provide relatively high levels of tensile strength but relatively low values of elastic modulus and shear strength. The coefficient of thermal expansion of glass fiber composites is comparable to that of concrete. The coefficient of thermal expansion of aramid fiber composite varies with temperature; its value is generally small and can even be negative. The tensile performance of glass fiber composites is not influenced by their moisture content; in the case of aramid fiber composites, there is a relatively small (less than 10%) and reversible loss of tensile performance upon saturation.

A comprehensive durability investigation of different composite systems was conducted. The effects of the following accelerated aging conditions on tensile performance were assessed: sustained loading in salt solution, extended immersion in alkali solution at room temperature and 60°C, extended immersion in salt solution, repeated wetting-drying in salt solution, repeated freezing-thawing, extended immersion in neutral water at room temperature and 80°C, extended exposure to ultraviolet radiation, fatigue loading, extended exposure to cold temperature, and repeated temperature cycling. Major adverse effects on tensile strength of glass fiber composites were caused by extended immersion in alkali solution at 60°C and in hot water at 80°C. The tensile strength of aramid (Technora®) fiber composites, on the other hand, was relatively stable under accelerated aging effects. Aramid (Technora®) fiber composite was then selected for further consideration.

Aramid fiber composite rods with deformed surfaces, when compared with steel reinforcing bars, provided about 20% higher bond strength per unit area to concrete. The fact that the tensile strength of aramid fiber composites is twice that of steel, however, implies that a

4

longer development length would be needed for aramid fiber composite bars when compared with steel bars of similar diameter. Bond failure is more brittle with aramid fiber composite bars when compared with steel reinforcing bars.

Concrete slabs reinforced with aramid fiber composite and steel bars were designed based on flexural criteria, and were fabricated and tested in unaged condition and also after the following accelerated aging effects: repeated freezing-thawing in salt solution, repeated wetting-drying, and repeated temperature cycling. Both steel and aramid fiber composite reinforced concrete slabs exhibited a tendency towards shear failure. Accelerated aging effects on the performance of aramid fiber composite and steel reinforced slabs were relatively small.

Design methodologies were developed for bridge decks reinforced with composite bars. These methodologies emphasize the punching shear mode of failure where the elastic modulus of reinforcement is a key design criterion. The relatively low elastic modulus of aramid fiber composites, in spite of their relatively high tensile strength, raises the required level of reinforcement. Typical steel and aramid fiber composite bridge decks were designed using this methodology, and were fabricated at a scale factor of 1.5 (i.e., linear dimensions of concrete and areas of reinforcement were reduced by a factor of 1.5 and 1.5^2, respectively). These slabs were subjected to static and fatigue tests simulating truck load application on bridge decks. Both steel and aramid fiber composite reinforced bridge decks exhibited satisfactory fatigue performance. In static tests a tendency towards punching shear mode of failure was observed with both steel and aramid fiber composite reinforced decks. The overall performance characteristics of both systems were comparable, and the design methodology developed for aramid fiber composite reinforced decks proved to be satisfactory. A field demonstration project was implemented to verify performance characteristics of aramid fiber composite reinforced bridge decks under actual load and exposure conditions in Michigan. This project is subjected of long-term monitoring efforts.

1.0 INTRODUCTION

Fiber reinforced polymer (FRP) composites comprise continuous fibers (glass, aramid, carbon, etc.) embedded in a resin matrix. Resins used are thermoset (polyester, vinyl ester, etc.) or thermoplastic (nylon, polyethylene terephthalate, etc.). FRP composites have been traditionally used to produce diverse consumer and construction products. The pultrusion process, which is a prevalent method used for the manufacturing of FRP rods, brings together continuous forms of reinforcement and combines them with a resin to produce directionally oriented FRP products of high fiber content. Efforts towards application of FRP composites for the reinforcement of concrete members have been quite intense in recent years. These efforts address some critical issues, including mass production at reduced cost, modification of design and construction systems to suit FRP, and optimization of fiber and resin systems for compatibility with concrete.

The primary interest of the concrete industry in FRP reinforcement is as a corrosion-resistant alternative to steel. Depending on the constituents of an FRP composite, however, other deterioration phenomena can occur. FRP reinforcement provides the following beneficial features for use in concrete: light weight, high specific strength and modulus, corrosion resistance, and chemical and environmental resistance. Corrosion has been a major problem with steel reinforced concrete in highway bridges. Application of deicer salt in colder climates accelerates corrosion of the reinforcing steel. Corrosion products would expand and cause fracture of concrete. The first solution was a galvanized coating applied to the reinforcing bars. Conventional measures to control corrosion of reinforcing steel includes epoxy coating of steel rebars and use of stainless steel bars (or stainless steel cladding on bars).

Research on FRP reinforcement started in late 1970's; the objective of this research was to determine if it presents a significant improvement over epoxy coated steel. In the 1980's FRP reinforcing bars were used increasingly in applications with special performance requirements or where reinforcing bars were subjected to severe chemical attack. The largest market was for reinforced concrete structures supporting or surrounding magnetic resonance imaging

medical equipment, where glass FRP reinforcing bars have been preferred over non-magnetic stainless steel. FRP reinforcing bars are now considered for a broader range of concrete applications, including concrete floor slabs in aggressive chemical environments, bridge decks in cold climates, industrial roof decks, and base pads for electrical and reactor equipment. The research reported herein focuses on the use of composites as reinforcement in concrete bridge decks where severe exposure conditions and complex modes of failure present a high demand on diverse mechanical and durability performance of the reinforcement system.

2.0   LITERATURE REVIEW

2.1   MATERIALS AND PROCESSES

FRP reinforcing systems for concrete comprise continuous fibers glued together with a resin. The continuous fibers are usually stiffer and stronger than the matrix. The performance of composites depends on their constituent materials, the arrangement of fibers which are the primary load-bearing elements, and the interaction between fibers and matrix.

2.1.1   The Polymer Matrix

While fibers are the primary structural constituents in composites, the important role of the polymer matrix cannot be ignored. The polymer matrix transfers stresses between reinforcing fibers and the surrounding structure, and protects the fibers against environmental and mechanical damage. Interlaminar shear is a critical design consideration for FRP structures under bending loads; in-plane shear is important for torsional loads. The polymer matrix properties influence the interlaminar shear as well as the in-plane shear properties of the composite. The polymer matrix also provides lateral support against fiber buckling under compression loading. Polymer matrices are further discussed below.

Polymer matrix materials differ from metals in several aspects that can affect their behavior in critical structural applications. The mechanical properties of composites depend strongly on ambient temperature and loading rate. In the Glass Transition Temperature (T_g) range, polymeric materials change from a hard, often brittle solid to a soft, tough solid. The tensile modulus of polymer matrix can be reduced by as much as five orders of magnitude. The polymer matrix material is also highly viscoelastic. When an external load is applied, it exhibits an instantaneous elastic deformation followed by slow viscous deformation. As the temperature is increased, the polymer changes into a rubber-like solid, capable of large, elastic deformations under external loads. If temperature is increased further, thermoplastics reach highly viscous liquid states. The glass transition temperature of a thermoset is controlled by varying the amount of cross-linking between molecules. For a very highly cross-linked

8

polymer, the transition temperature and softening may not be observed. For a thermosetting matrix polymer such as a polyester, vinyl ester or epoxy, no "melting" occurs. In comparison to most common engineering thermoplastics, thermosetting polymers exhibit greatly increased high-temperature and load-bearing performance. Normally, thermosetting polymers char and eventually burn at very high temperatures.

The effect of loading rate on mechanical properties of a polymer is opposite to that due to temperature. At high loading rates or in the case of short durations of loading, the polymeric solid behaves in a rigid, brittle manner. At low loading rates, or for long durations of loading, the same materials may behave in a ductile manner and exhibit improved toughness values.

Reinforcing fibers are impregnated with polymers by a number of processing methods. Thermosetting polymers are almost always processed in a low viscosity, liquid state. Therefore, it is possible to obtain a good fiber wet-out without resorting to high temperature or pressure. To date, thermosetting polymers (polyesters, vinyl esters and epoxies) have been the materials of choice for the great majority of structural composite applications, including composite reinforcing products for concrete. Thermosetting matrix polymers are low molecular-weight liquids with very low viscosities. The polymer matrix is converted to a solid by using free radicals to which cause cross linking and curing. Thermosetting matrix polymers provide good thermal stability and chemical resistance. They also exhibit reduced creep and stress relaxation in comparison to thermoplastic polymers. Thermosetting polymers generally have a short shelf-life after mixing with curing agents (catalysts), low strain-to-failure, and low impact strength.

Themoplastic polymers, on the other hand, have high impact strength as well as high fracture resistance. Many thermoplastics have a higher strain-to-failure than thermoset polymers. There are other potential advantages which can be realized in a production environment, including unlimited storage life in dry environments, shorter molding cycles, secondary formability, ease of handling and damage tolerance. Despite such potential advantages, the progress of commercial structural uses of thermoplastic matrix polymers has been slow. A major obstacle is that thermoplastic matrix polymers are much more viscous and are difficult

9

to combine with continuous fibers in a viable production operation. Recently, however, a number of new promising process options, especially for filament winding and pultrusion, have been developed.

In the case of common commercial composite products, the polymer matrix is normally the major ingredient of the composite. However, this is not the case for structural applications such as composite reinforcing bars for concrete. In unfilled, fiber reinforced structural composites, the polymer matrix will range between 25% and 50% (by weight), with the lower end of the range being more characteristic of structural applications.

Fillers can be added to thermosetting or thermoplastic polymers to reduce resin cost, control shrinkage, improve mechanical properties, and impart a degree of fire retardancy. In structural applications, fillers are used selectively to improve load transfer and also to reduce cracking in unreinforced areas. Clay, calcium carbonate, and glass milled fibers are frequently used depending upon the requirements of the application. Filler materials are available in a variety of forms and are normally treated with organo-functional silanes to improve performance and reduce resin saturation. Although minor in terms of the composition of the matrix polymer, a range of important additives, including UV inhibitors, initiators (catalysts), wetting agents, pigments and mold release materials are frequently used.

Epoxy resins are approximately twice as expensive as polyester materials. Compared to polyester resins, epoxy resins provide the following general performance characteristics: (1) a range of mechanical and physical properties can be obtained due to the diversity of input materials; (2) no volatile monomers are emitted during curing and processing; (3) low shrinkage during cure; (4) excellent resistance to chemicals and solvents; and (5) good adhesion to a number of fillers, fibers, and substrates. There are some drawbacks associated with the use of epoxy matrix polymers: (1) matrix cost is generally higher than for isopolyester or vinyl ester resins; (2) epoxies must be carefully processed to maintain moisture resistance; (3) cure time can be lengthy; and (4) some hardeners require special precautions in handling, and some hardeners can cause skin sensitivity reactions in production operations.

In processing of composites for structural applications, the matrix resin must have high fibers contents for load-bearing purposes. In the absence of sufficient fiber reinforcement, the resin matrix may shrink excessively, can crack, or may not carry the load imposed upon it. Fillers, specifically those with a high aspect ratio, can be added to the polymer matrix resin to obtain some measure of reinforcement. However, it is difficult to selectively place fillers, and thus fillers can reduce the volume available for load-bearing fibers. Another controlling factor is the polymer matrix viscosity. Reinforcing fibers must be fully wetted by the polymer matrix to ensure effective coupling and load transfer. Thermoset polymers of major commercial utility either have suitably low viscosity, or processing methods are selected to suit their viscosity. Processing methods for selected thermoplastic polymers, which have inherently higher viscosity, are just now being developed to a state of practicality.

2.1.2 The Reinforcing Fibers

Principal fibers in commercial use of composites for civil engineering applications, including reinforcement of concrete, are glass, carbon, and aramid. The properties of a fiber-reinforced composite depend strongly on the direction of measurement in relationship to the direction of fibers. Tensile strength and modulus of a unindirectionally reinforced composite are maximum when these properties are measured in the longitudinal direction of fibers.

Metals exhibit yielding and plastic deformation or ductility under load. Most fiber reinforced composites are elastic in their tensile stress-strain characteristics. The heterogeneous nature of fiber/polymer composites provides mechanisms for energy absorption on a micro-scale. Many fiber reinforced composites exhibit high internal damping properties. This leads to better vibrational energy absorption within the material, and reduces transmission of vibration to adjacent structures. This aspect of composite behavior may be relevant to civil engineering structures such as bridges that are subject to loads that are more transitory and of shorter duration than sustained loads.

The matrix gives form to the composite product, and protects fibers against external environmental effects. Chemical, thermal, and electrical performance can be affected by the

choice of the matrix resin; the matrix also maintains the position of fibers. Under loading, the matrix resin deforms and distributes the stress to the higher-modulus fiber constituents. The matrix should have an elongation at break greater than that of fibers. It should not shrink excessively during curing to avoid placing internal strains on reinforcing fibers. Fiber composites are able to withstand higher stresses than can their constituent materials because the matrix and fibers interact to redistribute the stresses caused by external loads. How well the stresses are distributed internally within the composite structure depends on the nature and efficiency of fiber-to-matrix bonding. Both chemical and mechanical bonding mechanisms are thought to be operational in any given structural situation. Coupling agents are used to improve the chemical bond between reinforcement and matrix, noting that the fiber-matrix interface is frequently in a state of shear when the composite is under load.

Glass has been the predominant fiber for many civil engineering applications because it offers a desirable balance of cost and specific strength properties. Glass fibers are commercially available in E-Glass formulation, the most widely used general-purpose form for composite reinforcement, high strength S-2 formulation, and ECR formulation (a modified E glass which provides improved acid resistance). Other glass fiber compositions include AR (alkali-resistant), R and Te. Although considerably more expensive than glass, other fibers including carbon and aramid are used for their strength or modulus properties, or in special situations as hybrids with glass. Properties of common high-performance reinforcing fibers are presented in Table 1.

Table 1. Comparison of Fiber Properties (per ASTM D 2343).[1]

	Specific Gravity	Tensile Strength, MPa	Tensile Modulus, Gpa
E-Glass	2.58	2689	72.4
S-2-Glass®	2.48	4280	86.0
ECR-Glass*	2.62	3625	72.5
K-49 Aramid	1.44	3620	131.0
AS4 Carbon	1.80	3790	234.0

* Mechanical Properties – Single Filament at 72°F per ASTM D-2101

Glass fibers are hydrophilic and very surface-active. They can be easily damaged in handling. A protective film-former is applied immediately as the first step after the fiber-forming process. Sizing solutions containing the film former also contain an adhesion promoter. Adhesion promoters are usually organo-functional silanes which function as coupling agents. The film former also provides processability and moisture protection. The adhesion promoter acts to improve coupling between fibers and the polymer resin matrix. Fiber suppliers select their adhesion promoters and film formers depending on the matrix resins and processing parameters of the end products.

Glass fibers are elastic until failure, and exhibit negligible creep under controlled dry conditions. Generally, it is agreed that the modulus of elasticity of monofilament E glass is approximately 73 GPA. The ultimate fracture strain is in the range of 2.5 to 3.5%. The general stress-strain characteristics of glass fibers are compared in Figure 1 with those of other fibers and materials. The fracture of the actual strand is a cumulative process in which the weakest fiber fails first and the load is then transferred to the remaining stronger fibers which fail in succession. Glass fibers are much stronger than a comparable glass formulation in bulk form such as window glass or bottle glass. The strength of glass fibers is well-retained if the fibers are protected from moisture and air-borne or contact contamination.

When glass fibers are held under a constant load at stresses below the instantaneous static strength, they will fail at some point as long as the stress is maintained above a minimum value. This is called 'creep-rupture.' Atmospheric conditions play a role, with water vapor being most deleterious. It has been theorized that the surface of glass contains sub-microscopic voids that act as stress risers. Moist air can contain weakly acidic carbon dioxide. The corrosive effect of such exposure can affect the stress in voids within glass fiber filaments until failure occurs. In addition, exposure to high pH environments may cause aging or a rupture associated with time. These potential problems were recognized in the early years of glass fiber manufacture and have been the subject of continuing development of protective treatments. Such treatments are universally applied at the fiber-forming stage of manufacture. A number of special organo-silane functional treatment have been developed for thus purpose. Both multi-functional and environment-specific chemistries have been developed for the classes of matrix materials in current use. Depending upon the resin matrix

used, the result of these developments has been to limit the loss of strength to 5 to 10% after a 4-hour water boil test.
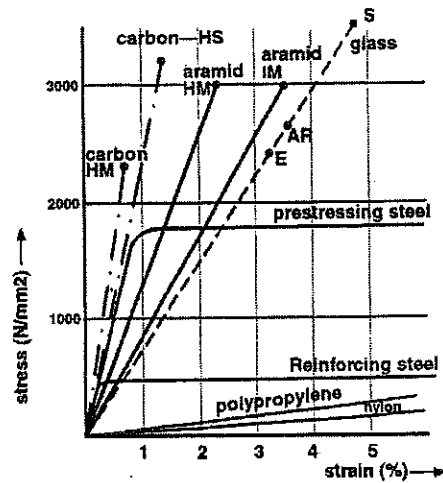

Figure 1. Tensile Stress-Strain Relationships.[2]

Commercial carbon fibers are derived from three sources: pitch (a by-product of petroleum distillation), PAN (polyacrylonitrile), and rayon. There are two types of carbon fiber: the high-modulus, and the high-strength type. Carbon fibers are not easily wet by resins; this is particularly true for higher-modulus fibers. Surface treatments that increase the number of active chemical groups (and sometimes roughen the fiber surface) have been developed for some resin matrix materials. Carbon fibers are frequently shipped with an epoxy size treatment applied to prevent fiber abrasion, improve handling, and provide an interface which is compatible with the epoxy resin matrix. Fiber-matrix interfacial bond strength approaches the strength of the resin matrix for lower-modulus carbon fibers. However, higher-modulus fibers show substantially lower interfacial bond strengths. Failure in high-modulus fibers occurs at surface layers in much the same way as with aramid. Table 2 presents typical properties of commercial carbon and other fibers.

Carbon fibers are available as 'tows' or bundles of parallel fibers. The range of individual filaments in the tow is normally from 1,000 to 200,000 fibers. Carbon fibers are also available in the form of a prepreg, and also as unidirectional tow sheets. There are several organic fibers available that can be used for structural applications. However, cost, and in some cases service temperature or durability factors, restrict their use to

14

specific applications. The most popular of the organic fibers is aramid. Kevlar 49 and Twaron 1055 are the major forms of aramid fibers used today because of their higher modulus. Kevlar 29 and Twaron 2000 are used for ballistic armor and applications requiring increased toughness. Ultra-high modulus Kevlar 149 is also available. Aramid fibers are available in tows, yarns, rovings, and various woven cloth products. The properties of aramid fibers are also presented in Table 2.

Table 2. Typical Properties of Commercial Reinforcing Fibers.[3]

Fiber	Typical Diameter (microns)	Specific Gravity	Tensile Modulus GPa	Tensile Strength GPa	Strain To Failure (%)	Coefficient Of Thermal Expansion $10^{-6}/^{\circ}C$	Poisson's Ratio
GLASS							
E-Glass	10	2.54	72.4	3.45	4.8	5.0	0.2
S-Glass	10	2.49	86.9	4.30	5.0	2.9	0.22
CARBON							
PAN-Carbon T-300[a]	7	1.76	231	3.65	1.4	-0.1 to -0.5 (longitudinal) 7-12 (radial)	-0.2 ... ...
As[b]	7	1.77	220	3.1	1.2	-0.5 to -1.2 (longitudinal) 7-12 (radial)	... ...
t-40[a]	6	1.81	276	5.65	2.0	... ...	... ...
HSB[b]	7	1.85	344.5	2.34	0.58	... ...	... ...
Fortafil3™ C	7	1.80	227	3.80	1.7	-0.1	... .
Fortafil5™ C	7	1.80	345	2.76	0.8	... ...	
PITCH-Carbon							
P-555[a]	10	2.0	380	1.90	0.5	-0.9 (longitudinal)	... ...
P-100[a]	10	2.16	758	2.41	0.32	-1.6 (longitudinal)	
ARAMID							
Kevlar™49[d]	11.9	1.45	131	3.62	2.8	-2.0 (longitudinal) +59 (radial)	0.35
Twaronr™1055[e]	12.0	1.45	127	3.6	2.5	-2.0 (longitudinal) +59 (radial)	0.35

a Amoco   c Akzo-Nobel/Fortafil Fibers   d DuPontde Nemours & Co.   e Akzo-Nobel Fibers   * minimum lot average values

2.1.3 Processing Systems

There are several methods of achieving reliable placement of fibers within the polymer matrix. The common fabrication processes are described below.

Filament winding (Figure 2) uses continuous fibers in the form of parallel strands (rovings) impregnated with matrix resin, and winds them on a rotating cylinder. The resin-impregnated rovings are made to traverse back and forth along the length of the cylinder. A laminate with controlled thickness, wind angle and fiber volume fraction is thereby created. The material is cured on the cylinder and then removed. Pipes, torsion tubes, storage tanks, airplane fuselages and the like are made by this process.
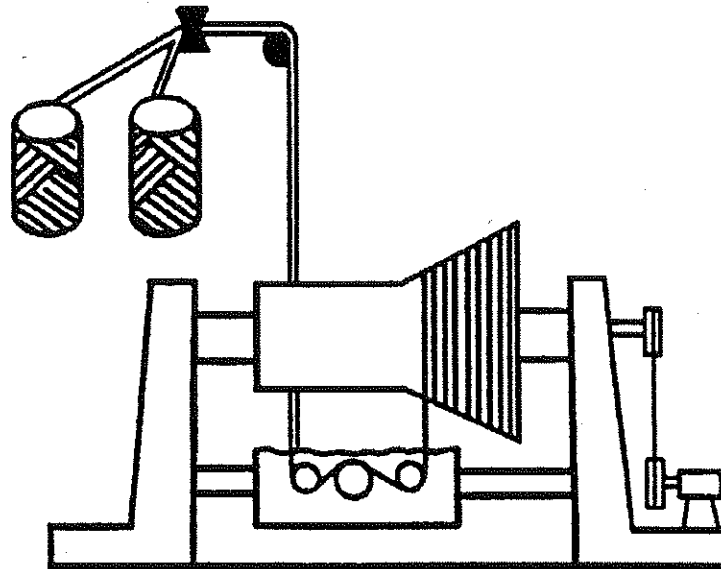

Figure 2. Filament Winding Process.[4]

Pultrusion (Figure 3) makes products with constant cross-section and unlimited length, with the length constrained only by building and shipping limitations. The pultrusion process uses continuous fibers; all the fiber rovings necessary for the cross-section of the part are drawn to a wet-out bath that contains the resin matrix, catalyst (or hardener), and other additives. The rovings are impregnated in the bath. Excess liquid resin is removed and returned to the bath, while the wet-out roving enters the pultrusion die. These dies are generally 0.9 to 1.3 m long and are heated electrically or by hot oil. In some cases, a radio-frequency pre-heating cabinet

is employed to increase the ease of curing thick sections. Throughput rate is generally about 0.9 m per minute. Complex and thick sections may require more time for complete cure, while very thin sections may require less time. Polyester resin and vinyl elsters are the major matrix materials used in the pultrusion process. Examples of products produced by pultrusion include reinforcing and prestressing rods, structural shapes, grating, automobile drive shafts, ground anchors and tie backs, sheet piling, and window frame sections.
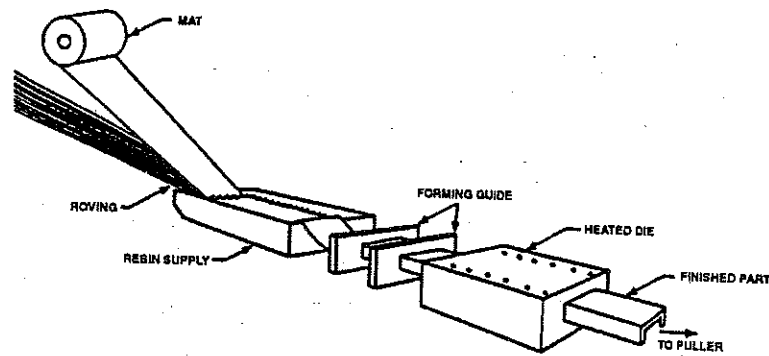

Figure 3. The Pultrusion Process.[5]

Vacuum compaction processes (Figure 4) atmospheric pressure against a material system, that has been sufficiently evacuated of entrapped air, for compression and compaction of the uncured laminate. In some forms of the process, a pre-impregnated arrangement of fibers is placed on a mold in one or more laminar thicknesses. A covering sheet of stretchable film is placed over the lamina array and secured to the mold surface. A vacuum is drawn from within the covered area by a hose leading to a vacuum pump. As air is evacuated, the stretchable sheet is pressed against the fiber prepreg array to compact the lamina. The entrapped air is thereby removed from between the plies. If the resin matrix is heated by one of a number of methods (infrared lamps, heated mold, steam autoclave, etc.), the resin viscosity drops and additional resin densification can take place before the increase in resin viscosity associated with curing.
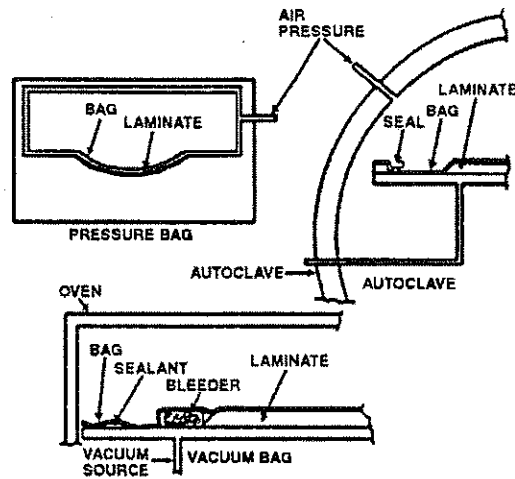
Figure 4. Vacuum Compaction Processing.[6]

Matched mold processing techniques cover a range of processes and materials. The molds in these processes defines the shape and thickness of the part, this approach generally uses a press.

2.2 ENGINEERING PROPERTIES

2.2.1 Physical and Mechanical Properties

In discussions related to the properties of FRP bars, the following points must be kept in mind. First, an FRP bar is anisotropic, with the longitudinal axis being the strong axis. Second, unlike steel, mechanical properties of FRP composites vary significantly from one product to another. Factors such as volume and type of fiber and resin, fiber orientation, dimensional effects, and quality control during manufacturing, play major roles in establishing product characteristics. Furthermore, mechanical properties of FRP composites, like all structural materials, are affected by such factors as loading history and duration, temperature, and moisture.

18

While standard tests have been established to determine the properties of traditional construction materials, such as steel and concrete, the same cannot be said for FRP materials. This is particularly true for civil engineering applications, where the use of FRP composites is in its infancy. It is therefore necessary to determine the exact loading and exposure conditions in advance, and to obtain (in consultation with the manufacturer, the material characteristics corresponding to those conditions.

2.2.1.1   Specific Gravity

FRP bars have a specific gravity ranging from 1.5 to 2.0, they are nearly four times lighter than steel. The reduced weight leads to lower transportation and storage costs and decreased handling and installation time on the job site as compared to steel reinforcing bars. This is an advantage to consider in cost analysis for product selection.

2.2.1.2   Thermal Expansion

Reinforced concrete itself is a composite material where the reinforcement acts as the strengthening medium and the concrete as the matrix. It is therefore imperative that behavior under thermal stresses for the two materials be similar so that the differential deformations of concrete and the reinforcement are minimized. Depending on mix proportions, the linear coefficient of thermal expansion for concrete varies from 6 to 11 x 10^{-6}/°C. Listed in Table 3 are the coefficients of thermal expansion for typical FRP products.

2.2.1.3   Tensile Strength

FRP bars reach their ultimate tensile strength without exhibiting any material yielding. A comparison of the properties of FRP and steel reinforcing bars is shown in Table 3. The mechanical properties of FRP reported here are measured in the longitudinal (i.e. strong) direction. Values reported for FRP materials cover some of the more commonly available products. Unlike steel, the tensile strength of FRP bars is a function of bar diameter. Due to

shear lag, fibers located near the center of the bar cross section are not subjected to as much stress as those near the outer surface of the bar.[7] This phenomenon results in reduced strength and efficiency in larger diameter bars. For example, for GFRP reinforcement produced by one U.S. manufacturer, tensile strength ranges from nearly 480 MPa for 28.7 mm bars to 890 MPa for 9.5 mm bars.[8]

Some FRP tendons were made by stranding seven GFRP (S-2 Glass) or CFRP pultruded bars of diameter ranging from 3 to 4 mm. The ultimate strength of these tendons was comparable to that of a steel prestressing strand. For GFRP tendons, ultimate strength varied from 1380 to 1724 MPa; for CFRP tendons, it varied from 1862 to 2070 MPa.[9]

2.2.1.4   Tensile Elastic Modulus

As noted in Table 3, the longitudinal modulus of elasticity of GFRP bars is approximately 25% that of steel. The modulus for CFRP tendons, which usually employ stiffer fibers, is higher than that of GFRP reinforcing bars.

Table 3. Comparison of Mechanical and Physical Properties (longitudinal direction)[7, 10].

	Steel Reinfg. Bar	Steel Tendon	GFRP Bar	GFRP Tendon	GFRP Tendon	AFRP Tendon
Tensile Strength, MPa	483-690	1379-1862	517-1207	1379-1724	165-2410	1200-2068
Yield Strength, MPa	276-414	1034-1396	Not Applicable			
Tensile Elastic Modulus, Gpa	200	186-200	41-55	48-62	152-165	50-74
Ultimate Elongtion, mm/mm	>0.10	>0/04	0.035-0.05	0.03-0.045	0.01-0.015	0.02-0.026
Compressive Strength, Mpa	276-414	N/A	310-482	N/A	N/A	N/A
Coeff. Of Thermal Exp. $(10\text{-}6/^{o}C)$	11.7	11.7	9.9	9.9	0.0	-1.0
Specific Gravity	7.9	7.9	1.5-2.0	2.4	1.5-1.6	1.25

Note: All properties refer to unidirectional reinforced coupons

Properties vary with the fiber volume (45-70%), coupon diameter, and grip system

N/A = Not Available

2.2.1.5 Compressive Strength

FRP bars are weaker in compression than in tension. This is the result of difficulties in accurately testing unidirectional composites in compression, and is related to gripping and aligning procedures, and also to stability effects of fibers. However, the compressive strength of FRP composites is not a primary concern for most applications. Compressive strength also depends on whether the reinforcing bar is smooth or ribbed. Compressive strengths in the range of 317 to 470 MPa have been reported for GFRP reinforcing bars having a tensile strength in the range of 552 to 896 MPa.[10] Higher compressive strengths are expected for bars with higher tensile strength.

2.2.1.6 Compressive Modulus

Unlike tensile stiffness, compressive stiffness varies with FRP reinforcing bar size, type, quality control in manufacturing, and length-to-diameter ratio of the specimen. The compressive stiffness of FRP reinforcing bars is smaller than the tensile modulus of elasticity. Based on tests of samples containing 55 to 60% volume fraction of continuous E-glass fibers in a matrix of vinyl ester or isophthalic resin, a modulus of 34 to 48 GPa has been reported.[10] Another manufacturer reports a compressive modulus of 34 GPa, which is approximately 77% of the tensile modulus for the same product.[11]

2.2.1.7 Shear Strength

In general, shear strength of composites is very low. FRP bars, for example, can be cut very easily in the direction perpendicular to the longitudinal axis with ordinary saws. This shortcoming can be overcome in most cases by orienting the FRP bars such that they will resist the applied loads through axial tension. Special shear tests have been developed;[12] these procedure have been applied to obtain shear properties for FRP dowel bars.

2.2.1.8   *Creep and Creep Rupture*

Fibers such as carbon and glass have excellent resistance to creep, while the same is not true for most resins. Therefore, the orientation and volume of fibers have a significant influence on the creep performance of reinforcing bars and tendons. One study reports that for a high-quality GFRP reinforcing bar, the additional strain caused by creep was estimated to be only 3% of the initial elastic strain.[9] Under loading and adverse environmental conditions, FRP reinforcing bars and tendons subjected to the action of a constant load may suddenly fail after a time period, referred to as the endurance time. This phenomenon, known as creep rupture, exists for all structural materials including steel. For steel prestressing strands, however, this is not a concern. Steel can endure the typical tensile loads, which are about 75% of the ultimate strength, indefinitely without any loss of strength or fracture. As the ratio of the sustained tensile stress to short-term strength of the FRP increases, endurance time decreases. Creep tests were conducted in Germany on GFRP composites with various cross sections; the results indicated that creep-rupture does not occur if sustained stress is limited to 60% of the short-term strength.[13] This limit on stress may be of little concern for most reinforced concrete structures since the sustained stress in reinforcement is usually below 60%. It does, however, require special attention in application of FRP composites as prestressing tendons. It must be noted that other factors, such as moisture, also impair creep performance and may result in a shorter endurance time. Short-term (e.g., 48 hour) and long-term (e.g., 1-year) sustained load corresponding to 50% of the ultimate strength have been applied to GFRP and CFRP tendons at room temperature. The specimens showed very little creep, and tensile modulus and ultimate strength did not change significantly after the application of sustained loads.[14,15]

2.2.1.9   *Fatigue*

FRP bars exhibit good fatigue resistance. Most research on this issue has been on high-modulus fibers (e.g. aramid and carbon) subjected to large cycles of tension-tension loading which is relevant to aerospace applications. In tests where loading was repeated for 10 million cycles, it was concluded that carbon-epoxy composites have better fatigue strength

than steel, while the fatigue strength of glass composites is lower than steel at low stress ratios.[6] Other research[12] showed good fatigue resistance of GFRP dowel bars in shear subjected to 10 million cycles. In another investigation, GFRP bars constructed for prestresing applications were subjected to repeated cyclic loading with a maximum stress of 496 MPa and a stress range of 345 MPa. The bars could stand more than 4 million cycles of loading before failure initiated at the anchorage zone.[16] CFRP tendons exhibited good fatigue resistance as shown in tension-tension fatigue tests under 2 million cycles. The mean stress was 60% of the ultimate strength, with minimum and maximum stress levels of 55% and 64% of the ultimate strength, respectively. The modulus of elasticity of tendons did not change after the fatigue tests.[17]

2.2.2 *Factors Affecting Mechanical Properties*

Mechanical properties of composites are dependent on many factors including load duration and history, temperature, and moisture. These factors are interdependent and, consequently, it is difficult to determine the effect of each one in isolation while the others are held constant.

2.2.2.1   *Moisture*

Excessive absorption of water in composites could result in significant loss of strength and stiffness. Water absorption produces changes in resin properties and could cause swelling and warping in composites. It is therefore imperative that mechanical properties required of the composites be determined under the same environmental conditions where the material is to be used. There are, however, resins which are formulated to be moisture-resistant and may be used when a structure is expected to be wet at all times. In cold regions, the effect of freeze-thaw cycled must also be considered.

2.2.2.2   *Fire and Temperature*

Many composites have good to excellent properties at elevated temperatures. Most composites do not burn easily. The effect of high temperature is more severs on resin than on

fiber. Resins contain large amounts of carbon and hydrogen, which are flammable, and research is continuing on the development of more fire-resistant resins.[6] Tests conducted in Germany have shown that E-glass FRP bars could sustain 85% of their room-temperature strength, after half an hour of exposure to 300°C temperature while stressed to 50% of their tensile strength.[16] While this performance is better than that of prestressing steel, the strength loss increases at higher temperatures and approaches that of steel. The problem of fire for concrete members reinforced with FRP composites is different from that of composite materials subjected to direct fire. In this case, the concrete serves as a barrier to protect the FRP from direct contact with flames. However, as the temperature in the interior of the member increases, the mechanical properties of the FRP may change significantly. It is therefore recommended that the user obtain information on the performance of a particular FRP reinforcement and resin system at elevated temperatures when potential for fire is high.

2.2.2.3   Ultraviolet Rays

Composites can be damaged by the ultraviolet rays present in sunlight. These rays cause chemical reactions in a polymer matrix, which can lead to degradation of properties. Although the problem can be solved with the introduction of appropriate additives to the resin, this type of damage is not of concern when FRP elements are used as internal reinforcement for concrete structures, and therefore not subjected to direct sunlight.

2.2.2.4   Corrosion

Steel reinforcement corrodes and the increase in material volume produces cracks and spalling in concrete to accelerate further deterioration. A major advantage of FRP materials is that they do not corrode. It must be noted, however, the composites can be damaged as a result of exposure to certain aggressive environments. While GFRP bars have high resistance to acids, they can deteriorate in an alkaline environment. In a recently completed study for prestressed concrete applications, a particular type of glass-epoxy FRP strand embedded in concrete was subjected to salt water tidal simulation, which resulted in water gain and loss of strength.[18] Although these results cannot be generalized, they highlight the importance of the selection of

correct fiber-resin system for a particular application. FRP tendons made of carbon fibers are resistant to most chemicals.[19]

2.2.2.5 *Accelerated Aging*

Short-term needs for long-term weathering data has necessitated the creation of such analytical techniques as accelerated aging to predict the durability of composite structures subjected to harsh environments over time. Some long-term aging predictions, made over a very short period of time and at higher temperatures have correlated well with real weather aging.[20] Based on these findings, researchers[21] developed two equations for accelerated aging of FRP composites. The first equation gave an acceleration factor based on the mean annual temperature of a particular climate. The second equation showed a relationship between bath temperature and number of acquired accelerated aging days per day in bath.[21,22] By using these two equations, dowel bars composed of E-glass fibers encapsulated in a vinyl ester resin were aged at an elevated temperature of 60°C for nine weeks. Specimens were aged in water, lime, and salt bath solutions. An accelerated aging period of 63.3 days at an elevated temperature of 60°C in the solution was utilized without appreciable degradation for a lime bath. This accelerated aging was equivalent to approximately 50 years.

2.3   TEST METHODS

2.3.1 Introduction

Test methods are important to evaluate the properties of resin, fiber, FRP composite, and structural components. This section deals with test methods related to FRP composites for civil engineering applications. The resin groups included are: polyester, vinyl ester, epoxy, and phenolic. The fibers included are: E-glass, S-2 glass, aramid, and carbon. FRP composites made of a combination of the above resins and fibers with different proportions are used for the reinforcement of concrete members. Only continuous fiber reinforcement is included in this report. ASTM standards divide the test methods relative to FRP composites

into two sections; one dealing with glass FRP composites, and one dealing with high-modulus FRP composites using fiber types such as carbon.

2.3.2 Gripping Mechanisms

The design and development of a suitable gripping mechanisms for FRP bars in tension tests and in pre- and post-tensioned concrete applications have presented major difficulties to researchers and practitioners. Due to the low strength of FRP reinforcing bars and tendons n the transverse direction, the forces introduced by the grips can result in localized failure of the FRP within the grip zone. Clearly, the use of longer grips to reduce the stresses in the grip zone is impractical in most cases.

One type of reusable grip[23] consists of two steel plates 178 by 76 by 19 mm with a semi-circular groove cut out of each plate. The groove diameter is 3 mm larger than the diameter of the bar to be tested. Fine wet sand on top of an epoxy-sand coating is used to fill the groove. Two plates are carefully brought together at each end of the bar to be tested. The grips are then placed inside the jaws of a universal testing machine. Although these grips may allow a slight slippage of the bar, this limitation is not a major concern when the bar is being tested to failure. It has been reported[24] that a set of such grips was successfully used for tensioning FRP reinforcing bars. In this application, six high-strength bolts were used to clamp the two plates together.

A method of stressing FRP cables using steel chucks 15 mm (0.6 in) in diameter was developed.[9] Two steel chucks are used at each end to develop the full strength of the cable. Other researchers[21] have developed a gripping method where FRP bars were bonded with epoxy into a copper pipe. Tensile testing studies using these grips have produced a procedure for gripping FRP specimens without crushing the bar. More than 200 tensile specimens were successfully tested using a long length between grips. Consistent tensile values were produced that reasonably match the theoretical specimen tension strengths. Aluminum grips with sandblasted circular surfaces are also used. Testing methods with flat jaws may be used

for determining the tensile strength, elastic modulus and ultimate strain of carbon fiber composite bars.

2.3.3 Tension Test

Pultruded glass fiber composite (GFRP) bars made with continuous glass fiber and ranging in diameter from 3.2 to 25.4 mm (0.12 to 1.00 in) can be tested for tensile strength using ASTM D 3916. This test determines the ultimate strength, elastic modulus, percentage elongation, ultimate strain, and Poisson's ratio. Test methods and fixtures used for glass FRP bars could be used for carbon fiber FRP (CFRP) composites, but may not be entirely suitable as higher stress levels are needed to attain tensile failure

2.3.4 Flexural Strength

Flexural strength tests on pultruded GFRP bars can be conducted using ASTM D 4476. This test provides modulus of rupture and modulus of elasticity in bending. Test methods for high modulus FRP composites (e.g. CFRP) are not listed in ASTM, but the methods recommended for glass FRP bars can be used for evaluation of carbon pultruded bars.

2.3.5 Horizontal Shear Strength

Horizontal shear strength of pultruded GFRP bars can be determined using ASTM D 4475 which is a short beam test method.

2.3.6 Creep and Relaxation

Aluminum grips can be used to hold a specimen between special steel jigs as shown in ASTM D 3916. This jig provides a self-straining frame condition to apply a constant load. The specimen extension can be measured by a dial gage or strain gage to determine the increase in strain under sustained load with time.

2.3.7 Nondestructive Testing

Acoustic emission (AE) technique was used to monitor the behavior of GFRP bars subjected to direct tension.[25,26] AE signals emitted by breakage of matrix and fibers were monitored using two AE sensors.

2.4 DESIGN PROCEDURES WITH COMPOSITE REINFORCEMENT

For flexural analysis, the fundamental principles include equilibrium on the cross section, compatibility of strains, (typically the use of plane sections remaining plane), and constitutive behavior.[27, 28] For concrete, the constitutive behavior model uses the Whitney rectangular stress block to approximate the concrete stress distribution at ultimate strength. For FRP reinforcement, the linear stress versus strain relationship to failure must be used. These models work very well for members where the FRP reinforcement is in tension. More work is needed for the use of FRP in compression zones due to possible buckling of the individual fibers within the reinforcing bar.

There is limited research available on the use of FRP shear reinforcement. The literature review presented later suggests that the lower modulus of elasticity of the FRP shear reinforcement allows the shear cracks to open wider than comparable steel reinforcement. A reduction in shear capacity would be expected since concrete contribution is reduced.

The use of FRP materials as reinforcement for concrete beams requires the development of design procedures that ensure adequate safety from catastrophic failure. With steel reinforcement, a confident level of safety is provided by specifying that the flexural strength of a section should be at least 25% less than its balanced flexural strength ($\rho_{actual} < 0.75\ \rho_{bal}$). This ensures the steel will yield before the concrete crushes, therein, guaranteeing a ductile failure. The result is the ability of the failed beam to absorb large amounts of energy through plastic straining in the reinforcing steel. FRP materials respond linearly and elastically to failure at which point brittle rupture occurs. As a result, failure, whether the result of shear, flexural

compression or flexural tension, is unavoidably sudden and brittle. Building codes and design specifications will eventually recognize the advantages and disadvantages of FRP material when defining analytical procedures on which engineers will rely for design. This may require lower flexural capacity reduction factors to be more compatible with the specific performance limitations of FRP materials.

2.4.1 Ductility

A formal definition of ductility is the ratio of the total deformation or strain at failure to the deformation or strain at yielding. FRP reinforcement has a linear stress versus strain relationship to failure. Therefore, by the above definition, the behavior of FRP reinforced members cannot be considered ductile.

The 1995 edition of ACI 318 contains an Appendix with alternative provisions for the establishment of capacity reduction factors. Part of ACI 318-95 defines the maximum reinforcement ratio for tension controlled sections by the ratio that produces a net tensile strain of not less than 0.005 at nominal strength. The net tensile strain is measured at the level of the extreme tension reinforcement at nominal strength due to factored loads, exclusive of effective prestress strain.[29] This provision was enabled to allow for members with various reinforcing materials including high strength steel reinforcement and steel prestressing strands, which have markedly different yield strains than ordinary reinforcement. Using the above definition, ductility of FRP reinforced member may be replaced by the concept of tension controlled section which is defined as one having a maximum net tensile strain of 0.005 or more.

If a pseudo-ductile model is used, the designer must realize that the member recovery will be essentially elastic. Minor damage to the concrete will occur at large deformations, but no 'yielding' of the reinforcement will occur. In seismic zones, there will be little or no energy dissipation resulting from the large deformations.

2.4.2 Constitutive Behavior and Material Properties

Since variation in fiber content and manufacturing quality control will affect both the strength and the elastic modulus, a designer should verify the properties of the actual material being used. The ultimate tensile strength of the FRP reinforcement must include consideration of the statistical variation of the product. Some researchers suggest that the maximum strength be taken as the average strength minus three standard deviations.[30] This assumes that statistical records are available and that they are representative of FRP production.

Use of the Whitney rectangular stress block is satisfactory for determination of the concrete strength behavior, although several researchers have used more complex constitutive rules for the concrete stress versus strain behavior.

The specific material properties lead to a number of design considerations. First, the modulus of elasticity of most FRP reinforcement are lower than that of steel. This means that larger strains are needed to develop comparable tensile stresses in the reinforcement. If comparable amounts of FRP and steel reinforcement are used, the FRP reinforced beam will have larger deflections and crack widths than the steel reinforced section.

FRP reinforcements' strength is time-dependent. Like a concrete cylinder, FRPs will fail at a sustained load considerable lower than their short-term static strength. At the present time, most designers and researchers are limiting the sustained load in FRP reinforcement to 50-60% of the static tensile strength. It was reported that the time-dependent creep strength of Polestar GFRP is about 70% of the short-term strength.[31] However, others reported a linear relationship between sustained stresses and logarithm of time.[32] In light of these results, a lower sustained stress is advisable for GFRP reinforcement in the presence of aggressive environments.

2.4.3 Flexural Behavior

The flexural design of reinforced concrete members with FRP reinforcement proceeds from basic equilibrium on the cross section and constitutive behavior of the concrete and the FRP

reinforcement. Unlike steel reinforcement, no constant tensile force may be assumed after yield point. The stress in reinforcement continues to increase with increasing strain until the reinforcement ruptures. The only condition of known forces in an FRP reinforced beam is the balanced condition where the concrete fails in compression at the same time that the reinforcement ruptures. This could be defined as the balanced ratio, ρ_{br}, and is given as:[33]

$$\rho_{br} = 0.85 \; \beta_1 \; (f'_c / f_{pu}) \; \varepsilon_{cu} / (\varepsilon_{cu} + \varepsilon_{pu})$$

where:

ε_{cu} is the ultimate concrete strain

ε_{pu} is the ultimate strain of the composite reinforcement

f'_c is the compression strength of the concrete

β_1 is a material property to define the location of the neutral axis from the depth of the compression block

f_{pu} is the ultimate tensile stress of the composite reinforcement

If the reinforcing ratio ρ is slightly less than ρ_{br}, failure will occur by rupture of the composite reinforcement, and the concrete will be near its ultimate stress condition. If $\rho << \rho_{br}$, the flexural member will fail by rupture of the composite reinforcement and the concrete stress state must be determined to locate the compression centroid. If $\rho > \rho_{br}$, compression failure of the concrete will occur first. The percentage of reinforcement should be selected to ensure formation of cracks and considerable deformation before failure to provide the warning behavior.

At the present time, there is insufficient data to accurately define a capacity reduction factor, $\varnothing$, for bonded FRP reinforced beams. For beams with a $\rho < \rho_{br}$, a $\varnothing$ factor of 0.85 may be a reasonable assumption since the failure can be made analogous to a shear failure. However, it has been shown that this condition is practically unattainable in non-prestressed flexural members since deflection becomes excessive.[34] For $\rho > \rho_{br}$, a $\varnothing$ factor of 0.70 may be more appropriate since failure is due to crushing of the concrete in compression. A minimum amount

of flexural reinforcement should be used to provide an adequate post-cracking strength to prevent brittle failure at first cracking.

Researchers [35,36] have reported that ACI 318 Code strength equations conservatively predict the flexural strength of FRP reinforced members. If the reinforcement ratio is near ρ_{br}, the ACI equations will be conservative because there is a reserve tensile capacity in the reinforcement. ACI strength equations are not valid for $\rho > \rho_{br}$.

2.4.4 Flexural Cracking

Excessive cracking is undesirable because it reduces stiffness, enhances the possibility of deterioration, and adversely affects the appearance of the beams. Since FRP reinforcement is not subject to the same corrosion mechanisms as steel, the oracle width limitations established by ACI Committee 318 may not be applicable. The crack width will be dependent upon the physical bonding characteristics of the reinforcement and its modulus. Available research outcomes for glass FRP reinforcement. Guidance for other FRP materials and configurations is not readily available.

2.4.5 Deflections

The deflection of FRP reinforced members will be greater than comparable steel reinforced members because of the lower modulus of elasticity of FRP. This leads to greater strains to achieve comparable stress levels and to lower transformed moment of inertia. Deflection limitations proposed by ACI 318 are independent of the concrete strength and reinforcement. They should remain applicable to FRP reinforced sections.

Three approaches are possible for the prediction of deflection in FRP reinforced members. The first method involves solving for curvature at several sections along the member and integrating the moment curvature diagram. This is a first principal approach and is applicable to all FRP materials. The other two approaches use the effective moment of inertia.

A modified moment of inertia for glass FRP reinforcement will be described later. This approach has the benefit of extensive correlation with test data.[37,38] An alternative approach is to use the existing ACI deflection equations. The cracked moment of inertia uses the transformed FRP section.

2.4.6 Development Length

The development length depends upon the surface of the FRP reinforcement. While guidance is available for helically wrapped glass FRP reinforcement, these results may not be universally applicable to all FRP reinforcement. For example, Mitsui's FiBRA™ has a deformed surface due to braiding and Tokyo Rope's CFCCY™ has a roughened surface due to the final fiber wrapping. Technora's® rod [39] has an external helical wrap while Mitsubishi's Leadline™ has a depression in the rod surface. These conditions are sufficiently different to suggest that more research is needed prior to the establishment of generic design guidelines.

2.4.7 Shear Design

The vast majority of the research data is for members that are not shear critical. There are a very small number of tests with FRP shear reinforcement. Experimental results of shear anchorage indicate that the stirrups will fail in the corners due to premature failure at the bend. The few tests that have been completed with FRP stirrups suggest that the shear resistance is less than predicted. This may be due to the large cracks that result from the lower modulus of elasticity of the stirrups. The larger cracks can reduce several components of the concrete contribution to shear resistance. Members with FRP longitudinal reinforcement and steel stirrups have not shown unusual shear behavior.[40] Special attention should be devoted to the reduced dowel contribution of FRP reinforcement in the presence of shear cracks.[41]

2.5   STRUCTURAL BEHAVIOR

2.5.1   Strength of Beams and Slabs Reinforced with FRP

The wide-spread implementation of FRP as a reinforcement for concrete structural members requires: (1) a comprehensive understanding of how these two materials behave together as a structural system, and (2) analytical techniques that reliably predict the composite behavior. In this regard, three important physical characteristics of FRP materials must be considered: (1) high tensile strength, (2) low modulus of elasticity, and (3) linear-elastic brittle behavior to failure. Substitution of FRP for steel on an equal area basis typically results in significantly higher deflections with wider crack widths and greater flexural strength. As a consequence, deflection limitations will likely be an important parameter in design considerations. This behavior is due to higher tensile strength and lower modulus values of FRP, assuming good force transfer.

Flexural failure of concrete members reinforced with currently available FRP materials can be categorized as relatively brittle. Failure occurs either as a result of concrete crushing or FRP tensile rupture. This behavior differs from the behavior of concrete beams under-reinforced with steel. However, one can still design FRP reinforced concrete beams, of reasonable ductility which fail by cracking of concrete, prior to rapture of FRP. In addition, shear capacity is also likely to be significantly reduced as a result of increased crack width and reduced size of compressive stress blocks.

2.5.2   Flexural Strength

Monotonic testing of 20 simply supported rectangular beams reinforced with GFRP and steel reinforcing bars has been reported.[42] Samples were loaded with two concentrated loads applied at the third span points. All beams were 178 mm deep by 89 mm wide by 1800 mm long with an effective depth that varied slightly from 159 mm to 165 mm. The beams were grouped in five series of four beams each. The four beams in each series included: two beams reinforced with FRP reinforcing bars with a bar diameter = 3 mm; one beam reinforced with an equal

number of steel bars with a steel bar diameter = 3.2 mm; and one beam reinforced with FRP bars and with chopped steel wire in the concrete mixture. Stirrups were not provided in any of the beams. The reinforcement ratio varied from 0.19% to 0.41% for FRP reinforced beams and from 0.22% to 0.45% for steel reinforced beams. Tensile strength and modulus of elasticity for the FRP were 1.1 GPa and 50.3 GPa, respectively. Concrete strength ranged from 28.3 MPa to 35.4 MPa. The test revealed an increase in ultimate moment capacity for steel reinforced beams as the percentage of reinforcement was increased. The reinforcing ratio of FRP beams did not affect moment capacity because the beams failed by compression of the concrete, thus not developing the full capacity of the FRP. The authors suggested that because the modulus of FRP is only slightly higher than that of concrete, limited tensile stress can be transmitted from the concrete to the FRP reinforcement. Thus, most of the tensile load is initially absorbed by the concrete. When the tensile strength of concrete is exceeded, cracks form and this cracking process continues until the cracks extend over three-fourths of the beam span at a spacing of approximately 102 mm to 152 mm. When further load was applied, the concrete crushed.

In another study[43], 14 simply supported beams were tested, 12 of which were longitudinally reinforced with glass FRP bars. No shear reinforcement was used. All beams were 3000 mm long by 127 mm wide and 305 mm deep with an effective depth of 286 mm and loaded with two concentrated loads at the one-third span points. FRP reinforcement ranged from 0.65% (2 FRP bars) to 2.28% (7 FRP bars). The FRP reinforcing bars were of 6.4 mm diameter and had tensile strength and modulus values of 723 MPa and 24.8 GPa, respectively. Concrete strength ranged from 29.6 MPa to 40 MPa. Analysis of test results indicated that the behavior of beams with respect to cracking, ultimate load, and deflection could be predicted with the same degree of accuracy as for steel reinforced concrete beams. The ratio of the observed to calculated moment capacity was close to 1.0, with a mean value of 1.09 and a standard deviation of 0.18. With respect to serviceability, a working load stress level in FRP of 15% of its tensile capacity was discussed for concrete strengths between 27.6 MPa and 34.5 MPa.

Flexural and shear performance of concrete beams reinforced only with GFRP reinforcing bars and in combination with steel reinforcing bars have been reported.[44] The study used test results to determine if the theory used for steel reinforced concrete can be used to predict the

performance of concrete beams reinforced with GFRP reinforcing bars. Four beam specimens, 152 mm wide by 152 mm high, with 25 mm of cover, and 1500 mm of length were cast. Beams one and two were simply supported and loaded at a single location; beams three and four were simply supported and loaded at two locations. Beam one was reinforced with three 12 mm diameter steel bars; beam two with two FRP and one 12 mm diameter steel reinforcing bar; beam three with three 12 mm diameter FRP reinforcing bars, and beam four with two 12 mm diameter steel and one 12 mm diameter FRP reinforcing bars. Concrete strength for beams one and two was 29.2 MPa and for beams three and four 25.7 MPa. FRP modulus and tensile strength were 41.4 GPa and 1.0 GPa, respectively. Deflections were calculated using the moment of inertia of the cracked transformed section, neglecting the tensile strength of concrete below the neutral axis. Ultimate load capacities were calculated using (a) transformed sections (b) linearly elastic composite sections, (c) limiting concrete compressive strength to f_c, (d) equilibrium, and (e) nonlinear stress-strain distribution for concrete.

A flexural failure occurred in beam one by yielding in the steel and was followed by concrete crushing. Diagonal tension failures occurred in beams two, three, and four; therefore, theoretical flexural strength could not be compared with test results and no conclusion was derived regarding the accuracy of flexural strength prediction for concrete beams reinforced with FRP. The authors recognized that a methodology for shear strength prediction of FRP reinforced concrete needs to be developed independently from steel/concrete equations.

Tests on six concrete beams, reinforced longitudinally and in shear with different combinations of GFRP and steel reinforcing bars, have been reported.[45] The FRP tensile strength and modulus values were 1.2 GPa and 53.1 GPa, respectively. All beams had a clear span of 3.05 m, and were simply supported, were loaded at two points with a shear span of 1300 mm. Sample cross-sections were 203 mm wide by 457 mm high. The study focused on experimentally determining the feasibility of using FRP bars as reinforcement for concrete beams. Steel stirrups provided adequate shear strength to the longitudinal GFRP reinforced beams to result in either a flexural compression failure or a tension failure (tensile rupture of the FRP bar). Based on the large number of uniformly distributed cracks, it was concluded that a good mechanical bond developed between the FRP bars and concrete. Specimens reinforced

with FRP stirrups and steel longitudinal reinforcement failed as a result of yielding in the longitudinal bars. This was followed by large plastic deformations until a concrete compression failure occurred. Calculated maximum loads using FRP properties were reasonably close to the experimental measured values.

Four simply supported concrete beams each with a different type of fiber reinforcement have been tested.[46] The type of reinforcement, the area of reinforcement, and the respective modulus of elasticity are given in Table 4. All samples were 1000 mm in length by 200 mm wide by 150 mm high with an effective depth of 120 mm, were simply supported, and were loaded at two points with a shear span of 500 mm. All beams were reinforced with steel stirrups 10 mm in diameter at a spacing of 70 mm. All four samples failed in flexure. The ratios of experimental failure load to predicted flexural strength (using elastic theory) for beams reinforced with AFRP, CFRP, GFRP grids and steel bars are 0.75, 0.86, 0.98, and 1.04, respectively. The tensile stress in the reinforcement was measured using bonded strain gauges located at mid-span. Experimental reinforcement strain results compared well with predicted values calculated using elastic theory. Based on these results, the authors concluded that the failure load for concrete beams reinforced with FRP can be calculated using the elastic theory applicable for reinforced concrete members. Theoretical load-deflection behavior was predicted using an effective moment of inertia. Experimental load-deflection behavior was reported to agree well with theoretical predictions.

Table 4. Reinforcing Bars.[19]

Reinforcement Type	Area mm^2	Modulus of Elasticity x 10^8 psi (GPa)
Aramid	37.75	10.30 (71)
Carbon	43.63	50.76 (350)
Glass	82.38	10.73 (74)
Steel	126.7	27.70 (191)

The cyclic response of concrete beams, 1800 mm long, 203 mm wide and 101 mm high, reinforced with a two dimensional FRP grid has been investigated.[47] Tensile strength and

modulus of the FRP were 827 MPa and 41.4 GPa, respectively. Concrete strength was between 29 MPa and 31.7 MPa. Test samples were reinforced at 110% of balanced strain condition. Samples were simply supported and loaded at two locations with a shear-span of 610 mm. The following two cyclic load schedules were used: the first series was subjected to 20 cycles of 0 to 50% of maximum monotonic capacity; the second series was subjected to 10 cycles for each loading case as follows: 0 to 20 %, 0 to 35%, 0 to 20%, 0 to 50% and 0 to 80% of maximum monotonic capacity for a total of 80 cycles. The results of the first series showed an increase in deflection with each cycle. The amount of increased deflection decreased with each cycle asymptotically. Also, the increase in permanent deflection was about half the increase in maximum deflection. Results from the second test series showed an increase in deflection each time the maximum applied load was increased, for example from 35 % to a 50 % load case. There appeared to be no increase in deflection when the load was reduced and cycled at 20% of maximum. The load-deflection curve (drawn with the first load-deflection points occurring each time a larger load was cycled), appeared to follow the load-deflection curve of a monotonically loaded sample of identical design. Only minor differences in crack pattern between cyclically and monotonically loaded samples was observed indicating that crack propagation stabilized after a relatively few number of cycles.

Seven full-size concrete bridge deck slabs, six of which were reinforced with pultruded GFRP gratings and one with steel reinforcing bars, have been tested.[48] The test span length was 2400 mm, with a projection of 305 mm on either side of the supports. Slab width was 1220 mm and total depth was 216 mm. A 32 mm cover was used and concrete strength was 34 MPa. The slabs were designed for a live load moment designated by AASHTO using a nominal HS-25 loading with a live load impact factor of 30% bringing the nominal service load to 11.8 MN. This load was then used to calculate a service limit slab deflection of 3.3 mm. One slab of each grating type and the steel reinforced slab were tested monotonically to 11.8 MN, then subjected to 10 loading unloading cycles of 0 to 11.8 MN, and then loaded monotonically to failure. The loading-unloading cycles for the 3 remaining slabs were as follows: 0 to 11.8 MN for 10 cycles, 0 to 23.6 MN for 10 cycles, 0 to 11.8 for 10 cycles, and 0 to failure. Behavior of all FRP reinforced slabs was similar. Initial cracking occurred between 4.5 and 6.8 MN followed by development of flexural cracks. At loads near ultimate, flexural shear cracking was observed.

Failure was the result of concrete crushing followed immediately by propagation of a flexural-shear crack in a diagonal path towards the outer support. This crack was intercepted by the top surface of the FRP grating and redirected horizontally along the top surface of the grating to the free end. No failure of the FRP grating was observed. The steel reinforced slab failed by yielding of the reinforcing bars and subsequent crushing of the concrete. Service load mid span deflections for all FRP reinforced slabs were close to the allowable limit of 4.9 mm. Deflection was found to stabilize after a limited number of cycles. All slabs failed at loads in excess of three times the service load.

The flexural performance of simply supported rectangular concrete beams with an effective length of 2700 mm, reinforced with GFRP reinforcing bars and subjected to load applied at two locations, have been reported.[49] Tensile strength of the FRP reinforcing bars ranged from 551 MPa for 25 mm diameter bars to 896 MPa for 10 mm diameter bars while the concrete strength ranged from 29 MPa to 69.0 MPa. The 27 concrete test beams were 152 mm in width, 305 mm in height and contained different configurations of FRP reinforcements (i.e. reinforcing bar size, type of reinforcing bar), and type of stirrups (steel, FRP smooth, FRP ribbed). Five groups of beams were tested, details of the test beams are given in Table 5.

Table 5. Specimen Details

# of Bars	Longitudinal Type	Shear Reinforcement
3	10 mm diameter coated or deformed FRP	6 mm diameter steel or 10 mm diameter deformed FRP
2	12 mm diameter deformed FRP	6 mm diameter smooth FRP bars or 10 mm diameter deformed FRP bars
2	25 mm diameter deformed FRP	6 mm diameter steel or 10 mm diameter deformed FRP
2	10 mm diameter deformed FRP	6 mm diameter steel or 10 mm diameter deformed FRP
5 or 3	10 mm diameter sand coated FRP 12 mm diameter sand coated FRP	10 mm diameter deformed FRP

From the test results, it was concluded that in order to take advantage of the high FRP reinforcing bar ultimate strength (i.e. 551 to 896 MPa), use of high-strength concrete instead of normal-strength concrete (69 MPa vs. 27.6 MPa) is essential. The ultimate moment capacity of high-strength concrete beams (69 MPa) was increased by 90% when an equal area of FRP reinforcing bars of ultimate tensile strength 896 MPa were used in lieu of mild steel reinforcing bars (414 MPa). The ultimate moment capacity of concrete beams reinforced with sand-coated FRP reinforcing bars is about 70% higher than that of beams reinforced with steel reinforcing bars for the same area and concrete strength; the use of sand-coated FRP reinforcing bars, in addition to high strength 41 to 69 MPa concrete, was found to increase the cracking moment of the beams and to reduce the crack widths in addition to eliminating the sudden propagation of cracks toward the compression zone. This behavior was related to a better force transfer between the sand-coated FRP reinforcing bar and concrete. The crack pattern was very similar to a pattern expected of a beam reinforced with steel reinforcing bars; beams cast with higher strength concrete and reinforced with two 10 mm diameter, three 10 mm diameter, and two 12 mm diameter FRP reinforcing bars failed when the FRP bars reached ultimate tensile strength, and beams reinforced with two 25 mm diameter FRP reinforcing bars failed in shear before reaching the ultimate tensile strength of the bars; using high strength concrete of 51.7 MPa compressive strength increased the moment capacity by 50% over beams cast with normal strength concrete of 29 MPa compressive strength.

The flexural and shear behavior of simply supported rectangular concrete beams, approximately 76.2 mm wide by 114.3 mm deep and 2400 mm long, loaded at two locations and reinforced with a three-dimensional continuous carbon fiber fabric, has been reported.[50] The three-dimensional fabric was roughly 41 mm wide by 91 mm high. Longitudinal reinforcing bars were spaced at 20 mm intervals across the fabric width and 30 mm intervals through its depth. Transverse bar elements (shear reinforcement) were longitudinally spaced at 30 mm intervals. Total gross cross sectional area of the 12 longitudinal FRP bars was 127.8 mm^2. Tensile strength and modulus of CFRP were 1.24 GPa and 113 GPa, respectively. Three beams were tested in flexure with a shear span of 990 mm and a 457 mm region of constant moment. Concrete strength for these three samples were 16.2 MPa, 19.4 MPa and 20.3 MPa, respectively. The beams were under-reinforced relative to a balanced design. After initial

cracking and increasing load, many closely spaced small vertical cracks developed. At ultimate load, the longitudinal carbon FRP bars ruptured successively from the lowest layer upward.

Nine slabs simply supported and loaded at two locations, having shear-span to effective depth ratios of approximately three (a/d=3) and reinforced with a variety of molded and pultruded GFRP gratings have been tested.[51] Slabs of two different sizes were fabricated. The first six slabs measured 1.4 m long by 305 mm wide by 102 mm thick and the second group of three slabs measured 1100 mm long by 305 mm wide by 102 mm thick, one of which was reinforced with epoxy-coated steel reinforcing bars. Reinforcement was placed in the tension side with 13 mm of cover. Concrete strength ranged from 18.3 MPa to 28.3 MPa. In addition to load and deflection data, strain was measured on the FRP grating and on the concrete. Following initial cracking, flexural cracks developed in the constant moment region at regular intervals of about 76 mm. With increasing load, diagonal tension shear cracking developed in the shear span. Flexural compression failure occurred in three of the first six slabs, and the remaining slabs failed in shear. The slabs that failed in compression had the lowest concrete strength. In several of the shear failures, the concrete below the reinforcement in the shear-span was completely separated from the slab. In all slabs, the experimental shear force V_{exp} was significantly larger than ($V_c = 2.0 \ (f'c)^{0.5} \ bd$). The effective flexural stiffness EI of the slabs was calculated using deflection data, strain data, and a transformed cracked-section theoretical method. Reasonable agreement between these three methods was achieved, indicating that the effective stiffness of FRP-reinforced concrete slabs can be predicted using theoretical methods with some degree of confidence.

The performance of four full-scale concrete slabs 6100 mm by 1200 mm by 216 mm, doubly reinforced (top and bottom) with 51 mm deep, commercially produced pultruded FRP gratings having longitudinal bar intervals of 76 mm and 51 mm on-center, respectively, and transverse bars located at 152 mm intervals has been reported. The cross-sectional profile of the longitudinal bars had an approximate area of 350 mm². A fifth sample reinforced with 16 mm diameter steel bars with 415 MPa yield strengths located 114.3 mm on center (top and bottom) and having the same dimensions as the four FRP slabs was tested for control purposes. All samples were provided with 25 mm concrete cover, top and bottom, and supported as

continuous beams over two spans of 2400 mm. Two equal loads were placed 1000 mm from the center support and applied over 254 mm by 635 mm by 51 mm thick steel plates. The FRP tensile strength and modulus values (as reported from manufacturers' data) were 414 MPa and 34.5 GPa, respectively. Slabs were loaded as follows: first, under a monotonically increasing load to 11.8 MN, then subjected to 10 loading unloading cycles 0 to 11.8 MN, and finally loaded monotonically to failure. Slab performance was evaluated with respect to ultimate and serviceability limit state criteria. The behavior of all FRP grating-reinforced slabs was similar. Flexural cracks developed early in both the positive and negative moment regions and were in line with the transverse bar locations. All slabs experienced shear failure in the short shear-span between the middle support and the load point. The ratios of failure to service load for FRP reinforced slabs were 4.26, 3.89, 4.17, and 4.16. For the steel reinforced slab, this ratio was 3.34. No evidence of shear cracking was observed prior to failure. At higher loads, nonlinear compressive strain was recorded in all FRP gratings. This was assumed to be the result of localized compression failure in the gratings. The local radius of curvature in the positive moment region generally satisfied a recent AASHTO draft serviceability specification. However, in the negative moment region this criterion was violated. Service load deflections were well below the L/500 limit, where L is the length of the beam.

Five concrete beams reinforced with hybrid reinforcing bars, steel deformed bars, and FRP reinforcing bars have been tested.[52,53] A beam length of 1.2 m and cross-sectional dimensions of 100 mm wide by 150 mm deep were used. Samples were simply supported and loaded at two locations with a shear span of 350 mm and a constant moment length of 100 mm. Each beam was reinforced with four identical reinforcing bars, two in the compression zone and two in the tension zone. In all beams, shear reinforcement consisted of closed stirrups made of smooth steel wire (f_y= 483 MPa; E=195.2 GPa), 4 mm in diameter and spaced at 40 mm. Clear cover at all surfaces was 17 mm. Concrete compressive strength was 43.6 GPa. The only parameter varied in the five specimens was the type of longitudinal reinforcement provided. The five beams were reinforced as follows:

Deformed steel bars f_y = 373 MPa; E=208.9 GPa.
Braided aramid FRP reinforcing bars f_u = 1489 MPa; E=64.9 GPa.

Same as above, but the FRP reinforcing bars were coated with silica sand to improve mechanical bond.

Hybrid reinforcing bars consisting of high-strength steel core f_y = 1,390 MPa; E= 196 GPa and a braided aramid FRP skin f_u = 489 MPa; E=64.9 GPa. Same as above, but the FRP skin was coated with silica sand to improve mechanical bond.

Load-deflection behavior for the different reinforcing bar types were characterized as follows: (1) for steel reinforcing bars, a typical three-stage behavior of an under-reinforced concrete beam consisting of uncracked-section, cracked-section linear elastic to yield, and post-yield of reinforcement; (2) for FRP reinforcing bars, a two-stage behavior reflecting uncracked section and cracked-section linear elastic to failure; and (3) for hybrid reinforcing bars, a three-stage behavior typical of under-reinforced steel beam characterized by uncracked section and linear-elastic response followed by steel core yielding before ultimate failure.

Test results showed that sand-coated reinforcing bars performed better than the corresponding uncoated reinforcing bars. Relative to ultimate flexural capacity, coating the FRP reinforcing bars and hybrid reinforcing bars with sand increased flexural capacity by approximately 25%. Smaller crack widths and higher post-crack flexural rigidity were also reported for the sand-coated reinforcing bars as compared with the corresponding uncoated reinforcing bars. For all beams, it was stated that ultimate strength could be predicted on the basis of the material properties of concrete and reinforcement as is done with conventional reinforced concrete.

The behavior of full-size concrete bridge decks 3700 mm long by 2100 mm wide and 203 mm deep reinforced with sand-coated FRP reinforcing bars has been investigated by Faza and GangaRao (1993). The slabs were supported on steel stringers running transverse to the 3700 mm slab length. Three test sets, each consisting of two tests, were run; the first set was non-composite construction (studs welded to the stringers passed through holes in the concrete deck to eliminate shear transfer) with stringer spacing of 914 mm for one slab and with 1524 mm stringer spacing for the other. The second set developed composite action (the space surrounding the studs in the deck holes was grouted). The third set was composite construction (the decks were cast on the stringers) with stringer spacing of 1800 mm. The decks were designed for one-way bending, two 1800 mm long stirrups were used to create a single

temperature and shrinkage reinforcing bar. A three-point bending setup was used; the center load was either a pad load or a load distributed over the 2134 mm width. In all cases, the load-deflection curve was linear. Measured strains on the FRP longitudinal reinforcement were greater than those in the transverse reinforcement.

2.5.3 Shear strength

Shear testing has been carried out on six simply supported samples[50]. For this test a single concentrated load at center span was applied with shear span-to-depth ratios of 2.13, 2.55, and 3.62. In all cases no shear failure developed. Failure was, instead, due to tensile rupture of the longitudinal FRP bars.

A series of eight FRP-grating/concrete composite slabs, in which the shear span-to-depth ratio and concrete deck thickness were varied in an attempt to force different types of failures, have been tested.[27] Concrete deck thickness ranged from 44 mm to 140 mm. All specimens were simply supported and loaded at two locations with a/d ranging from 3.94 to 9.49. Four of the eight slabs were also reinforced with 6.35 mm vertical studs consisting of either FRP reinforcing bars or steel bolts. Concrete strength ranged from 29.6 MPa to 32.1 MPa. Test results showed that for samples with a/d ratios of 7.7 or greater, failure occurred by crushing of the concrete. For these samples, the calculated flexural capacity was very close to the test results. For a/d ratios of five or less, failure occurred as a result of diagonal tension cracking. The vertical studs did not prevent shear failure.

2.5.4 Bond and development of reinforcement

The evaluation of bond characteristics of FRP reinforcements is important in the design of FRP reinforced concrete members. Due to variations in FRP reinforcing products, bond characteristics are quite variable. Bond characteristics are influenced by factors such as: size and type of reinforcement (wires or strands), surface conditions (smooth, deformed, sand-coated), Poisson's ratio, concrete strength, concrete confinement (e.g., helix or stirrups), type of loading (e.g., static, cyclic, impact), time-dependent effects, amount of concrete cover,

surface preparations (braided, deformed, smooth), and type and volume of fiber and matrix. Bond characteristics of GFRP bars have been investigated by testing 20 concrete specimens.[28] Different configurations of FRP reinforcement size, type (ribbed, sand-coated) and embedment lengths were tested. The specimens were tested as cantilever beams to simulate the beam portion adjacent to a diagonal crack. Twelve pull-out cylindrical specimens were tested. The following design equation was suggested for development length of GFRP:

$$\ell_d = k_1 \cdot f_u \cdot A_b / (f'_c)^{0.5}$$

where:

ℓ_d = development length (in); A_b = reinforcing bar cross sectional area (in²); f_u = reinforcing bar tensile strength (psi); f'_C = concrete compressive strength (psi); and k_i=1/16.

More than 70 pull-out tests to examine the bond strength of GFRP reinforcing bars (E-glass fiber), Kevlar 49 reinforcing bars (AFRP) and steel bars have been conducted.[56] Three different diameters of GFRP reinforcing bars, namely 6.4 mm, 9.5 mm and 12.7 mm and one diameter of FRP 9.5 mm were tested. Results indicated that AFRP and GFRP reinforcing bars exhibited similar behavior at a performance level below steel reinforcing bars. Two equations were proposed for calculating a safe development length (inches) for E-glass and Kevlar 49 FRP bars. They are K_1 = 1/20 and K_i= 1/18, respectively as defined in the above equation. The development length of GFRP reinforcing bars (E-glass fibers and polyester resin, with a sand-coated surface) has been evaluated.[57] Pull-out tests were undertaken using normal-strength concrete, high-strength concrete and grout. Three different rod diameters were used and the anchor length was varied from five times to ten times the rod diameter. A development length of $20d_b$ was recommended. The bond strength of GFRP bars (E-glass fibers and vinyl ester resin) by testing 30 beams having varying bar diameters and embedment lengths. All beams were 3000 mm long and 203 mm by 457 mm in cross-section. The study concluded that if shear reinforcement was provided for the entire length of the specimen, development lengths of 203 mm and 440 mm would be required to develop ultimate tensile strength for 16 and 23 mm

diameter GFRP bars, respectively. However, all specimens reinforced with 25 mm diameter bars failed in bond. The study identified the occurrence of premature bond failure under sustained load. [58]

A study on bond of GFRP reinforcing bars was conducted on 102 straight and 90-degree hook specimens[59] New limits for allowable slip were introduced as 0.064 mm at the free end, or 0.38 mm at the loaded end. According to this study, the basic development length ℓ_{db} of straight GFRP reinforcing bars should be computed knowing the ultimate strength of the reinforcement and $K_1 = 21.3$ given in the above equation. To account for the influence of concrete cover, a factor of 1.0 can be used with concrete cover of not less than two times the bar diameter. A factor of 1.5 can be used with cover of one bar diameter or less. The development length ℓ_d, computed as the product of the basic development length ℓ_{db} (inches) and the confinement factors (1.0 or 1.5), should not be less than:

$$\ell_{db} = 0.00035 d_b f_u$$

where d_b is the bar diameter (inches) and f_u in the ultimate strength (psi). The bond strength developed for top reinforcing bars was found to be less than that of bottom bars. Therefore, a factor of 1.25 can be used for top reinforcing bars. Moreover, the development length ℓ_d, computed as the product of the basic development length ℓ_{db} and the applicable top bar factor should not be less than 381 mm.

For hooked GFRP reinforcing bars with tensile strength equal to 75,000 psi, the basic development length, ℓ_{hb} (inches) should be computed as follows in terms of concrete compressive strength (f'_c, psi):

$$\ell_{hb} = 1820\, d_b / (f'_c)^{0.5}$$

For reinforcing bars with tensile strength other than 75,000 psi, a modification factor $f_u /75,000$ should be used. When side cover and cover on bar extension beyond hook are not less than 64

mm and 51 mm, respectively, a modification factor 0.7 should be used. Moreover, to prevent direct pull-out failure in cases where the hooked reinforcing bar may be located very near the critical section, the development length ℓ_{hb} computed as the product of the basic development length ℓ_{hb} and the applicable modification factors should be no less than eight times the bar diameter or 152 mm (6 inches).

Several weaknesses in standard pullout tests (simply supported beams or pullout specimens) have been identified because they do not sufficiently account for all types of mechanical behavior. Many attempts have been made to find a better standard test method. Researchers have developed a new technique that combines two test methods that individually account for these mechanisms.[60,61] Beams were cast with the cantilever section similar to the Ferguson and Thompson test [62], but they also included concrete outcroppings extending from the side of the beam (see Figure 5).[63] By loading beams on T sections, compressive effects of the load do not confine the reinforcement and therefore do not affect bond characteristics of the reinforcement. The cantilever section allows for investigation of FRP bars subjected to negative moments and can be adjusted by moving the reaction point, thus giving great flexibility in testing scenarios. FRP reinforced concrete cantilever beams have been successfully used in more than 100 full-scale tests. The embedment length. ℓ_d (in) for 7.5 mm and 12.5 mm diameters was derived to be the following:

$$L_d = (0.59 \, f_u \, A_b) / [c_b^2 \cdot (f_c')]^{0.5}$$

Where:

f_u = ultimate tensile strength of the reinforcement (psi)

A_b = area of the rod (in^2)

c_b = circumference of the rod

f_c' = compressive strength of concrete (psi)

The above equation is based upon zero end slip criteria. If 7.5 mm slip is allowed at the end of the embedment, the above equation becomes:

$$L_d = (0.42\, f_u\, A_b) / [c_b^2 \cdot (f'_c)]^{0.5}$$

6" 6" End view

Dogbones

Stirrups

6" 6"

8" 96" 8" 36"

148"

Plan view

Bond breaker FC rod

12"

Support Steel rebar Stirrups

Support

Elevation view
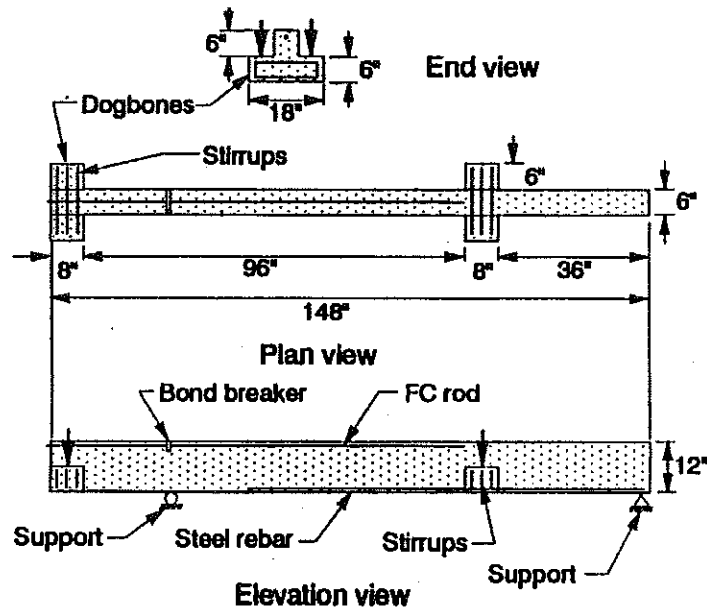
Figure 5. The Bond-Beam Test.[36]

2.5.5 Serviceability

Serviceability of FRP reinforced flexural members is described in terms of deflection and crack width limitations.

2.5.6 Deflection Considerations

Deflections of flat slabs reinforced with FRP have been estimated by the finite element (FE) method.[60] FE analyses closely predicted the deflections of both steel and FRP reinforced one-way slabs. The study found that a slab reinforced with a typical GFRP, having a tensile modulus of 40 GPa, will deflect three to six times more than a steel-reinforced slab. Using a typical CFRP with a higher modulus of 80 GPa, the deflection could be reduced by 50%. If drop panels are added, the deflections become comparable to those of steel-reinforced slabs.

The deflection of FRP reinforced beams at ultimate load has been determined to be approximately three times greater than that of the corresponding steel-reinforced beams.[64] The theoretical deflection predictions have been found to underestimated test results for loads above 50% of ultimate; deflection values were fairly well predicted at load levels up to approximately 30% of ultimate.[65] The study suggested a procedure in which values of curvature calculated at different sections of the beam should be used to obtain a better estimate of deflection values.

Reference 23 predicted deflections of FRP-reinforced beams to be underestimated using the effective moment of inertia, I_e, as prescribed by ACI 318-89. The authors introduced a new method of calculating the effective moment of inertia of concrete beams reinforced with FRP reinforcement. The new expression is based on the assumption that a concrete section between the point loads is assumed to be fully cracked, while the end sections are assumed to be partially cracked. Therefore, an expression for I_{cr} is used in the middle third section, and the ACI 318-89 I_e is used in the end sections. Using the moment-area approach to calculate maximum deflection at the center of the beam resulted in an expression for a modified moment of inertia as shown (independent of the unit system):

$$I_m = (23\ I_{cr}\ I_e)/(8\ I_{cr} + 15\ I_e)$$

2.5.7 Crack Width and Pattern

It has been found that beams reinforced with steel had fewer cracks than the corresponding FRP reinforced beams.[64] The large number of well-distributed cracks in the FRP reinforced beams indicated good mechanical bond was developing between the FRP bar and surrounding concrete. It has been determined that concrete beams reinforced with spiral deformed FRP reinforcing bars using normal-strength concrete, 27.6 MPa, exhibited crack formation which was sudden and propagated toward the compression zone soon after the concrete stress reached its tensile strength. Crack spacing was very close to the stirrup spacing, and cracks formed at or near the stirrups, which were spaced at intervals of 150 mm. This sudden propagation of cracks and wider crack widths decreased when higher strength concrete 50 to 70 MPa and sand-coated FRP reinforcing bars were employed. Another important observation in specimens tested with sand coated reinforcing bar and higher strength concrete is the formation of narrow cracks with

smaller crack spacing. The crack patterns of beams reinforced with sand-coated reinforcing bars resembled the crack patterns expected in beams reinforced with steel reinforcing bars, with shorter spacing at ultimate levels. Based on the assumption that maximum crack width can be approximated by an average strain in FRP reinforcing bar multiplied by expected crack spacing, this resulted in an expression for maximum crack spacing governed by the following parameters: (1) bond strength of FRP reinforcing bar; (2) splitting tensile strength of concrete; (3) area of concrete cross section in tension; (4) number of reinforcing bars in tension; (5) size of reinforcing bar; and (6) effective yield strength or working stress of FRP reinforcing bar.

The resulting expression for maximum crack width is:

$$W_{max} = [(f_r/E_f).2\,f_t^{'}\,A] / (\mu_m\,\Pi\,D)$$

where:

f_r = maximum stress (ksi) in FRP reinforcement at service load level with 0.5 fy to be used if no computations are available; A = the effective tension area of concrete surrounding the principal reinforcement divided by the number of reinforcing bars, defined as having the same centroid as the reinforcement (in^2); μ_m = maximum bond stress; and D = diameter of reinforcement.

The flexural behavior of concrete beams reinforced with GFRP bars have been compared to identical conventionally reinforced ones.[65] Two series of 3300 mm long concrete beams were loaded with two concentrated loads applied at the third span points. The section of the beams of series 1 was 200 mm wide 300 mm high and 200 mm by 550 mm for series 2. Each series consisted of two beams reinforced with two FRP bars 19.1 mm diameter and two others reinforced with two equal diameter steel bars. Tensile strength and modulus of elasticity of the FRP reinforcement were 700 MPa and 42 GPa, respectively. Compressive strength and modulus of concrete were 42MPa and 33 GPa. At 25% M_u the crack pattern and spacing in FRP reinforced beams were similar to those in conventionally reinforced beams. At service (50% M_u) and ultimate (90% M_u) loads, there were more and wider cracks than in the steel-reinforced

beams. At service and ultimate loads FRP-reinforced beams experienced maximum deflection three times higher than for steel-reinforced beams. Predicted deflections using the Branson expression for effective moment of inertia, I_e as prescribed in ACI 318-89, were underestimated. This is attributed to the width, depth, and spacing of the cracks. Based on experimental data a modified expression for the effective moment of inertia of a simply supported beam reinforced with FRP bars is (independent of the unit system):

$$I_{ef} = \alpha I_{cr} + (I_e / \beta - \alpha I_{cr}) \cdot (M_{cr} / M_u)^3$$

in which α and β are reduction factors equal to 0.84 and 7.0, respectively. These factors account for the reduced area of the compression section when the applied moment reaches $M_{cr.}$

2.6   DESIGN PROCEDURES

Based on a synthesis of the state-of-the-art in the field, the American Concrete Institute Committee 440 is developing "Provisional Design Guidelines for Concrete Reinforced with Fiber Reinforced Polymer (FRP)." These guidelines provide a reasonable basis to revise current bridge deck design procedures to suit FRP reinforced decks. This section presents a summary of the relevant parts of the most recent version of Provisional Design Guidelines for concrete Reinforced with Fiber Reinforced Polymer (FRP).

2.6.1   Flexural Design

Flexural design of structural members with FRP reinforcement shall be based on compression failure. Compression failure is preferable because of: (1) more gradual member failure as compared to FRP rebar rupture in a tension failure; (2) reduction in service load deflections and crack widths due to higher stiffness and lower FRP rebar stress (because of larger area of FRP reinforcement); and (3) higher moment of resistance (by involving higher forces in the internal force-equilibrium as compared to a tension failure).

51

The design (nominal) strength in flexure of a rectangular cross section (without compression reinforcement) may be expressed for beams as (independent of the unit system):

$$\phi M_n = \phi[0.85 \; f_c' \; a.b.\{d-a/2\}]$$

The strength reduction factor ϕ for flexure shall be taken as 0.7 because of compression failure (noting that the ϕ value for shear is also taken as 0.7 due to the nature of FRP rebars and due to the lack of research at this time).

Brittle-brittle strain condition exists at a rectangular cross section when the maximum strain at the extreme compression fiber just reaches 0.003 simultaneously with the first design nominal strain f_f/E_f in the tension reinforcement (f_f=nominal strength of FRP, and E_f=elastic modulus of FRP). The reinforcement ratio corresponding to brittle-brittle failure under flexure (ρ_{b-b}) depends on the shape of the cross section which is considered to be rectangular, failure strain of FRP rebar (ε_f) and the location of the reinforcement. For a compression failure, minimum reinforcement must be at least 1.33 times ρ_{b-b} (independent of the unit system):

$$\rho_{f, min} = 1.33 \; \rho_{b-b}$$

Where, ρ_{b-b} is the reinforcement ratio producing balanced conditions wherein strain in FRP reinforcement and concrete shall be assumed directly proportional to the distance from the neutral axis and maximum usable strain at extreme concrete compression fiber shall be assumed equal to 0.003:

$$\rho_{b-b} = [(0.85\beta_1 \; f'_c)/f_f].[0.003E_f/(f_f+0.003E_f)]$$

The minimum reinforcement ratio ($\rho_{f, min}$) is specified to prevent tension failure. The 1.33 safety factor presented above is approximately $1/(1-3\sigma)$, where σ is the standard deviation for ultimate moment capacity of concrete beams reinforced with FRP bars in compression failure (measured at 8.3% in the case of glass FRP reinforcement).

Sustained tensile stresses in FRP rebars shall not exceed 25% of f_f (their nominal strength, that is the average strength minus three times the standard deviation of measured strength values).

Beams and slabs shall be designed with a c/d ratio between 0.15 to 0.3 for GFRP reinforcement and between 0.25 to 0.5 for CFRP reinforcement to ensure compression failure and satisfy deformability criteria. In this expression, c is the distance from extreme concrete compression fiber to neutral axis, and d is the distance from extreme concrete compression fiber to centroid of tension reinforcement. Deformability is defined here as a ratio of energy absorption (area under moment-curvature curve) at ultimate to energy with respect to a limiting curvature based on serviceability criteria of deflection and crack width. For obtaining a deformability factor of 8 or higher, the maximum curvature limit at service load shall satisfy the following and should not exceed 0.006/d:

1. The serviceability deflection limit of l/180
2. The crack width limit of 0.4 mm.

Maximum curvature limit exceeding 0.006/d may not result in service level deflections within l/180 for beams with depths between l/d ratio of 8 to 13. Curvature at the load corresponding to limiting deflection or crack width shall be determined by calculating stress in FRP reinforcement or concrete at the extreme compression fiber. The strain in respective materials can then be calculated. For example, ε_f = stress / E_f. Curvature can be calculated as (ε_f / (d-c) or as (ε_f+ε_c)/d. Beams and slabs designed with a c/d ratio between 0.15 and 0.3 result in compression failure and satisfy deformability criteria. c/d ratios higher than 0.3 may not result in anticipated moment increase in compression failure modes.

In slabs, primary flexural reinforcement shall be spaced not further apart than two times the slab thickness, nor 305 mm. Maximum bar spacing criteria is based on the necessity to control deflection and crack width. Minimum FRP bar spacing criteria are suggested to be the same as those in ACI 318. The minimum limits were originally established to permit concrete

to flow readily into spaces between bars and between bars and forms without honeycomb, and to ensure against concentration of bars on a line that may cause shear or shrinkage cracking.

Use of compression reinforcement enclosed with closed stirrups is permitted in conjunction with additional tension reinforcement to increase the strength of flexural members. However, contribution of FRP compression reinforcement for further increase in the moment capacity may be limited, due to lower failure strains in the compression zone (ε_c=0.003 and ε_{fc}≈0.002 in compression zone at ultimate) and lower strength and stiffness values of FRP bars in compression as compared to tension. The stirrups enclosing compression bars shall be at least 10 mm diameter in size for longitudinal bars 25 mm or smaller diameter. Such stirrups shall be provided throughout the distance where compression reinforcement is used. Closed stirrups shall be formed in one piece by overlapping standard stirrup end hooks around a longitudinal bar, or formed in one or two pieces lap spliced with a lap length 1.3 l_d.

Development l_d is computed as the product of the basic development length, l_{db}, and a series of factors accounting for different conditions. Basic development length for 25 mm diameter (#8) and smaller bars l_{db} (inches) shall be:

$$l_{db} = K_1 \cdot (A_f \cdot f_f)/(f'_c)^{0.5}$$

where, A_f =cross sectional area of rebar, in^2

K_1=factor of rebar type since it is surface dependent, to be provided by manufacturer and traditionally ranges from 0.004 to 0.006.

All factors for the calculation of l_d are not yet available in the draft of code. Modification factors of 1.3 and 1.5 have been proposed for top cast bars and for cases with concrete cover of one bar diameter or less, respectively.

Flexural tension reinforcement shall be well distributed within the tension zone. This distribution of tension steel together with the proportioning of cross sections shall limit the maximum crack width (w_{max}), as calculated below, to specified levels.

$$w_{max} = 0.000076 \, K_f \, \beta \, f_{f,s} \, (d_c.A)^{1/3}$$

where, $K_f = 0.25 \, (3E_s/E_f + 1)$

A = effective tension area of concrete surrounding the flexural tension reinforcement and having the same centroid as that reinforcement, divided by the number of bars. When the flexural reinforcmeent consists of different bar sizes the number of bars shall be computed as the total area of reinforcement divided by the area of the largest bar.

d_c = thickness of concrete cover measured from extreme concrete fiber to center of bar located closest thereto, in.

$f_{f,s}$ = calculated stress at service load in FRP reinforcement, ksi

β = ratio of distances to the neutral axis from the extreme tension fiber and from the centroid of main tension reinforcement.

E_f = modulus of elasticity of FRP reinforcement.

E_s = modulus of elasticity of steel (for converting the equation developed originally for steel reinforced concrete to FRP reinforced concrete)

The following minimum concrete cover shall be provided for reinforcement:

Concrete cast against and permanently exposed to earth:	76 mm
Concrete exposed to earth or weather	
No. 6 through No. 12 bars:	51 mm
No. 5 and smaller:	38 mm
Concrete not exposed to weather or in contact with ground	38 mm

The above concrete cover requirements have been based upon crack width, cover delamination and fire resistance considerations. Appropriate fire-retardant resins shall be used

in the manufacturing process to provide acceptable degree of fire resistance to the structure based upon its location and importance. The condition of the concrete surface exposed to the weather refers to direct exposure to moisture changes and not just to temperature changes. Slabs are not usually considered directly "exposed" unless subject to alternate wetting and drying, including that due to condensation conditions or direct leakage from exposed top surfaces, run off, or similar effects.

Reinforced concrete members subjected to flexure shall be designed to have adequate stiffness to limit deflections that adversely affect the serviceability of a structure. Calculation of deflections shall be based on elastic analyses satisfying equilibrium of stress and compatibility of strains in concrete and reinforcement, considering effects of creep and shrinkage of concrete and reinforcement, and also effects of cracking. When calculating the strain or stress in a cracked section the concrete in tension shall be ignored. However, computation of deflections of cracked members may allow for the contribution of concrete in tension. Thus, at a cracked section, the mean curvature ψ_m can be used in computing deflections of members. The value of ψ_m shall be intermediate between values computed using an uncracked section and a value computed using a fully cracked section (i.e., concrete in tension ignored):

$$\psi_m = (1-\zeta)\psi_1 + \zeta\,\psi_2$$

where ζ is an interpolation coefficient given by (independent of the unit system):

$$\zeta = 1 - \beta_1\,\beta_2\,(f_t/\sigma_1)^2$$

where, β_1 = bond quality coefficient; should be taken 1.0 for high bond bars, and 0.3 where bond quality is known to be low such as for smooth FRP bars.

β_2 = loading case coefficient; should be taken 1.0 for first loading, and 0.5 for most practical applications.

$f_t = f_r$ = flexural strength of concrete when no axial force is applied ($f_r = 7.5\,(f'_c)^{0.5}$ for normal-weight concrete).

Unless stiffness values are obtained by a more comprehensive analysis, immediate deflections shall be computed with the modulus of elasticity E_c for concrete and with the effective moment of inertia I_e of a simply supported FRP reinforced concrete beam expressed as follows (independent of the unit system):

$$I_e = I_{cr} + (\beta I_g - I_{cr}).(M_{cr} / M_a)^3$$

where,

$$\beta = 0.5 (E_f / E_s + 1)$$

E_s = Steel Modulus of Elasticity

2.6.2 Shear Strength without Shear Reinforcement

The shear strength provided by concrete in members reinforced with FRP (V_{cf}) can be calculated as:

$$V_{cf} = V_c (E_f / E_s)$$

where E_f is the elastic modulus of FRP (flexural reinforcement), and E_s is the elastic modulus of conventional steel reinforcement. V_c in the above equation can be calculated per ACI 318. The factor E_f/E_s in used in the above equation to account for the fact that the equation for V_c in ACI 318 significantly overestimates the shear capacity of members reinforced by GFRP bars. It is our suggestion to follow the recommendation of ACI 318 and use only half of V_{cf} for members without shear reinforcement.

2.6.3 Durability and Practical Considerations

FRP reinforcement, comprising reinforcing fibers and polymer matrix, shall exhibit less than 15% loss in strength and stiffness when exposed to accelerated aging conditions and sustained strain levels simulating actual service conditions in concrete.

FRP bars should be protected from moisture, UV exposure and alkaline environment during storage. Design properties of bars stored for more than twelve months shall be based on additional tests.

At the time concrete is placed, reinforcement shall be free from mud, oil, or other coatings that decrease bond. Sand coated bars and bars with deformed surfaces shall be permitted.

Reinforcement shall be accurately placed and supported, preferably using plastic or plastic coated metallic chairs before concrete is placed.

Tolerance for depth d, and minimum concrete cover in flexural members shall be as follows:

	Tolerance on d	Tolerance on minimum cover
d < 200 mm	±10 mm	-10 mm
d > 200 mm	±12 mm	-12 mm

except that tolerance for the clear distance to formed soffits shall be minus 6 mm and tolerance for cover shall not exceed minus 1/3 the minimum cover required in the design drawings or specifications. Tolerance for longitudinal location of ends of reinforcement at discontinuous ends of members shall be ±12 mm.

3.0   EXPERIMENTAL EVALUATION AND SELECTION OF FRP BARS

3.1   INITIAL ASSESSMENT OF FRP BAR AVAILABILITY

Glass fiber composite bars, due to their relatively low cost, present attractive choices for the reinforcement of concrete bridge decks when compared with carbon and aramid fiber composite bars.   Given the susceptibility of glass fibers to alkali attack, selection of resin would be critical for ensuring the durability of composite rebars in concrete. The following resins have been subject of major studies for infrastructure applications, and promise to yield composites with good durability characteristics under sustained load and freeze-thaw exposures: (1) low viscosity, urethane modified vinyl ester; and (2) medium reactivity isopthalic unsaturated polyester.

Our focus in this project was on the selection of commercially available glass, carbon and aramid fiber composite rebars. We contacted the following manufacturers for this purpose.

- Mitsubishi Ksaei Corp (Japan - CFRP)
- Tokyo Rope Mfg. Co., Ltd. (Japan - CFRP)
- DFI, Inc. (USA - CFRP)
- Teijin Limited (Japan - AFRP)
- Asahi Glass Company (Japan - GFRP)
- IGI International Grating, Inc. (Houston, TX - GFRP)
- Tillco Company (Marshall, AR - GFRP)
- Poly Structures Co. (Little Rock, AR - GFRP)
- Creative Pultrusion, Inc. (Alum Ban, PA - GFRP)
- Corrosion Proof Composites, LLC (Tequesta, FL - GFRP)
- Marshall Industries Composites, Inc. (Lima, OH - GFRP)

3.2 EXPERIMENTAL INVESTIGATIONS

3.2.1 Tensile Testing of Composites

The following FRP reinforcing bars were acquired from manufacturers:

- Glass Fiber Composite from Corrosion Proof Composite, LLC

- Glass Fiber Composite from Tillco Co. (previously known as Marshall)

- Technora Aramid Fiber Composite from Teijin Limited

- Carbon Fiber Composite from Tokyo Rope Mfg. Co., Ltd (these bars were never shipped to us in spite of repeated requests).

We sought to establish a reliable and universally applicable tension test set-up for composite rebars. Our earlier set-up, which worked successfully with certain GFRP bars, failed in application to the two selected GFRP bars. The alternative set-ups we tried, and our experience with each set-up, are discussed below.

- FRP bars anchored in hydraulic grips: Bars crushed under grip pressure.

- FRP bar ends embedded in AD-932 epoxy resin (from Adtech Corp.) with square cross section, which were placed in grips (Figure 6). Failure in bars with total length of 375 mm was either by bar pull-out from the epoxy resin, or rupture of the bar at the edge of the epoxy.

- FRP bar ends embedded in same epoxy resin with circular cross section which were placed in grips (Figure 7). Most bars of 375 mm total length pulled out of the epoxy resin, and occasionally the epoxy failed.

- FRP bar ends surrounded by a thin 100 mm long soft metallic pipe (threaded inside), with the gap between pipe and FRP filled with Sikadur 33 epoxy resin from Sika Corp. or AD-932 epoxy resin from Adtech Corp. (Figure 8), and the pipe anchored in a hydraulic grip (Figure 9). Success rate was only 20% with GFRP bar pull-out or failure of epoxy occurring in most cases.

- FRP bar ends roughened with sandpaper and surrounded by a thin 125 mm long soft metallic pipe (threaded inside), with the gap between pipe and FRP bar filled with aluminum filled epoxy resins (EC-428 or EA-618) from Adtech Corp. (these epoxies offer low viscosity and longer work life, and we also allowed for a longer curing of 14 days), with new 100 mm jaws of circular groove shape for hydraulic grips (previous 75 mm jaws had grooves of square cross-section). Some composite bars pulled out of the pipe

- Same as above but using longer (750 mm) FRP bars which allow for 150 mm long soft metallic pipes placed at the ends, using EC-428 filled epoxy resins. Tests were generally successful

The tensile strength and elastic modulus test results of the three composite bars under investigation are compared in Table 6 with the corresponding manufacturers' values. The test results presented here are average values for about 10 measurements. The experimental results are generally close to, but somewhat below, manufacturers' values.
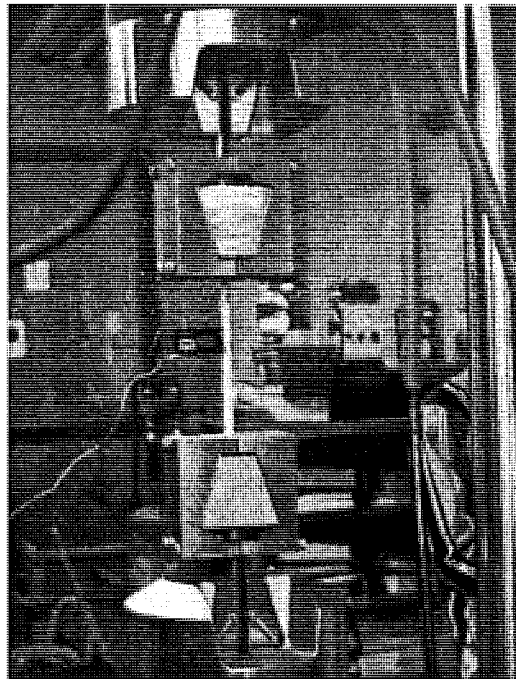
Figure 6. Square Grip Fixture
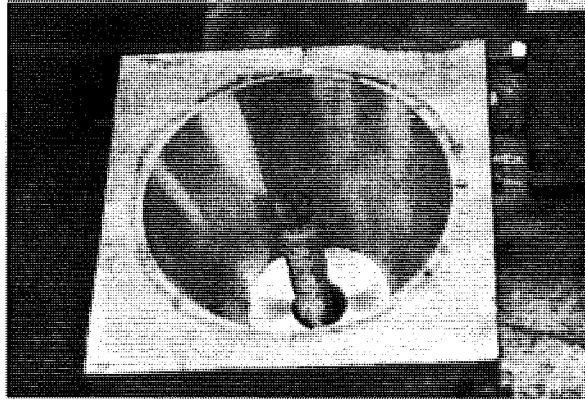
Figure 7. Circular Grip Fixture
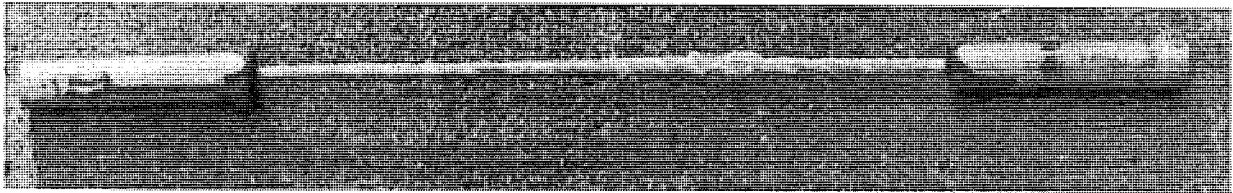
Figure 8. FRP Rebar Grip with Steel Pipe
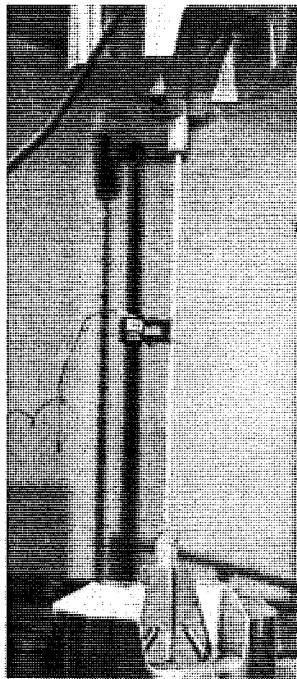
Figure 9. Pipe Anchorage in a Hydraulic Grip.

Table 6. Experimental Results.

PROPERTY	GFRC-Tillco			GFRC-COR PRF			AFRC-TEIJIN		
	Test		Manuf.	Test		Manuf.	Test		Manuf.
	mean	stdev		mean	stdev		mean	stdev	
Tens. Strength, MPa	893	179.8	966	811	35.14	900	1533	83.395	1800
Elastic Mod., GPa	49.2	9.76	53.8	46.1	5.413	48.3	55.5	1.663	54

3.2.2 Coefficients of Thermal Expansion

Figures 10 through 13 present the thermal expansion test results for two glass (Tillco and Corrosion Proof), one aramid (Teijin) and one carbon (Mitsubishi) fiber composite with temperature increasing from -40°C to +40°C. The two glass fiber composites exhibit a coefficient of longitudinal thermal expansion of 8.25 and 8.56 x 10^{-6}/°C, which are comparable to the coefficient of thermal expansion of normal concrete (about 8 x 10^{-6}/°C). Technora aramid fiber composite exhibits a variable coefficient of thermal expansion, which could even be negative, and can be as large as 0.41 x 10^{-6}/°C at higher temperatures. The same is true for carbon fiber composite, with coefficient of longitudinal thermal expansion reaching 1.42 x 10^{-6}/°C at higher temperatures. Thermal expansion mismatch between concrete and carbon or Technora aramid fiber composite bars may thus be a concern. Tests presented later involving temperature cycling of concrete reinforced with different FRP bars were used to examine the practical significance of this thermal expansion mismatch.
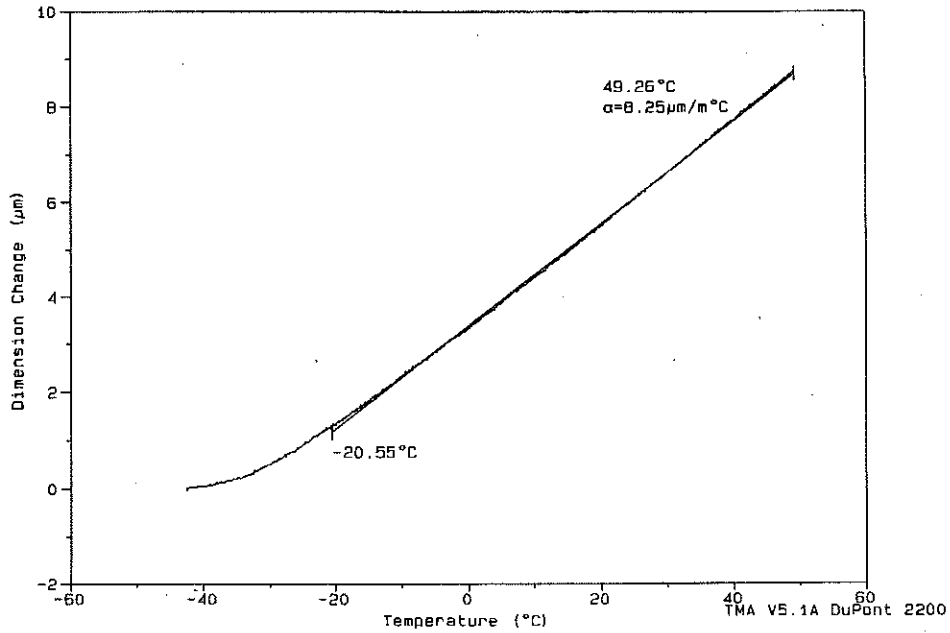
Figure 10. Thermal Expansion of 'Corrosion Proof' Glass Fiber Composite.
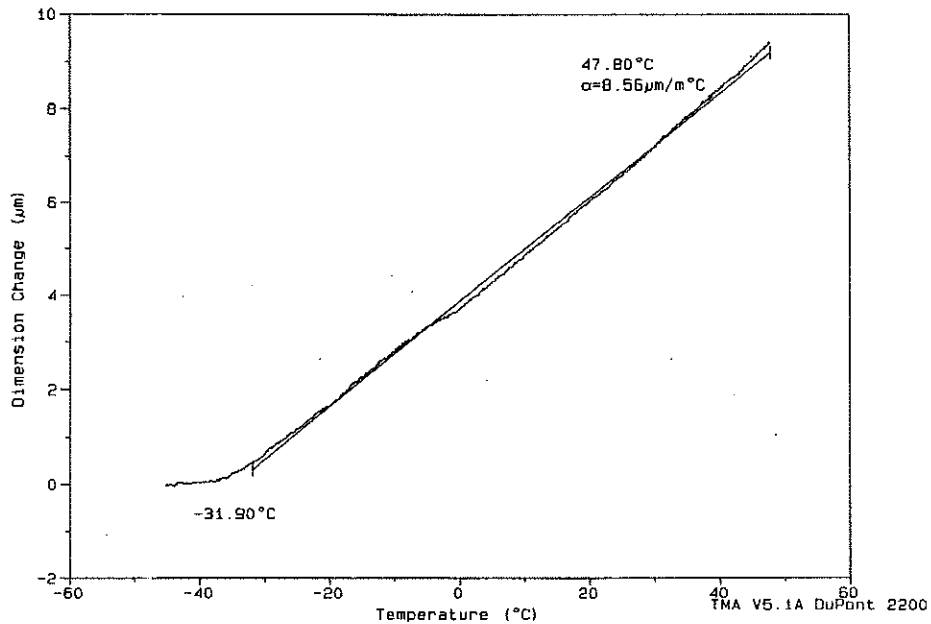
Figure 11. Thermal Expansion of 'Tillco' Glass Fiber Composite.

Sample: KEVLAR REINFORCED BAR   TMA   File: C:TMA-KEVLAR.200
Size: 13.1000 mm   Operator: MIKE RICH WITH PHIL C.
Method: -40 TO 40°C. 2°C/MIN   Run Date: 26-Aug-97 16:11
Comment: -40 TO 40 C. 2°C/MIN RAMP RATE
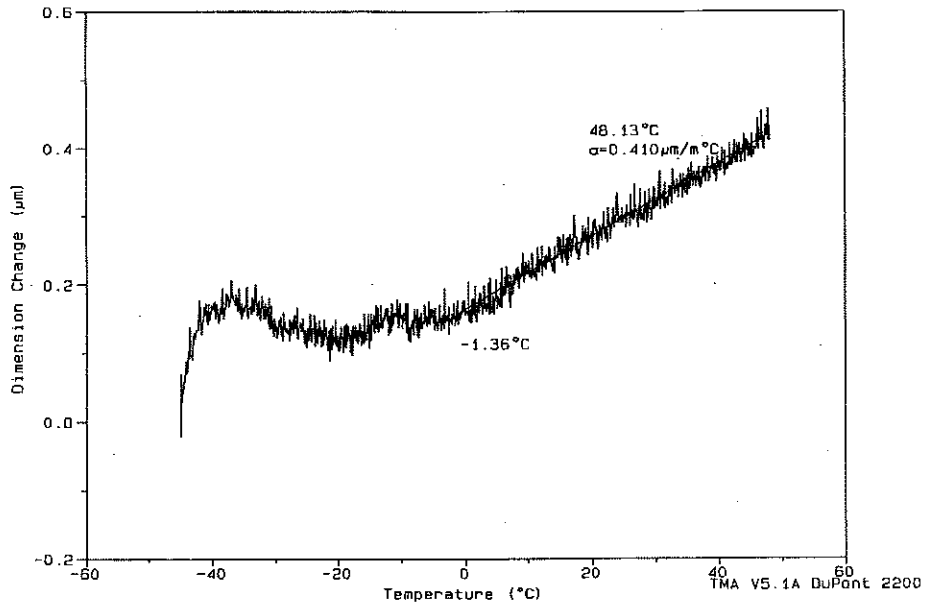
Figure 12. Thermal Expansion of Technora Aramid Fiber Composite.

Sample: CARBON FIBER REINFORMCEMNT BAR   TMA   File: C:TMA-CARBON.100
Size: 12.9700 mm   Operator: MIKE RICH WITH PHIL C.
Method: -40 TO 40°C. 2°C/MIN   Run Date: 21-Aug-97 16:41
Comment: -40 TO 40 C. 2°C/MIN RAMP RATE
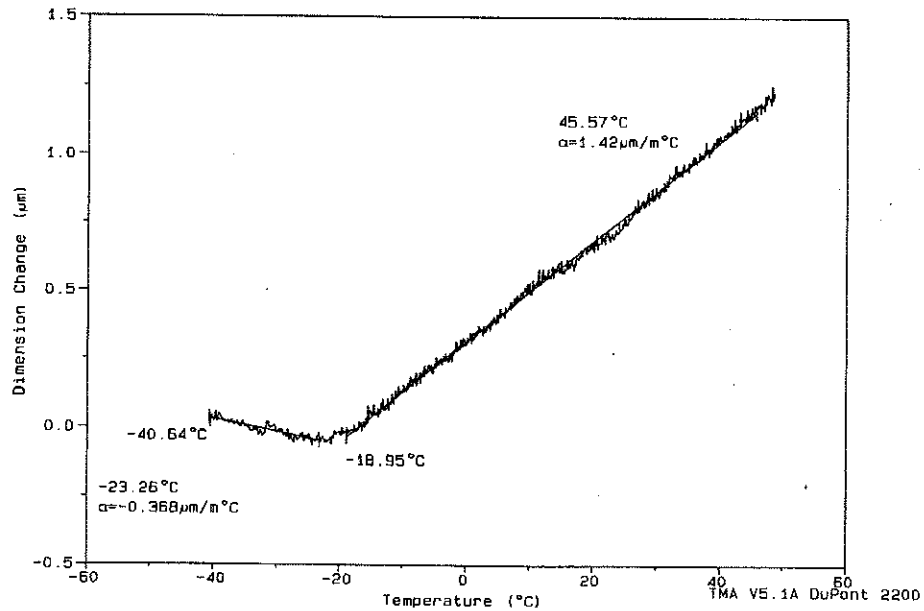
Figure 13. Thermal Expansion of Carbon Fiber Composite.

3.2.3   Shear Strength

Composite bars generally provide high tensile performance but lack shear resistance. The possibility of punching shear in slabs, however, leads to the application of shear forces on composite bars. In order to assess the shear resistance of composite bars relative to steel, the selected composite bars, as well as a low-strength smooth steel rod, were subjected to pure shear tests (Figure 14). Table 7 presents the shear and tensile strengths as well as the ratio of shear-to-tensile strength for various bars. Composites, as compared to steel, are observed to provide relatively low shear-to-tensile strength ratios. This implies that higher ratios of composite bars would be required in conditions such as punching shear failure when bars act in shear. Further tests results on dowel action of composite rebars in concrete will be presented later.
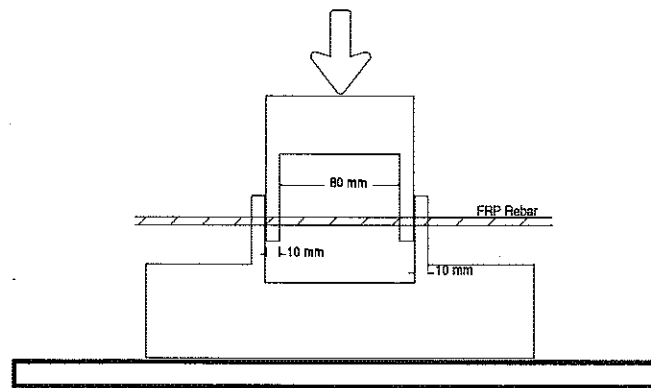
Figure 14. Shear Strength Test Set-Up.

Table 7. Shear Strength Test Results.

Bar	Shear Strength, MPa	Tensile Strength, MPa	Shear/Tensile Strength
GFRP-Tilco	464	893	0.52
GFRP-Corr Prf	487	811	0.60
AFRP	605	1533	0.39
Steel (4.7 mm diameter)	1568	237	6.6

3.2.4   MOISTURE EFFECTS ON TENSILE BEHAVIOR

For each FRP system (Tillco and Corrosion Proof glass FRP, and Technora aramid FRP), three specimens were tested after 30 days of exposure to 50% RH at 22°C, and three other specimens after 30 days of immersion in water at 22°C.

Figures 15a, 15b and 15c compare the tensile strength, elastic modulus and strain at peak, respectively, of wet vs. dry specimens of the three FRP systems. Table 8 presents the individual test results. The adverse effects of wetting on tensile performance are less than 10% for Technora aramid FRP and practically non-existent for glass FRP's. Tests where saturated specimens were first air-dried and then tested indicated that the effects of wetting on Technora aramid FRP are reversible upon drying.
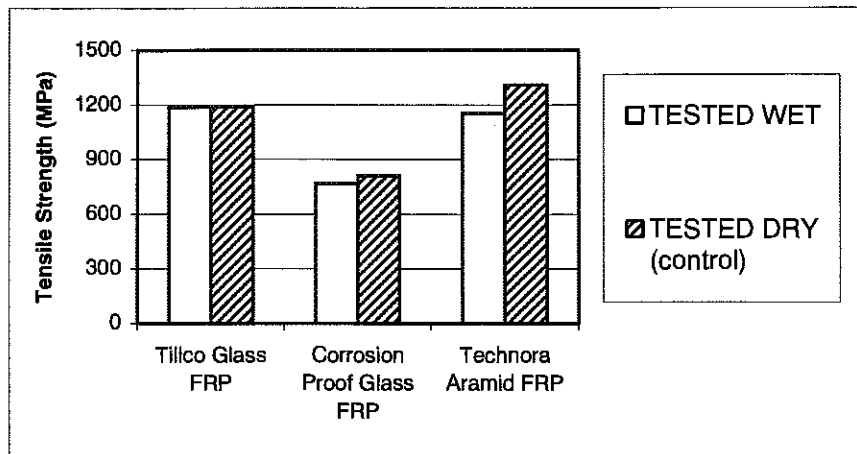
(a) Tensile Strength
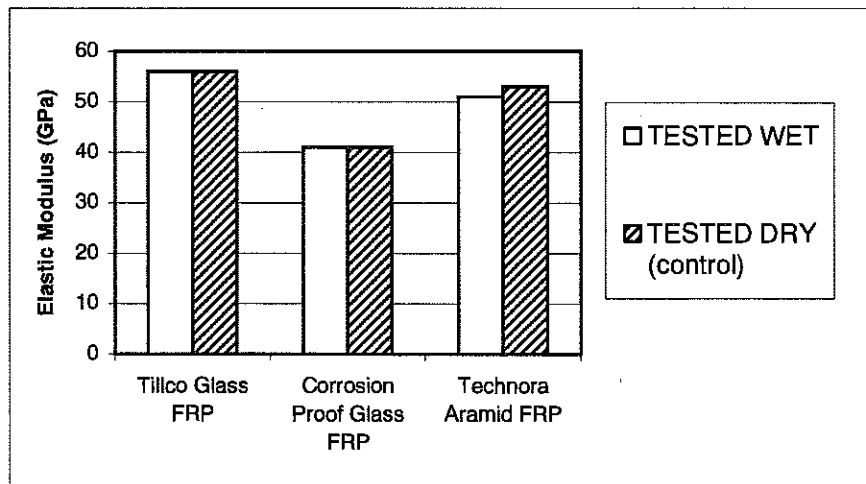
(b) Elastic Modulus
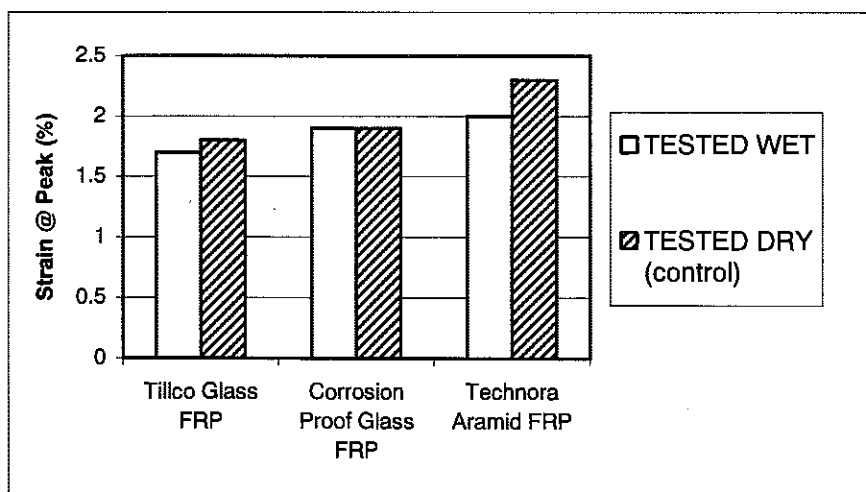
(c) Tensile Strength Strain at Peak

Figure 15. Effects of Wetting on Tensile Behavior of Different FRP System

Table 8. Wet Vs. Dry Tension Test Results

Wet 1 month/tested dry	50% R.H.	50% R.H.	50% R.H.
	Tensile Strength, Mpa	Elastic Modulus, GPa	Strain at Peak, %
Tillco, # 2 rebar			
1	1222.8	55.90	1.8
2	1205.4	55	1.8
3	1138.8	58.60	1.7
Average	1189.000	56.333	1.767
STDEV	44.336	2.084	0.058
Corrosion Proof, # 2 rebar			
1	808.4	40.00	2
2	810.8	39.70	2
3	812.7	42.40	1.8
Average	810.633	40.700	1.933
STDEV	2.155	1.480	0.115
Technora, # 3 rebar			
1	1262.6	51.40	2.3
2	1295.4	52.00	2.5
3	1367.8	55	2.3
Average	1308.600	52.800	2.367
STDEV	53.828	1.929	0.115

One Month in Water	Tested Dry	Tested Dry	Tested Dry
	Tensile Strength, Mpa	Elastic Modulus, GPa	Strain at Peak, %
Corrosion Proof # 2 Rebar			
1	750.02	40.50	1.8
2	805.7	44.30	1.8
3	746.32	40.5	2
Average	767.3466667	41.76666667	1.866666667
STDEV	33.26644155	2.193931023	0.115470054
Tillco Company rebar # 2			
1	1094.9	56.50	2
2	1083.9	52.90	1.84
3	1388.9	59.2	1.8
Average	1189.233333	56.2	1.88
STDEV	173.0038535	3.160696126	0.105830052
Technora # 3 Rebar			
1	1338.5	53.00	2.4
2	909.3	52.00	2.2
3	1205.3	53	2
Average	1151.033333	52.66666667	2.2
STDEV	219.6857149	0.577350269	0.2

Table 8. Wet Vs. Dry Tension Test Results (continued)

Wet 1 month/tested wet	Tested wet	Tested wet	Tested wet
	Tensile Strength, Mpa	Elastic Modulus, GPa	Strain at Peak, %
Tillco, # 2 rebar			
1	1230.1	58.80	1.7
2	1055.6	53	1.7
3	1276.3	58.80	1.8
Average	**1187.333**	**56.700**	**1.733**
STDEV	**116.400**	**3.637**	**0.058**
Corrosion Proof, # 2 rebar			
1	782.5	42.10	1.9
2	773.9	40.20	1.9
3	743.5	41.80	1.8
Average	**766.633**	**41.367**	**1.867**
STDEV	**20.490**	**1.021**	**0.058**
Technora, # 3 rebar			
1	1044.5	51.00	1.9
2	1310.1	51.20	2.3
3	1101.4	51.6	2
Average	**1152.000**	**51.267**	**2.067**
STDEV	**139.843**	**0.306**	**0.208**

3.2.5 Durability Characteristics

The polymer composite bars (two glass and one Technora aramid FRP) were subjected to the following accelerated aging tests:

- Sustained Load

- Sustained Load in Salt Solution

- Alkali Resistance at Room Temperature

- Resistance to Salt Solution

- Resistance to Repeated Wet-Dry in Salt Solution

- Freeze-Thaw

- Resistance to Hot Water at 80°C

- Resistance to Ultraviolet Radiation

- Fatigue Life

- Moisture resistance in neutral water was assessed through six months of immersion in water at 22°C, followed by 14 days of air drying at 50% RH.

- Alkali resistance at 60°C was assessed through two months of immersion in lime solution (pH 13) at 60°C, followed by 14 days of air drying at 50% RH.

- Resistance to freeze-thaw was assessed through exposure to 300 cycles of freeze-thaw (ASTM C666) in 3% sodium chloride solution.

- Resistance to extreme cold was determined through tension testing at –40°C.

- Resistance to temperature cycles was assessed through exposure to 100 cycles of heating to +40°C for 24 hours and cooling to –40°C for 24 hours.

All composite specimens were conditioned, after accelerated aging at 50% relative humidity and room temperature for two weeks prior to the performance of tests. Detailed accelerated aging test results are presented in Tables 9 through 11. These tables also indicate the statistical significance (S) or insignificance (I) of each accelerated aging effect on tensile behavior of different FRP rods at 95% level of confidence. Statistical significance of an effect was determined using statistical inference procedures and statistical distribution. Figures 16, 17 and 18 present the effects of different accelerated aging conditions on the tensile properties of Technora aramid, glass (Corrosion Proof) and glass (Tillco) FRP rods, respectively. Only those accelerated aging effects which are statistically significant (marked "S" in Table 9, 10 and 11) and also cause reduction of tensile properties are discussed below.
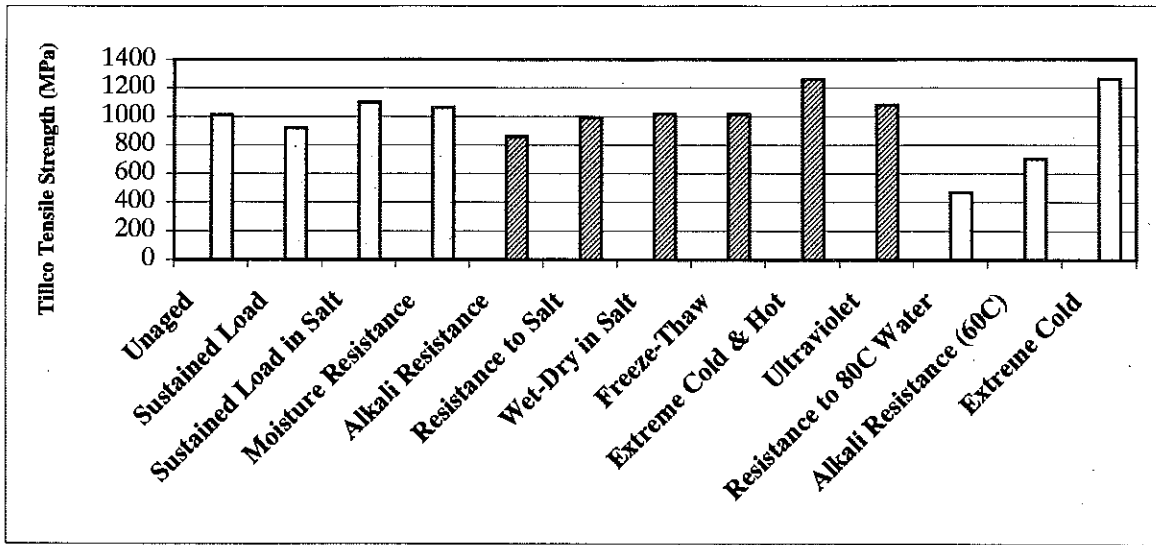
Figure 16a. Effects of Different Accelerated Aging Conditions on Tensile Strength of Tillco Glass FRP
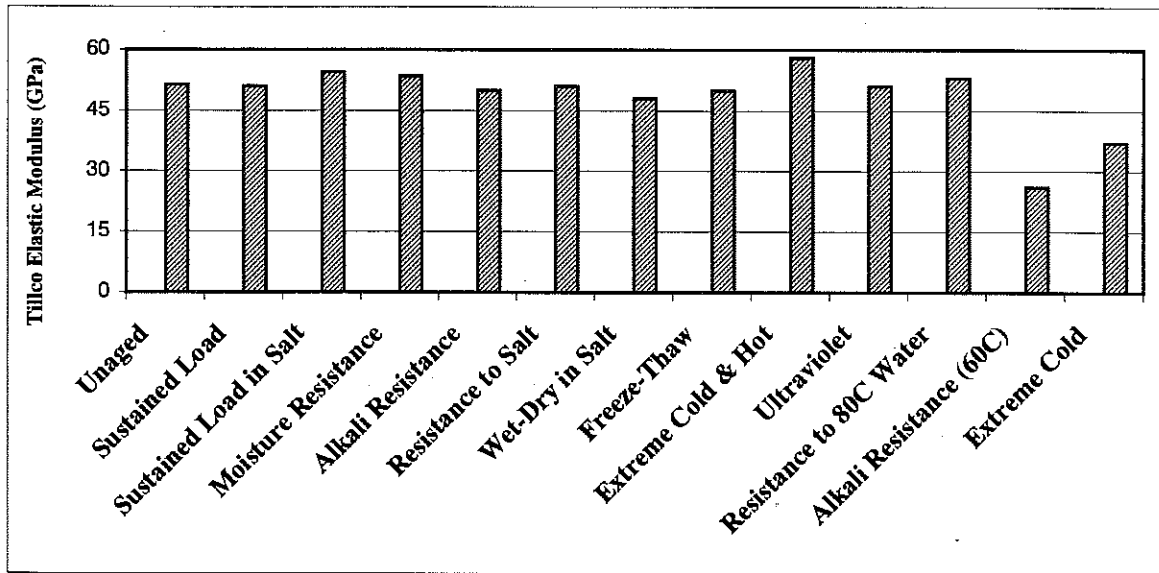
Figure 16b. Effects of Different Accelerated Aging Conditions on Elastic Modulus of Tillco Glass FRP
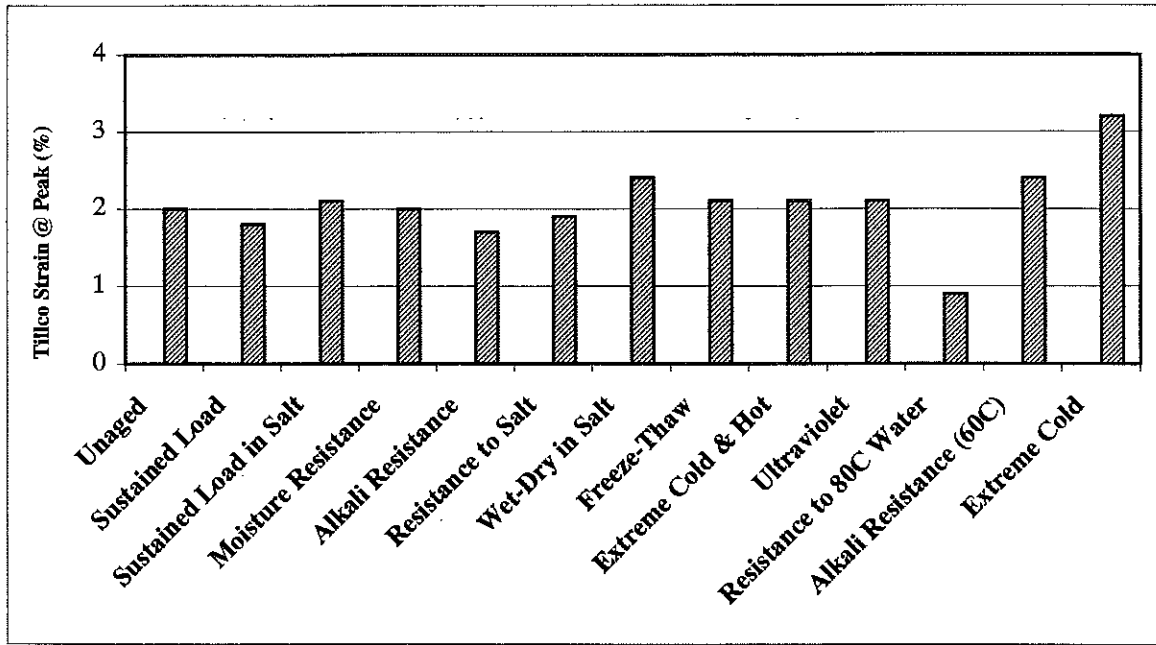
Figure 16c. Effects of Different Accelerated Aging Conditions on Strain at Peak of Tillco Glass FRP
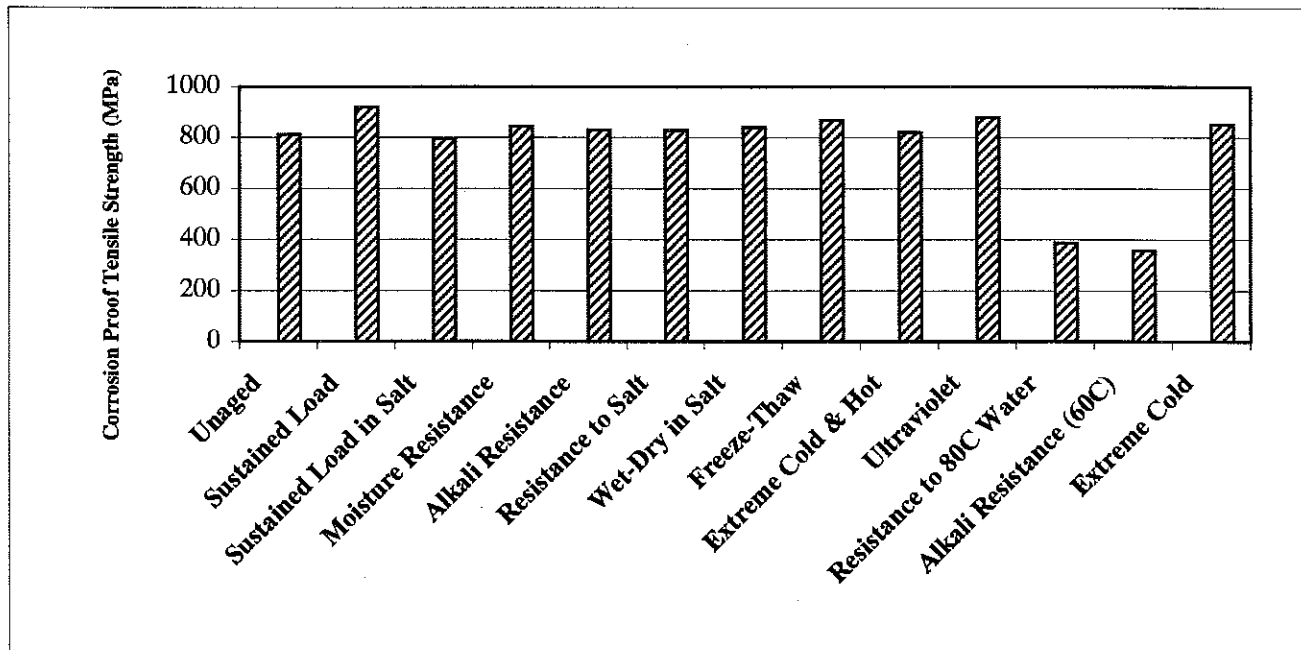
Figure 17a. Effects of Different Accelerated Aging Conditions on Tensile Strength of Corrosion Proof Glass FRP
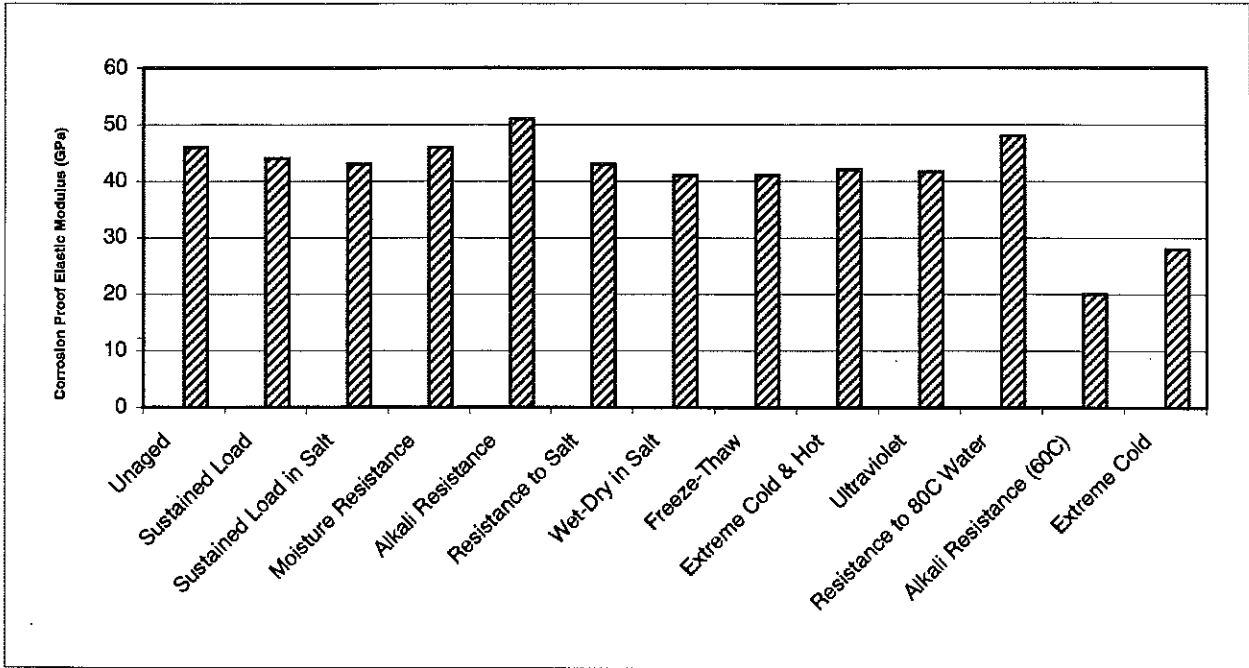
Figure 17b. Effects of Different Accelerated Aging Conditions on Elastic Modulus of Corrosion Proof Glass FRP
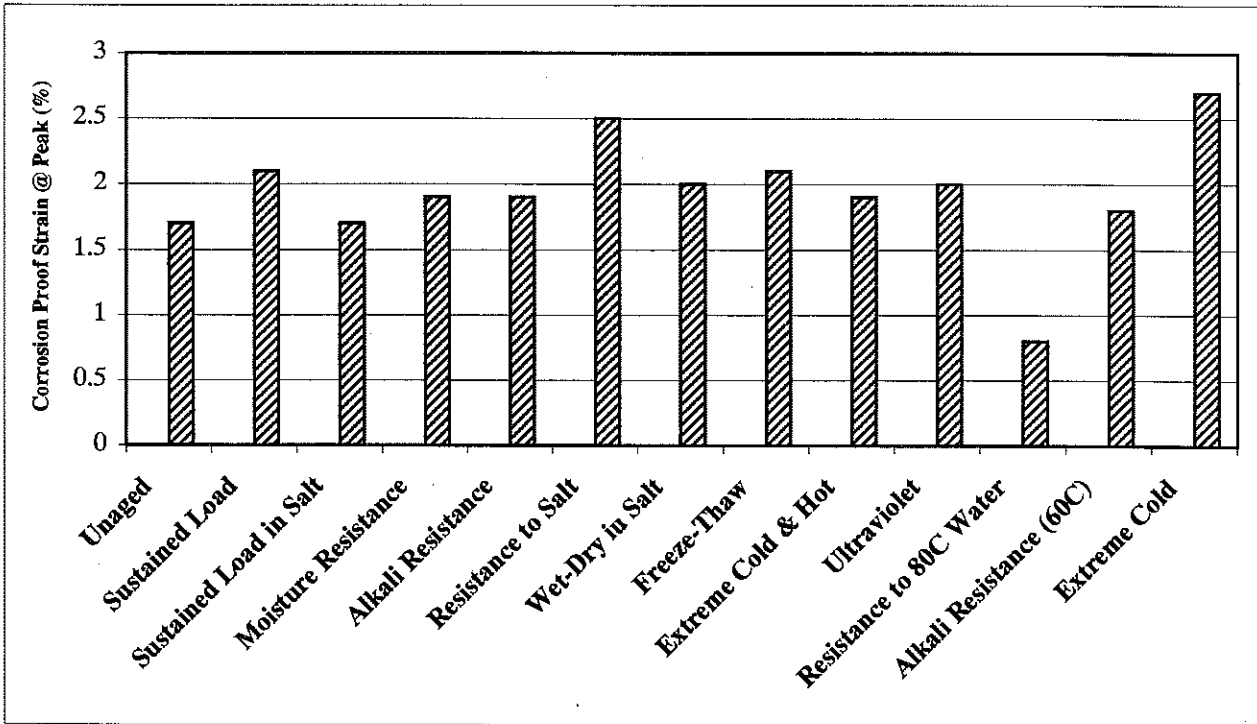
Figure 17c. Effects of Different Accelerated Aging Conditions on Strain at Peak of Corrosion Proof Glass FRP

74
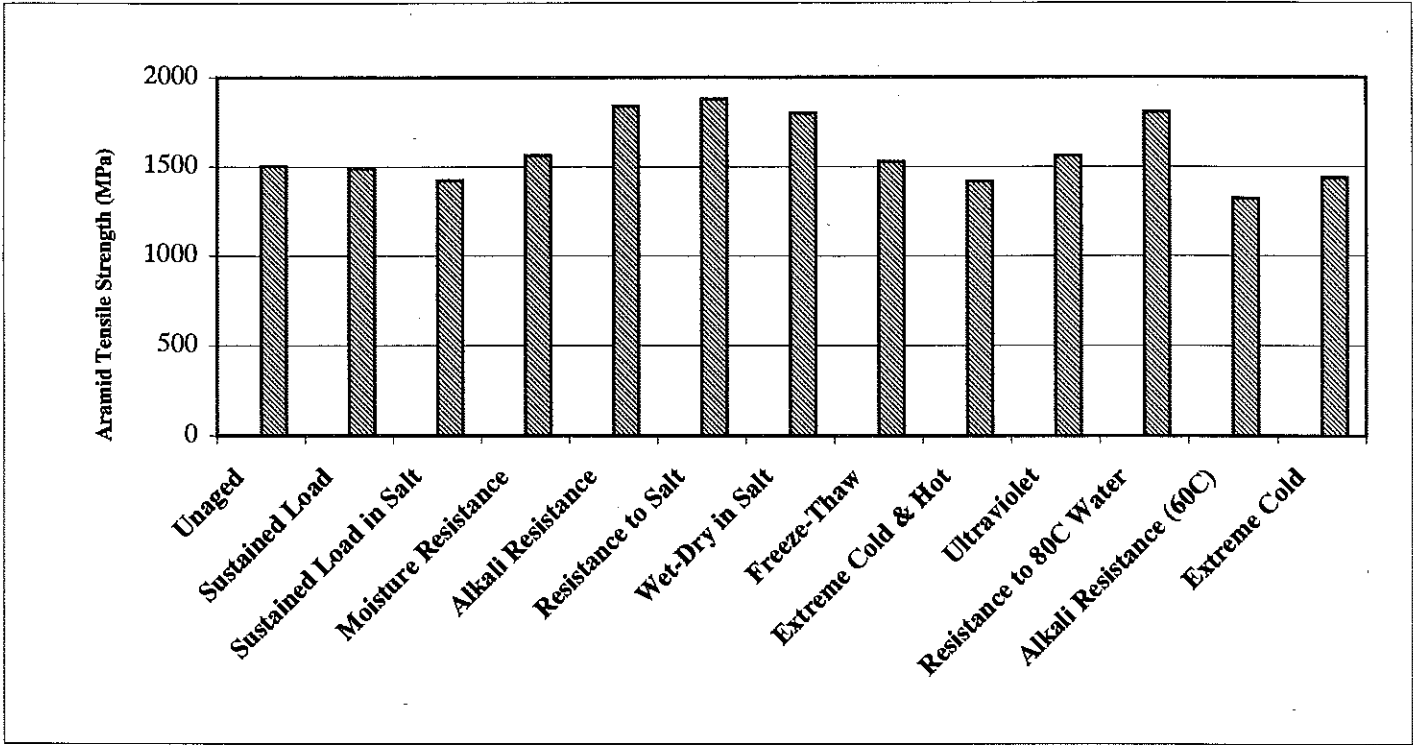
Figure 18a. Effects of Different Accelerated Aging Conditions on Tensile Strength of Technora Aramid FRP
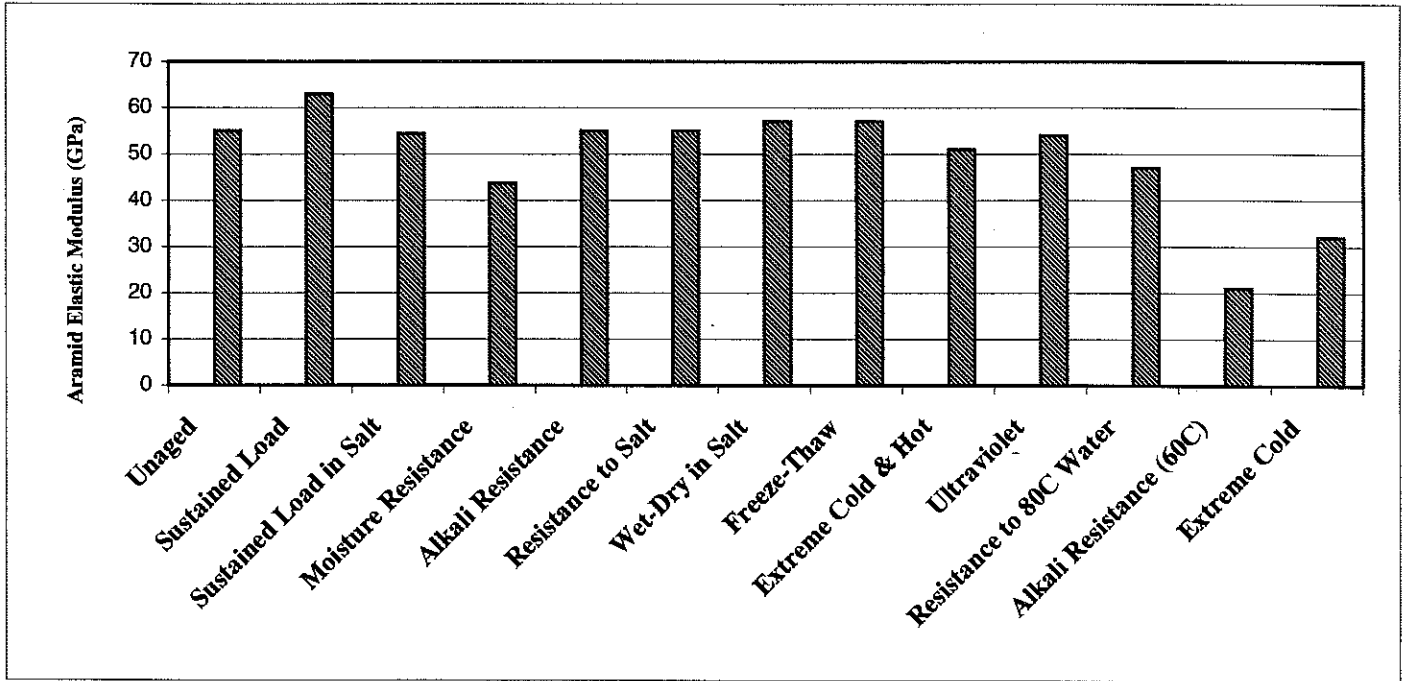
Figure 18b. Effects of Different Accelerated Aging Conditions on Elastic Modulus of Technora Aramid FRP
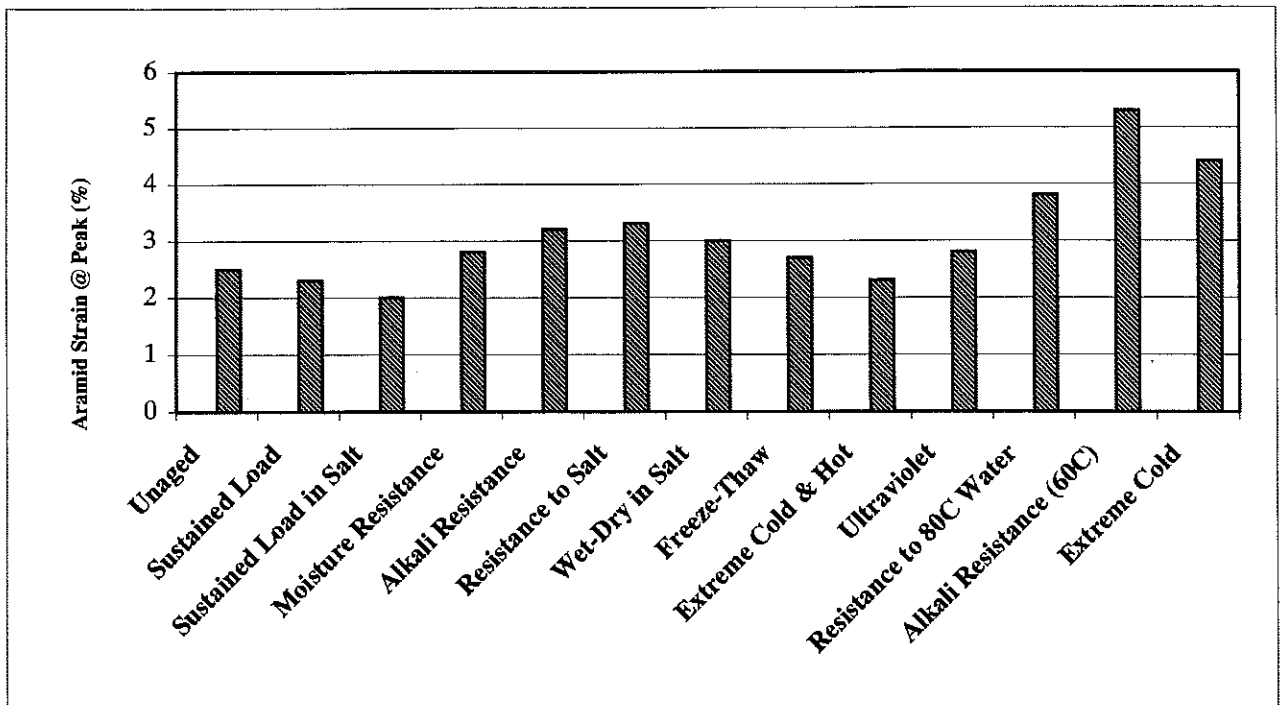
Figure 18c. Effects of Different Accelerated Aging Conditions on Strain at Peak of Technora Aramid FRP

Table 9. Accelerated Aging Effects on Tensile Behavior of Tillco Glass FRP

Tillco	Tensile Strength, MPa				
Aging	No	Mean	StDev	% Change	(S/I)
Unaged	10	1011.100	179.820	0.000	
Sustained Load	2	921.750	199.192	-8.837	I
Sustained Load in Salt	3	1097.267	81.742	8.522	I
Moisture Resistance	8	1062.688	47.246	5.102	I
Alkali Resistance	7	858.096	72.354	-15.132	S
Resistance to Salt	8	992.501	61.109	-1.839	I
Wet-Dry in Salt	8	1018.441	72.333	0.726	I
Freeze-Thaw	5	1016.760	163.100	0.560	I
Extreme Cold & Hot	8	1262.100	110.946	24.824	S
Ultraviolet	3	1081.470	1081.470	6.960	I
Resistance to 80C Water	8	468.538	24.244	-53.661	S
Alkali Resistance (60C)	5	702.820	26.177	-30.490	S
Extreme Cold	3	1262.000	46.027	24.815	S
Tillco	**Elastic Modulus, Gpa**				
Aging	No	Mean	StDev	% Change	(S/I)
Unaged	10	51.400	9.760	0.000	
Sustained Load	2	50.786	10.975	-1.195	I
Sustained Load in Salt	3	54.467	3.288	5.967	I
Moisture Resistance	8	53.575	2.969	4.232	I
Alkali Resistance	7	50.151	5.391	-2.430	I
Resistance to Salt	8	51.194	1.862	-0.401	I
Wet-Dry in Salt	8	47.535	2.327	-7.519	I
Freeze-Thaw	5	49.650	2.480	-3.405	I
Extreme Cold & Hot	8	57.960	3.806	12.763	S
Ultraviolet	3	51.442	1.747	0.082	I
Resistance to 80C Water	8	53.356	2.291	3.805	I
Alkali Resistance (60C)	5	25.280	2.770	-50.817	S
Extreme Cold	3	37.067	1.007	-27.885	S
Tillco	**Strain@Peak, %**				
Aging	No	Mean	StDev	% Change	(S/I)
Unaged	10	1.990	0.530	0.000	
Sustained Load	2	1.800	0.000	-9.548	I
Sustained Load in Salt	3	2.153	0.273	8.191	I
Moisture Resistance	8	2.018	0.237	1.407	I
Alkali Resistance	7	1.660	0.219	-16.583	I
Resistance to Salt	8	1.946	0.084	-2.211	I
Wet-Dry in Salt	8	2.388	0.587	20.000	I
Freeze-Thaw	5	2.160	0.430	8.543	I
Extreme Cold & Hot	8	2.157	0.151	8.399	I
Ultraviolet	3	2.097	0.195	5.377	I
Resistance to 80C Water	8	0.908	0.056	-54.372	S
Alkali Resistance (60C)	5	2.400	0.141	20.603	I
Extreme Cold	3	3.267	0.252	64.171	S

Table 10. Accelerated Aging Effects on Tensile Behavior of Corrosion Proof Glass FRP

Corrosion Proof	Tensile Strength, MPa				
Aging	No	Mean	StDev	% Change	(S/I)
Unaged	10	811.927	35.140	0.000	
Sustained Load	2	919.835	0.332	13.290	S
Sustained Load in Salt	3	795.933	4.864	-1.970	I
Moisture Resistance	8	843.830	64.707	3.929	I
Alkali Resistance	7	829.876	33.205	2.211	I
Resistance to Salt	8	828.098	67.609	1.992	I
Wet-Dry in Salt	8	840.548	46.133	3.525	I
Freeze-Thaw	6	868.130	58.310	6.922	S
Extreme Cold & Hot	8	820.029	28.961	0.998	I
Ultraviolet	3	878.900	31.776	8.249	S
Resistance to 80C Water	8	387.100	32.447	-52.323	S
Alkali Resistance (60C)	5	357.380	34.796	-55.984	S
Extreme Cold	3	851.133	21.309	4.829	S
Corrosion Proof	Elastic Modulus, Gpa				
Aging	No	Mean	StDev	% Change	(S/I)
Unaged	10	46.046	5.413	0.000	
Sustained Load	2	44.285	0.672	-3.824	I
Sustained Load in Salt	3	42.867	1.861	-6.905	I
Moisture Resistance	8	45.950	3.454	-0.208	I
Alkali Resistance	7	51.289	18.738	11.386	I
Resistance to Salt	8	43.269	1.390	-6.031	I
Wet-Dry in Salt	8	41.485	1.292	-9.905	S
Freeze-Thaw	6	41.330	1.370	-10.242	S
Extreme Cold & Hot	8	41.900	1.532	-9.004	S
Ultraviolet	3	41.610	0.863	-9.634	I
Resistance to 80C Water	8	47.751	1.441	3.703	I
Alkali Resistance (60C)	5	20.260	0.467	-56.001	S
Extreme Cold	3	28.233	5.410	-38.685	S
Corrosion Proof	Strain@Peak, %				
Aging	No	MEAN	StDev	% Change	(S/I)
Unaged	10	1.664	0.354	0.000	
Sustained Load	2	2.150	0.071	29.207	S
Sustained Load in Salt	3	1.730	0.082	3.966	I
Moisture Resistance	8	1.869	0.162	12.320	I
Alkali Resistance	7	1.933	0.495	16.166	I
Resistance to Salt	8	2.489	1.839	49.579	I
Wet-Dry in Salt	8	1.989	0.135	19.531	S
Freeze-Thaw	6	2.100	0.180	26.202	S
Extreme Cold & Hot	8	1.861	0.114	11.865	I
Ultraviolet	3	2.053	0.072	23.377	S
Resistance to 80C Water	8	0.825	0.052	-50.421	S
Alkali Resistance (60C)	5	1.800	0.200	8.173	I
Extreme Cold	3	2.667	0.058	60.276	S

Table 11. Accelerated Aging Effects on Tensile Behavior of Technora Aramid FRP

Technora Aramid	Tensile Strength, MPa				
Aging	No	Mean	StDev	% Change	(S/I)
Unaged	10	1502.892	83.395	0.000	
Sustained Load	3	1491.827	334.902	-0.736	I
Sustained Load in Salt	3	1423.333	459.559	-5.294	I
Moisture Resistance	8	1562.513	251.759	3.967	I
Alkali Resistance	8	1839.238	187.865	22.380	S
Resistance to Salt	8	1879.496	153.584	25.059	S
Wet-Dry in Salt	8	1799.126	192.150	19.711	S
Freeze-Thaw	6	1529.370	170.540	1.762	I
Extreme Cold & Hot	8	1390.386	206.304	-7.486	I
Ultraviolet	2	1561.500	66.327	3.900	I
Resistance to 80C Water	8	1804.674	303.925	20.080	S
Alkali Resistance (60C)	5	1319.960	268.830	-12.172	S
Extreme Cold	3	1437.567	66.618	-4.347	I
Technora Aramid	Elastic Modulus, Gpa				
Aging	No	Mean	StDev	% Change	(S/I)
Unaged	10	54.752	1.663	0.000	
Sustained Load	3	63.159	8.898	15.355	S
Sustained Load in Salt	3	54.367	4.362	-0.703	I
Moisture Resistance	8	43.725	8.670	-20.140	S
Alkali Resistance	8	55.079	1.958	0.597	I
Resistance to Salt	8	55.548	4.562	1.454	I
Wet-Dry in Salt	8	57.287	1.554	4.630	S
Freeze-Thaw	6	57.000	2.560	4.106	S
Extreme Cold & Hot	8	51.511	1.867	-5.919	S
Ultraviolet	2	54.015	0.675	-1.346	I
Resistance to 80C Water	8	46.748	1.951	-14.619	S
Alkali Resistance (60C)	5	20.600	0.354	-62.376	S
Extreme Cold	3	31.867	1.804	-41.798	S
Technora Aramid	Strain@Peak, %				
Aging	No	Mean	StDev	% Change	(S/I)
Unaged	10	2.517	0.213	0.000	
Sustained Load	3	2.257	0.636	-10.330	I
Sustained Load in Salt	3	2.050	0.132	-18.554	I
Moisture Resistance	8	2.863	0.885	13.747	I
Alkali Resistance	8	3.203	0.348	27.255	S
Resistance to Salt	8	3.350	0.356	33.095	S
Wet-Dry in Salt	8	3.074	0.297	22.130	S
Freeze-Thaw	6	2.660	0.220	5.681	I
Extreme Cold & Hot	8	2.271	0.390	-9.757	I
Ultraviolet	2	2.825	0.021	12.237	I
Resistance to 80C Water	8	3.844	0.617	52.721	S
Alkali Resistance (60C)	5	5.280	0.286	109.774	S
Extreme Cold	3	4.433	0.777	76.122	S

3.2.5.1 Tillco Glass FRP (Table 9)

- Resistance to 80°C Water: Six months of immersion in hot water at 80°C reduced tensile strength by 54% and strain at peak by 55%.

- Alkali Resistance at 60°C: Two months of immersion in lime solution (pH 13) at 60°C led to 30% and 50% drops in tensile strength and elastic modulus, respectively.

- Resistance to Extreme Cold: Testing at –40°C caused 27% drop in elastic modulus.

3.2.5.2 Corrosion Proof Glass FRP (Table 10)

- Resistance to 80°C Water: Six months of immersion in hot water at 80°C reduced tensile strength by 52% and strain at peak by 50%.

- Wet-Dry Cycles in Salt Solution: 100 cycles of drying (8 hrs)-wetting (16 hrs) in 3% sodium chloride solution reduced elastic modulus by 10%.

- Freeze-Thaw Resistance: 300cycles of freeze-thaw (ASTM C666) in 3% sodium chloride solution reduced elastic modulus by 10%.

- Ultraviolet Resistance: Exposure to ultraviolet reduced elastic modulus by 10%.

- Alkali Resistance at 60°C: Two months of immersion in lime solution (pH 13) at 60°C led to 35% and 56% drops in tensile strength and elastic modulus, respectively.

- Resistance to Extreme Cold: Testing at –40°C caused 38% drop in elastic modulus

3.2.5.3 Technora Aramid FRP (Table 11)

- Resistance to Extreme Cold-Hot Cycles: 100 cycles of repeated heating (+40°C)-cooling (-40°C) cycles reduced elastic modulus by 6% and strain at peak by 10%.

- Resistance to 80°C water: Six months of immersion in hot water at 80°C reduced elastic modulus by 15%.

- Alkali Resistance at 60°C: Two months of immersion in lime solution (pH 13) at 60°C led to 12% and 62% drop in tensile strength and elastic modulus respectively.
- Resistance to Extreme Cold: Testing at –40°C caused 41% drop in elastic modulus.
- Moisture Resistance: Six months of immersion in neutral water led to 20% drop in elastic modulus.

In evaluating of the above results one should note that strain measurement, which influences elastic modulus and strain at peak values, is more prone to experimental error than force measurement, which influences tensile strength values. Furthermore, in the case of Technora aramid FRP, the high tensile strength of bars made failure near or within end anchorage rather common. This could make the measured values of elastic modulus more variable. The drops in elastic modulus of Technora aramid FRP observed after some accelerated aging effects could be partly a consequence of experimental errors.

Based on the results presented above, glass fiber composites are susceptible to significant loss of tensile strength when exposed to the alkaline pore water of concrete. Hence, the project would focus on Technora's aramid fiber composite. It should be noted here that various grades of aramid are available, from different manufacturers, and the results presented here are strictly valid for the Technora grade of aramid FRP manufactured by Teijin Limited, Japan.

4.0   ASSESSMENT OF TECHNORA AFRP PERFORMANCE IN CONCRETE

4.1   TECHNORA AFRP SLAB DESIGN

4.1.1   Technora AFRP Bar Development Length

Assessment of Technora AFRP bond strength to concrete was the first step in the design process. Bond tests (see Figure 19 for test set-up) were performed according to ASTM C 234, using MDOT concrete mix grade D, with 2NS sand (Pit #19-46) and 6AA crushed limestone (Pit #95-5). This mix yielded 28-day compressive strength of 39.8 MPa in laboratory.
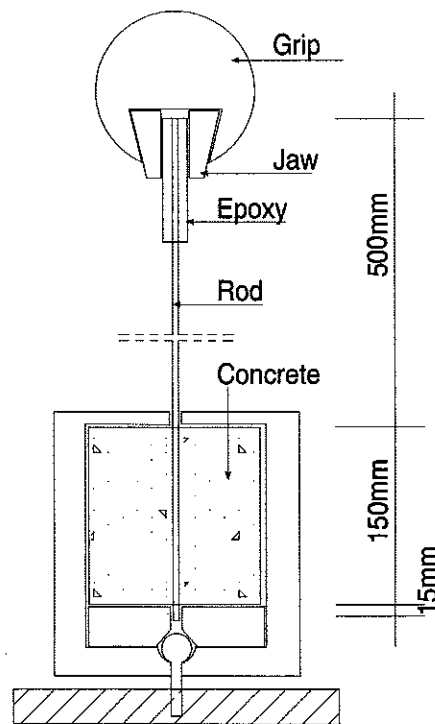
Figure 19. Bond Test Set-Up.

The bond stress-slip relationships for steel (9.5mm nominal diameter) and Technora AFRP (7.4mm nominal diameter) are presented in Figures 20a and 20b, respectively. One steel and one Technora AFRP bar ruptured, two steel and two Technora AFRP rods pulled out.
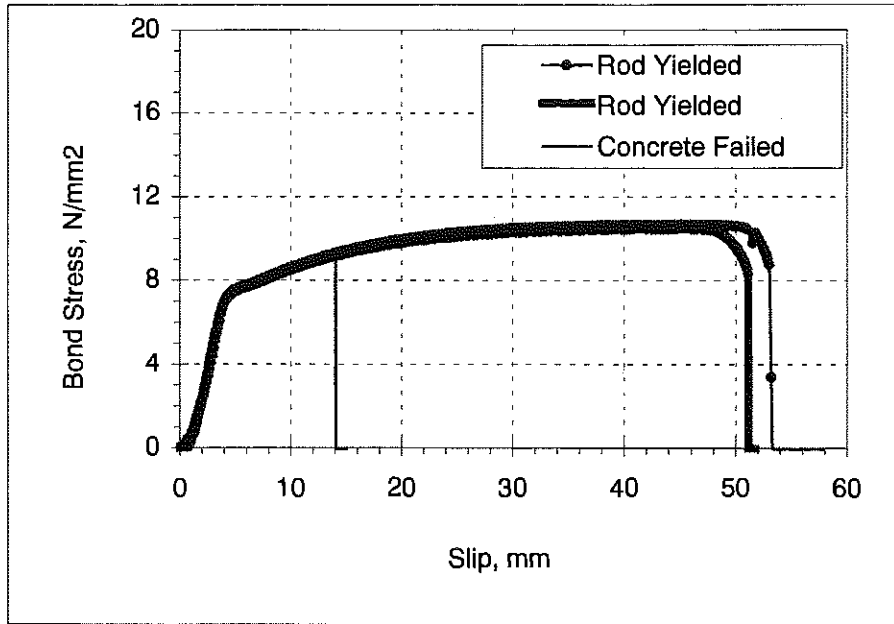
(a) Steel
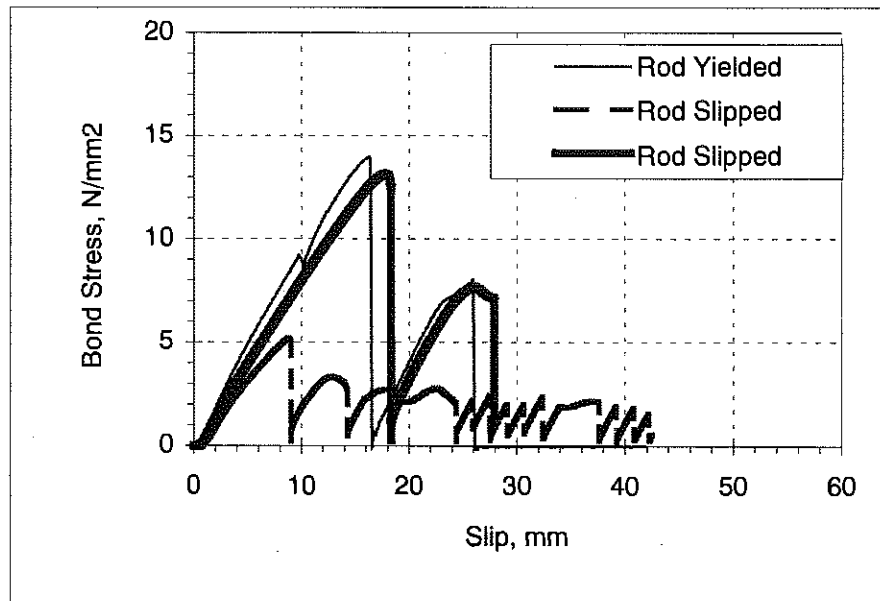
(b) Technora AFRP

Figure 20. Bond Stress-Slip Relationships

Figure 21 compares typical bond stress-slip relationships of steel and Technora AFRP rods (for pulled-out cases). Technora AFRP rods exhibited a higher bond strength, but their post-peak pull-out behavior was more brittle when compared with steel. The fact that the bond

strength of Technora AFRP is about 20% higher than that of steel provides a guide to verify the required development length of Technora AFRP during slab design.
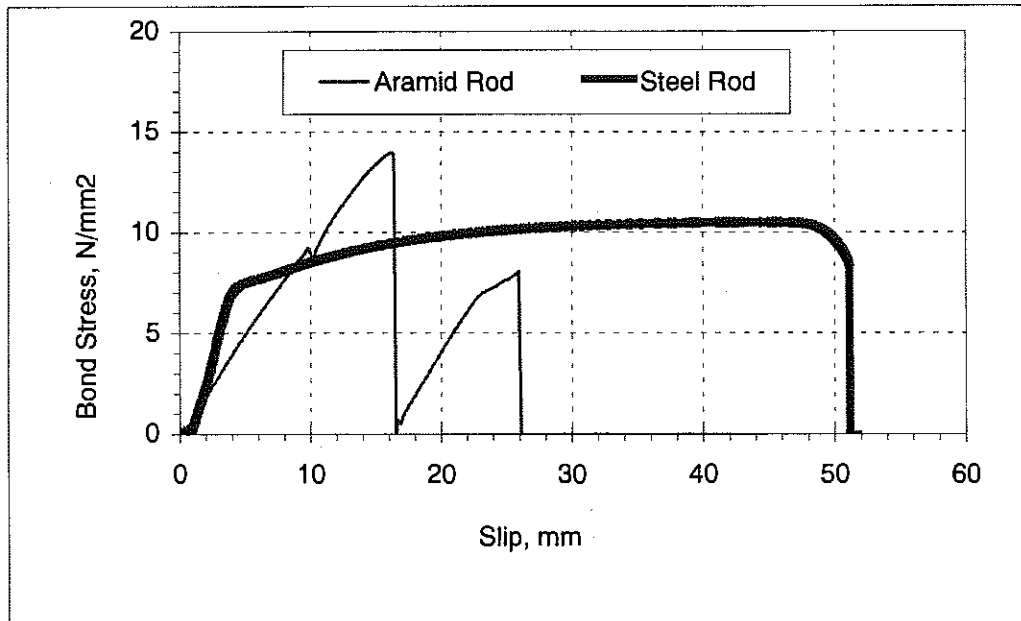
Figure 21. Typical Bond Stress-Slip Behavior of Technora AFRP vs Steel

Technora AFRP reinforced concrete slabs were designed following the ACI Committee 440 "Draft Design Guidelines for Concrete Members Reinforced with FRP Rebars".

In the case of the Technora AFRP rod, the development length l_{db} (in) can be calculated in terms of the rod cross-sectional area A_{fl} (in^2) and tensile strength f_{fl} (psi) as follows:

$$l_{db = 0.06} * (Af * f_{fl})/ \sqrt{f'_c}$$
$$= 0.06 * (0.0657 * 217,000) / \sqrt{5,736}$$
$$= 11.3" (287 \text{ mm})$$

The slab would be subjected to center-point loading on a simple span; the total bar length in the span direction should thus exceed 547 mm (twice the development length).

The steel bar to be used in the control slabs is #3, Grade 60. The basic development length (with sufficient concrete cover and bar spacing), per ACI 318 code, is:

$$l_d = (f_y \cdot d_b) / (25 \sqrt{f'_c})$$
$$= 60,000 * (0.375) / (25 \sqrt{5,736})$$
$$= 11.88" \ (300 \ mm)$$

In slabs subjected to center-point loading on simple spans, we would require total bar lengths in the span direction of 600mm.

The ultimate tensile force of the Technora AFRP rod used here is about twice that of steel and its periperal area is about 80% that of steel. The bond strength of Technora AFRP is about 20% greater than that of steel. Under these conditions, one would suspect that development length for Technora AFRP should be about twice that of steel. The (ACI Committee 440) required development length of 287 mm (compared to 300 mm for steel) thus seems unconservative.

The above equation for l_{db} was based on an earlier version of ACI Committee 440 Draft Design Guide. Later versions of this document included the additional requirement that l_{db} should not be less than $d_b f_{fl} / 2700$, which is equal to 23.2 in (589 mm) in this case and thus governs.

4.1.2   Limits on Reinforcement Ratio

For Technora AFRP reinforcement
$$\rho_{flmim} = 1.33 \ \rho_{bb}$$
$$= 1.33(0.85\beta_1 \ f'_c/f_f)*(0.003E_f/(\ f_f +0.003E_f)]$$

$$= 1.33 \ (0.85*0.85*5,736/217,000)*[0.003*7,800,000/(217,000+0.003*7,800,000)]$$

$$= 0.002$$

For steel reinforcement

$$\rho_{min} = 3\sqrt{f'_c}/f_f$$

$$= 3\sqrt{5{,}736}/60{,}000$$

$$= 0.0038$$

$$\rho_{max} = 0.75\ \rho_b$$

$$= 0.75\ (0.85)\ \beta_1\ (f'_c/f_y)*[87/\ (87+f_y)]$$

$$= 0.75(0.85*0.85*(5{,}736/60{,}000)*[(87/(87+60)]$$

$$= 0.03$$

4.1.3 Slab Design

Figure 22 presents the slab design used in this investigation. In the main (longer) direction, we used either three steel bars (0.009 reinforcement ratio) or three Technora AFRP rods (0.0055 reinforcement ratio). These reinforcement ratios fall within the limits established above.
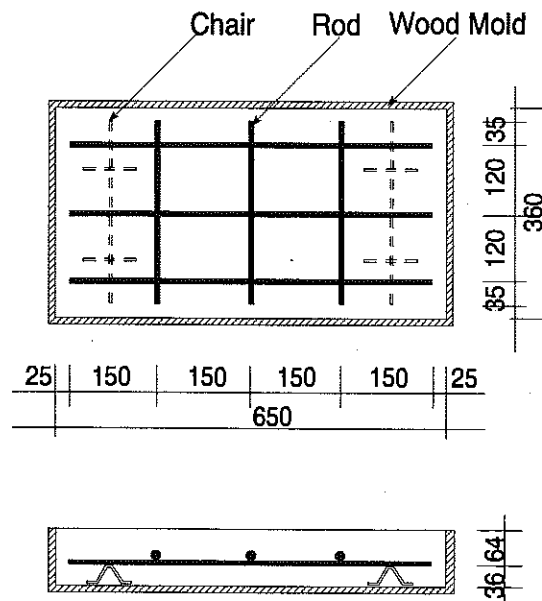
Figure 22. Slab Design

Ultimate flexural strength (M_u) with <u>Technora</u> AFRP reinforcement is calculated below.

$$a = A_f * f_f / (0.85 \ f'_c \ b)$$
$$=0.197*217,000/(0.85*5,736*14.2)$$
$$= 0.617"$$

$$M_u = 0.85 \ f'_c \ a.b \ (d-a/2)$$
$$= 0.85*5736*0.617*14.2 \ (2.52 - 0.617/2)$$
$$= 94,468 \ lb.in \ (10,664 \ KN.mm)$$

Ultimate flexural strength (M_u) with steel reinforcement is calculated below.

$$a = A_s * f_y / (0.85 \ f'_c \ b)$$
$$=0.33*60,000/(0.85*5,736*14.2)$$
$$= 0.286"$$

$$M_u = A_s * f_y / (d-a/2)$$
$$= 0.33*60,000/(2.52-0.286/2)$$
$$=47,065 \ lb.in \ (5,313 \ KN.mm)$$

The slabs were subjected to center-point loading on a simple span of 600 mm. The ultimate load capacities would thus be 71.1 and 35.4 KN for Technora AFRP and steel reinforced slabs, respectively.

4.2   SLAB TEST PROGRAM

A total of 32 slab specimens were made; 16 with Technora AFRP reinforcement, and 16 with steel reinforcement. Figure 23 shows the reinforcing bars inside wood molds.
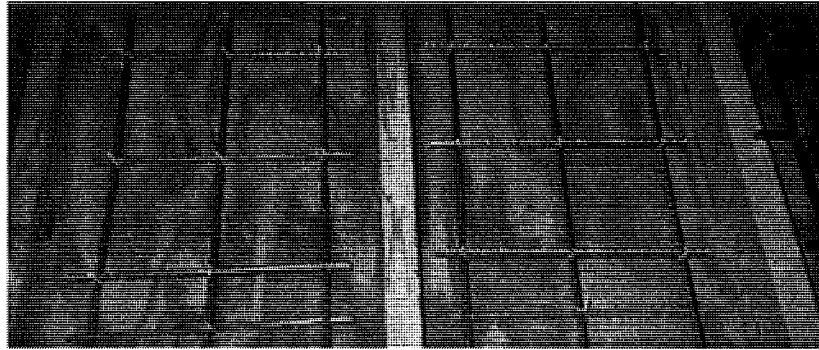
Figure 23. Reinforcing Bars in Wood Molds

The test program is presented below.

Reinforcement	Unaged	Freeze-Thaw	Wet-Dry	Temperature Cycle
Steel	4	4	4	4
Technora AFRP	4	4	4	4

All specimens were moist cured for 28 days at 22°C and 100% relative humidity, and then air-dried for 10 days. Unaged specimens were tested at the completion of this curing process.

The accelerated freezing-thawing process comprised 300 cycles (ASTM C 666) in 3% salt solution. The wetting-drying process comprised 100 cycles of wetting in water at 22°C For 16 hours followed by 8 hours of drying at 22°C, and the temperature cycling process comprised 30 cycles of exposure to 40°C for 24 hours and -40°C for 24 hours.

4.3   SLAB TEST RESULTS

The experimental load deflection curves are presented in Figures 24 and 25. Figure 26 compares typical load-deflection curves of Technora AFRP and steel reinforced slabs. The

concrete used in these slabs had a compressive strength of 35.4 MPa. The failure process of Technora AFRP reinforced slab was dominantly by bar pull-out. Steel reinforced slabs failed by a combination of yielding and pull-out of steel bars. Both Technora AFRP and steel reinforced slabs exhibited a tendency towards the punching shear mode of failure (see Figures 27 and 28). Figures 27 and 28 presented pictures of failed specimens. In the case of Technora AFRP, the average peak load was 42.6 KN, compared to the predicted value of 71.1 KN. This indicates that the development length (calculated using the ACI Committee 440 Draft Design Guide) should be almost doubled for the tensile strength of Technora AFRP rods to be fully utilized. The average peak load for steel reinforced slabs was 51.2 KN compared to the predicted value of 35.4 KN. It seems that the steel rebars have undergone post-yield hardening, and thus provided the slabs with higher post-yield peak strength than predicted. Technora AFRP reinforced slabs reach their peak load at deflections twice the peak load deflections of steel reinforced concrete slabs. This partly reflects on the lower elastic modulus of Technora AFRP compared to steel, and partly on the dominance of pull-out in the failure process of Technora AFRP reinforced concrete slabs.
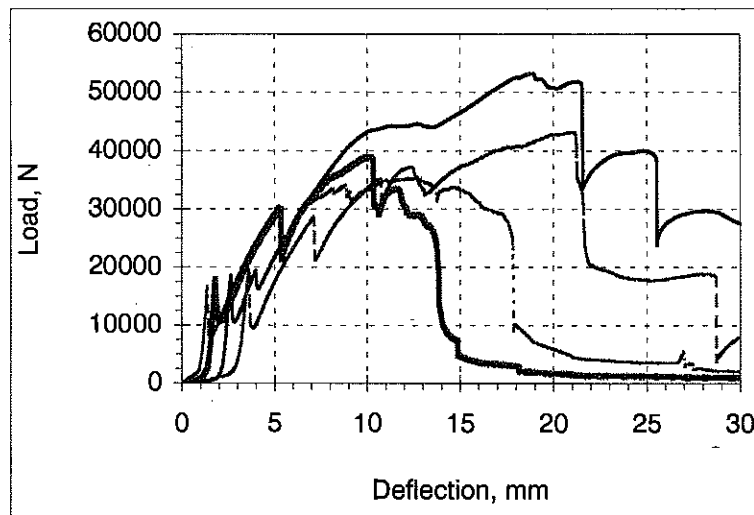
Figure 24. Experimental Load-Deflection Curves for Unaged Technora AFRP Reinforced Slabs.
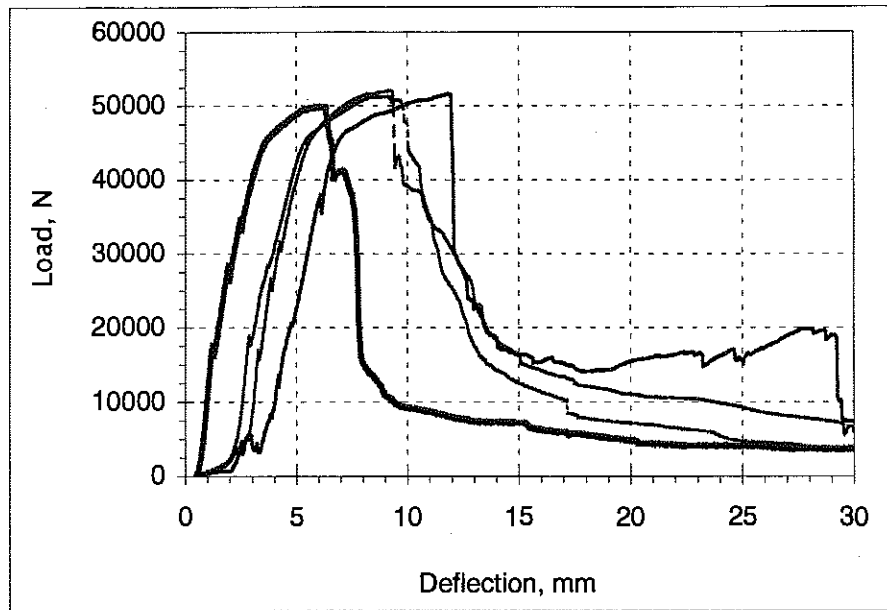
Figure 25. Experimental Load-Deflection Curves for Unaged Steel Reinforced Slabs.
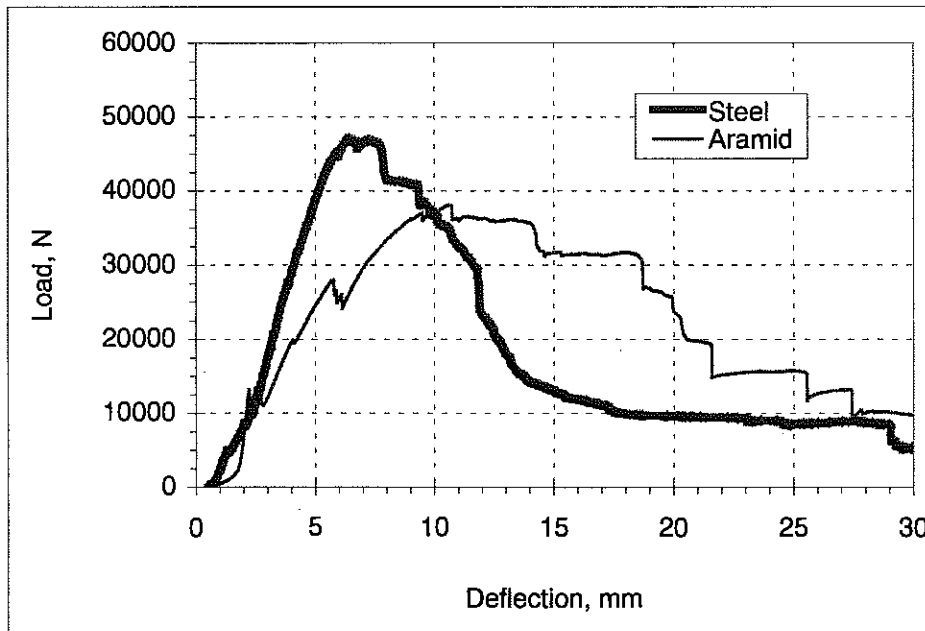
Figure 26. Typical Load-Deflection Curves for Unaged Technora AFRP Vs. Steel Reinforced
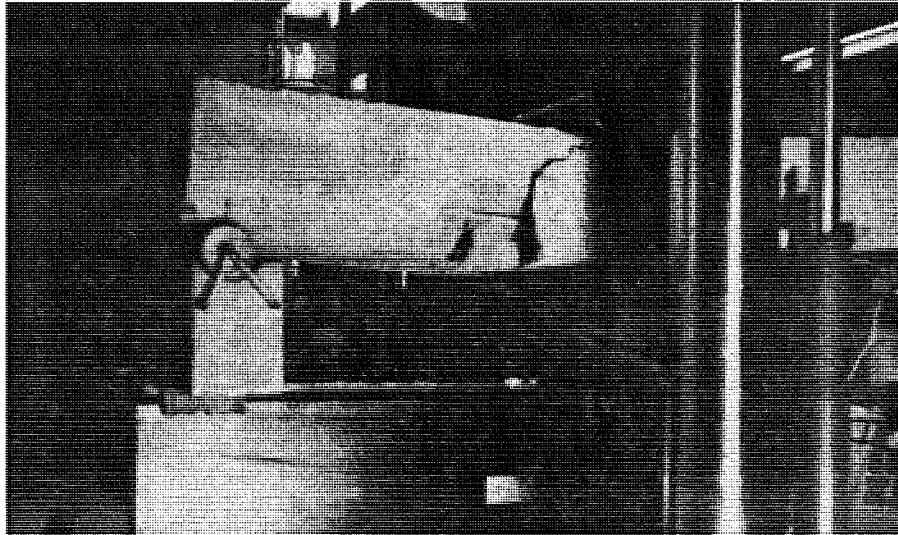
Slabs.

Figure 27. Picture of a Typical Failed Technora AFRP Reinforced Slab.
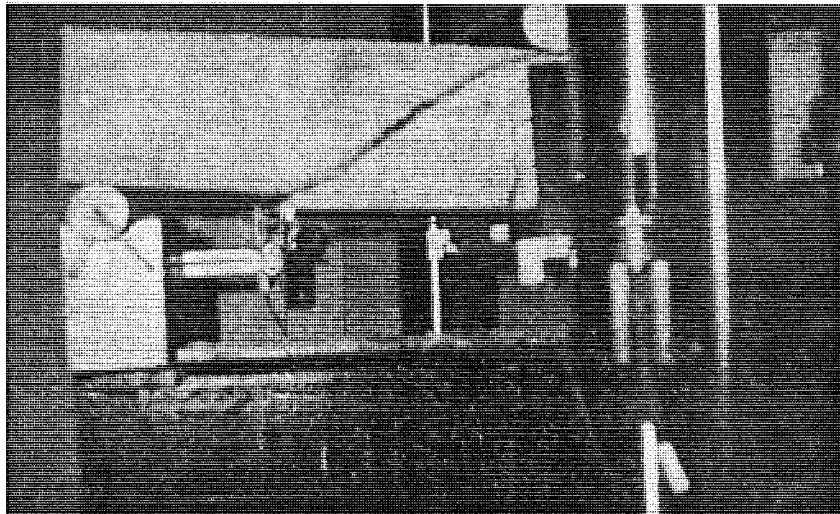
Figure 28. Picture of a Typical Failed Steel Reinforced Slab.

Aged Technora AFRP and steel reinforced slabs exhibited failure modes similar to unaged specimens. Figures 29 and 30 present the experimental load-deflection curves of aged Technora AFRP and steel reinforced slabs, respectively. Figures 31 and 32 compare typical unaged versus aged load-deflection curves for Technora AFRP and steel reinforced slabs, respectively. The accelerated aging conditions consider here are observed to have relatively small effects on Technora AFRP and steel reinforced concrete slabs (see Figure 33).
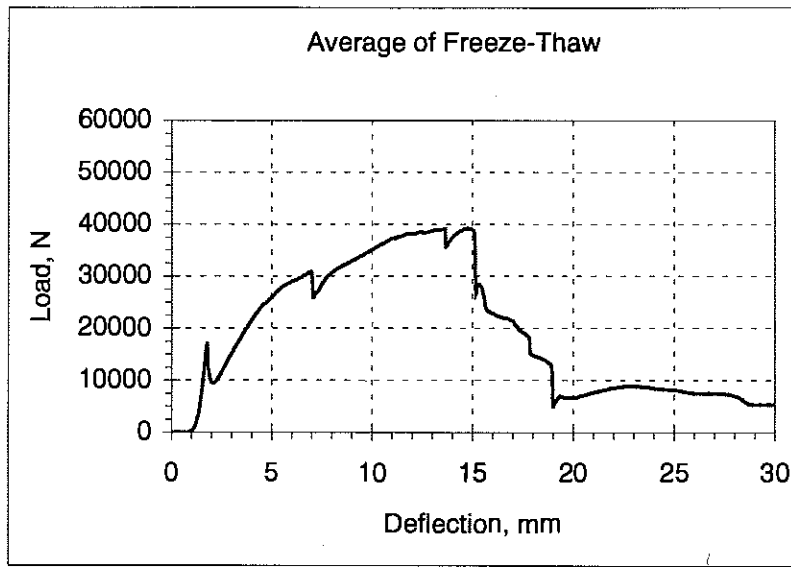
(a) Freeze-Thaw
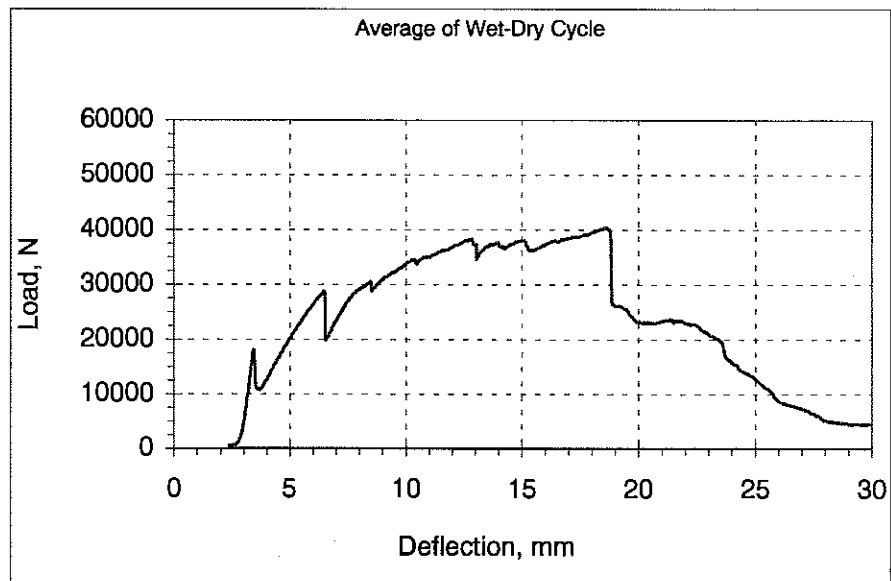
(b) Wet-Dry

Figure 29. Typical Load-Deflection Curves of Aged Technora AFRP Reinforced Slabs.
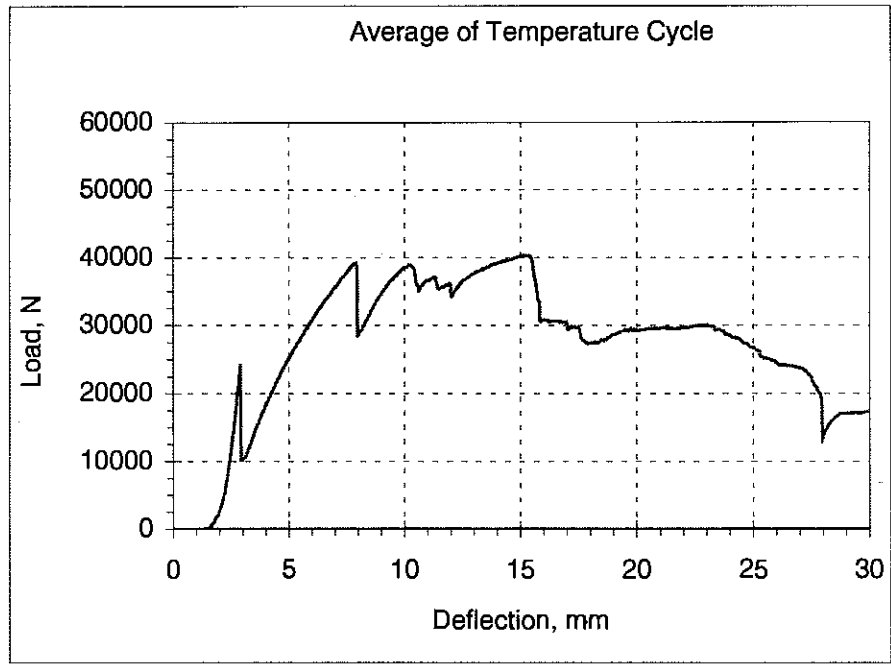
(c) Temperature Cycle

Figure 29 (continued). Typical Load-Deflection Curves of Aged Technora AFRP Reinforced
Slabs.
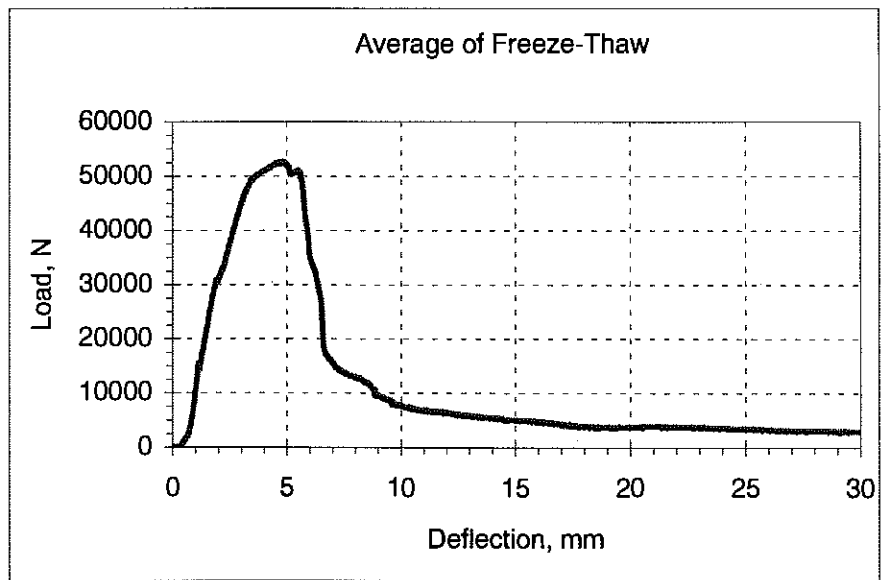
(a) Freeze-Thaw
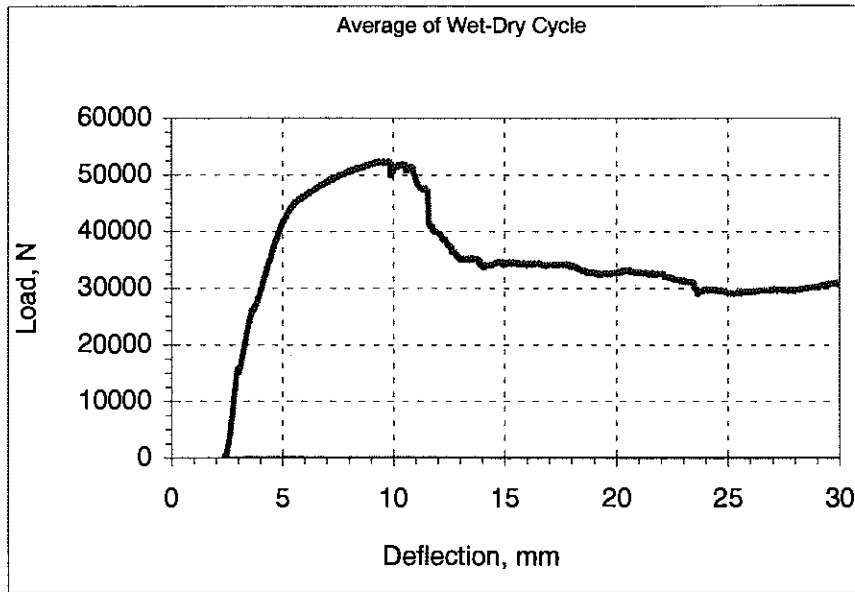
(b) Wet-Dry
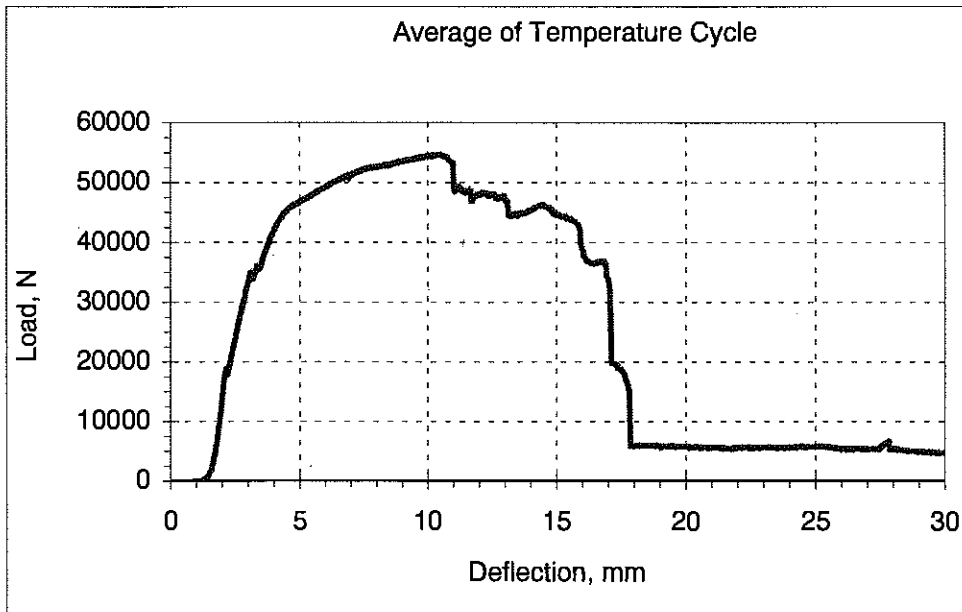
(c) Temperature Cycle

Figure 30. Typical Load-Deflection Curves of Aged Steel Reinforced Slabs.
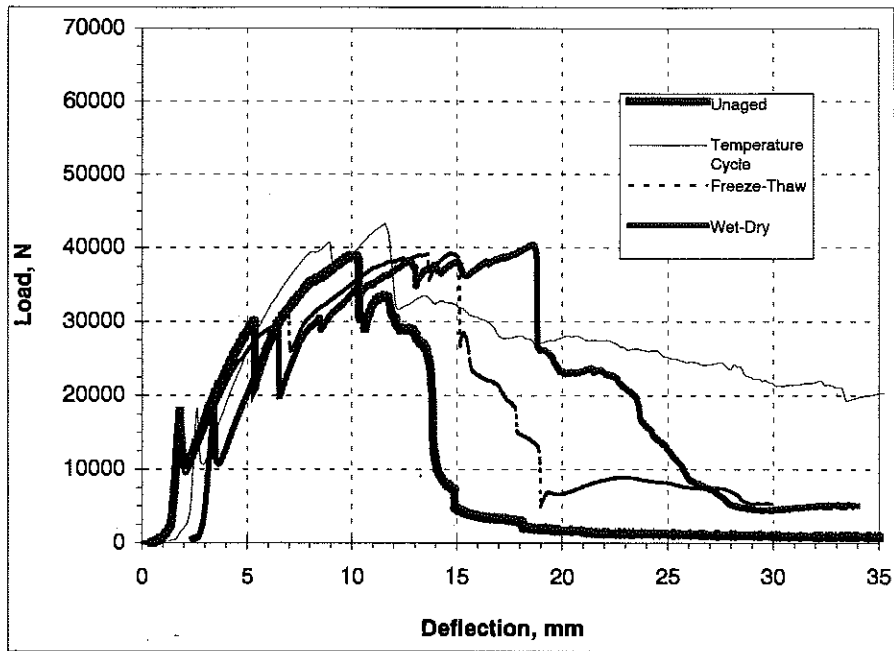
Figure 31. Typical Unaged Versus Aged Load-Deflection Curves for Technora AFRP Reinforced Slabs.
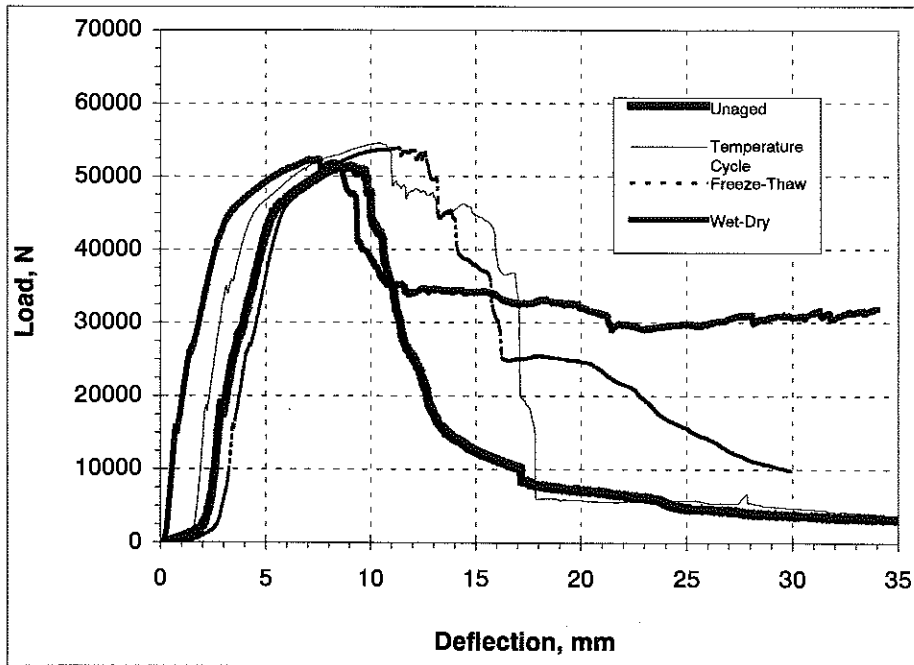
Figure 32. Typical Unaged Versus Aged Load-Deflection Curves for Steel Reinforced Slabs.

The above test results indicate that the ACI Committee 440 Draft Design Guides yield unconservative development lengths for AFRP bars. The Japanese Society of Civil Engineers (JSCE) "Recommendation for Design and Construction of Concrete Structures Using Continuos Fiber Reinforced Materials", requires a development length of 723 mm for AFRP bars for the conditions considered here (compared to 287 mm for ACI Committee 440 Draft Guide). This explains why Technora AFRP reinforced slabs provided only half their theoretical peak load. Also, the 723 mm development length of Technora AFRP rods (7.4 mm diameter) is greater than the steel rebar (9.5 mm diameter) development length of 300 mm, which is reasonable considering the relatively high strength of Technora AFRP rods.

Table 12 and Figure 33 summarize all peak load test results generated in this test program. Statistical analysis (of variance) of test results indicated that the accelerated aging effects considered here did not, at 90% level of confidence, cause any significant deterioration of steel and Technora AFRP reinforced concrete slabs.

Table 12. Summary of Test Results.

SLAB WITH STEEL REBAR							
	Peak Load (no aging)		Peak Load (wet/dry)		Peak Load (freeze/thaw)		Peak Load (hot/cold)
1	49896	1	53614	1	53830	1	57570
2	51279	2	52313	2	52537	2	52528
3	52025	3	51489	3	56312	3	52632
4	51612	4	50784	4	51279	4	56105
						5	57768
						6	54579
Stdv	923.21		1215.55		2150.65		2330.25
Mean	51203.00		52050.00		53489.50		54708.75
90% CI	759.27		999.70		1582.02		1916.46
SLAB WITH TECHNORA AFRP REBAR							
	Peak Load (no aging)		Peak Load (wet/dry)		Peak Load (freeze/thaw)		Peak Load (hot/cold)
1	35241	1	39067	1	39223	1	40489
2	43119	2	40368	2	36637	2	42092
3	38917	3	40712	3	33388	3	40282
4	53209	4	41945	4	36456	4	38136
						5	43135
						6	39032
Stdv	7757.52		1183.46		2387.33		1624.81
Mean	42621.50		40523.00		36426.00		40249.75
90% CI	6379.99		973.31		1963.40		1091.07
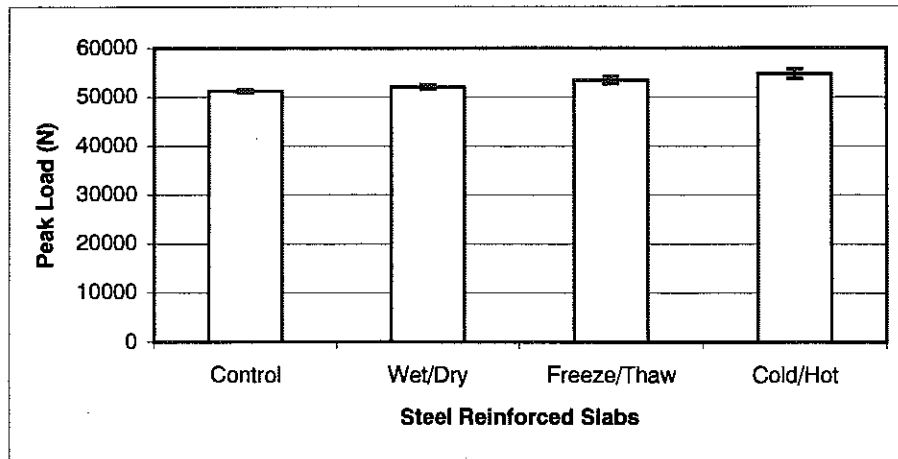
(a) Steel Reinforced Concrete Slabs
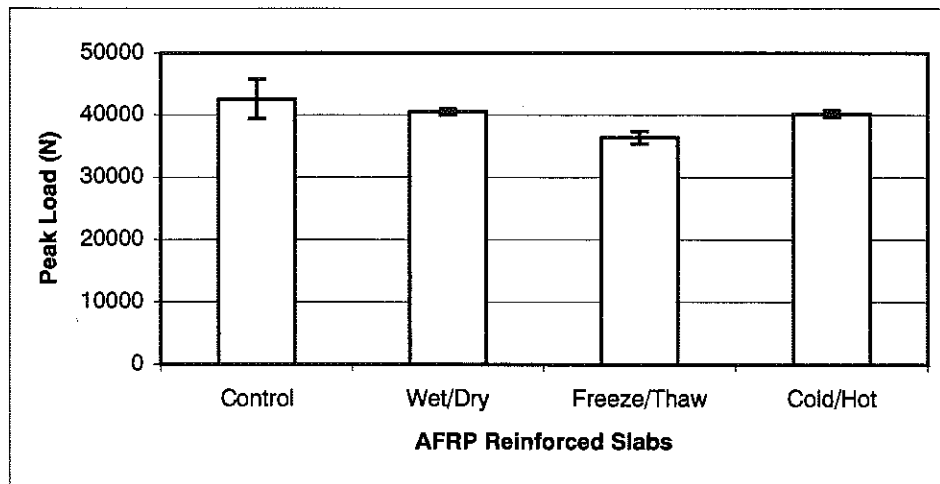
(b) Technora AFRP Reinforced Concrete Slabs

Figure 33. Mean Values and 90% Confidence Intervals of Peak Loads for Reinforced Concrete Slabs Loaded After Different Aging Conditions.

4.4   DOWEL TEST RESULTS

The tendency towards punching shear mode of failure (see Figure 27 and 28) implies that Technora AFRP and steel reinforcement in slab systems would be subjected to shear

98

(dowel) loads. Laboratory tests were thus conducted in order to compare the dowel action of Technora AFRP bars versus steel bars.

Steel and Technora AFRP rods of 9.5 and 7.4 mm diameters, respectively were subjected to dowel action using the set-up shown in Figures 36 and 37. The concrete used here had a compressive strength of 30 MPa. As shown in Figures 38 and 39, failure occurred by splitting of the concrete cover. The dowel load-deflection curves are shown in Figure 40. Steel and Technora AFRP dowel bars reached peak loads of 48.9 and 40.8 kN, respectively. This mode of dowel behavior does not indicate any particular weakness of Technora AFRP bars when compared with steel bars. The dowel test results presented in Figures 37 and 38, however, should be evaluated cautiously. Given the mode of failure, that is splitting of cover concrete, the area of concrete (i.e., the surface area of split crack) is an important factor influencing dowel strength. In other words, increasing the number of bars for the same concrete area does not proportionally increase the total dowel strength, the test set-up of Figure 36 may not reveal any weakness of Technora AFRP bars in dowel action.
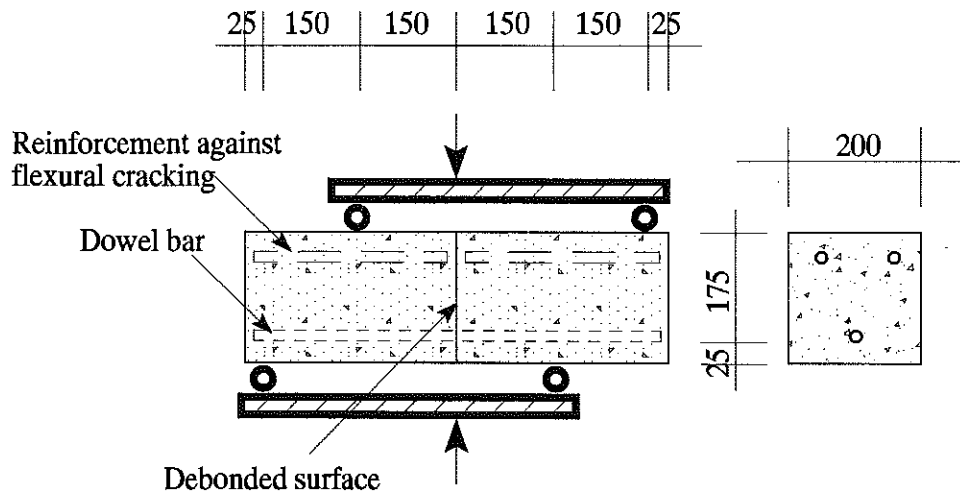
Figure 34. Dowel Test Set-Up.
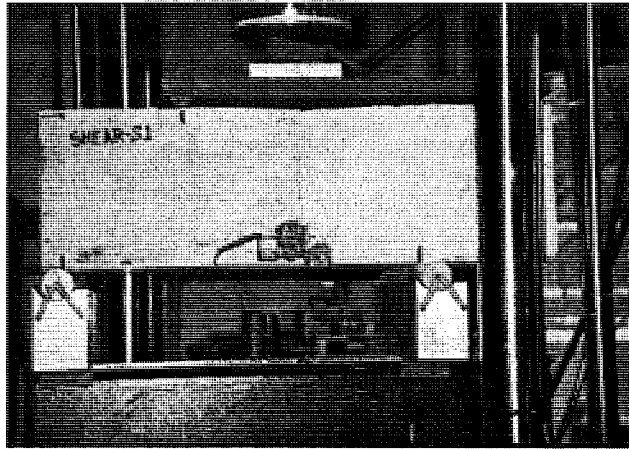
Figure 35. Picture of the Dowel Test Set-Up.
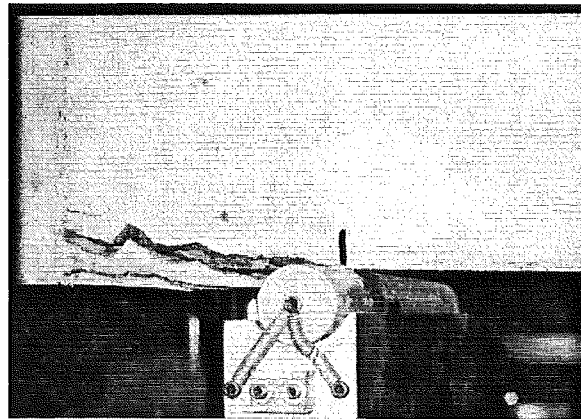
Figure 36. Initial Stage of Cover Splitting Under Dowel Load
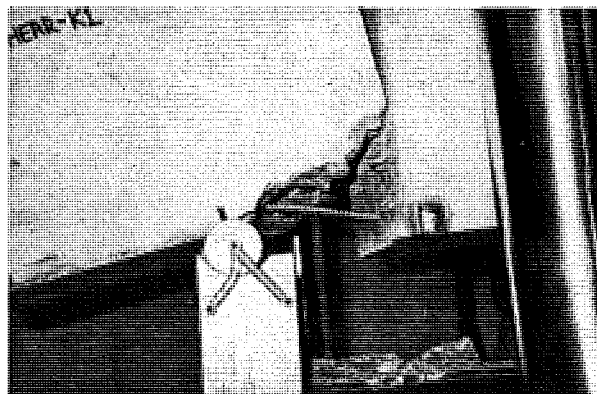
Figure 37. Later Stage of Dowel Bar Failure.
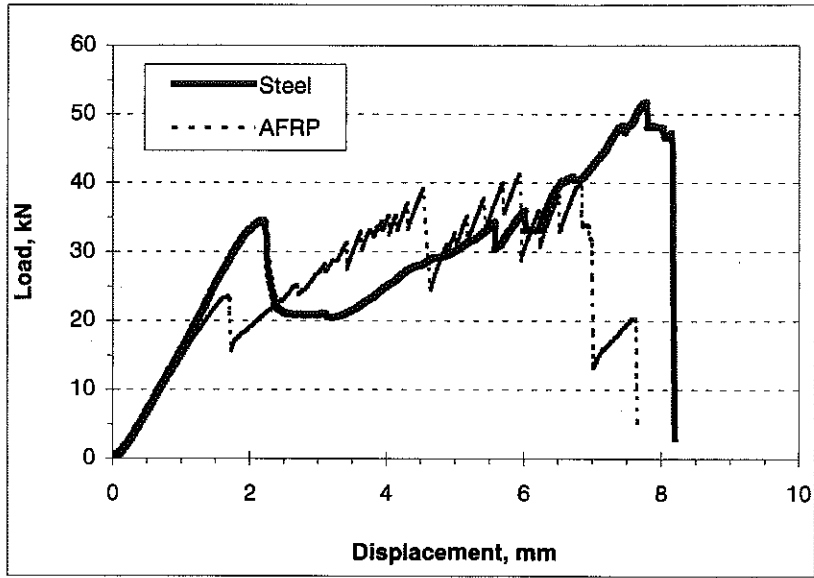
Figure 38. Dowel Load-Deflection Curve

5.0   BRIDGE DECK DESIGN AND LABORATORY EVALUATION

5.1   BASIC EVALUATION OF BRIDGE DECK DESIGN PHILOSOPHIES

The traditional approach to reinforced concrete bridge deck design assumes predominance of the flexural mode of failure. Structural failure of bridge decks has been a rare occurrence (many bridge deck replacements have been necessitated by the corrosion of reinforcing steel); the theory of flexural failure thus has not been thoroughly verified in field. Recent laboratory work, however, has suggested that bridge decks do not fail in flexure; punching shear has been suggested as the dominant mode of failure[26].

In order to assess failure processes of reinforced concrete bridge decks, a typical deck was analyzed under an example truck load. Some available design equations (for steel reinforced concrete slabs) were used to assess safety factors against flexural and punching shear modes of failure. The reinforced concrete bridge deck considered in this investigation is shown in Figure 39. The span length and total deck thickness are 2,134 and 229 mm, respectively.

f'_c =31 MPa

f_y =414 MPa
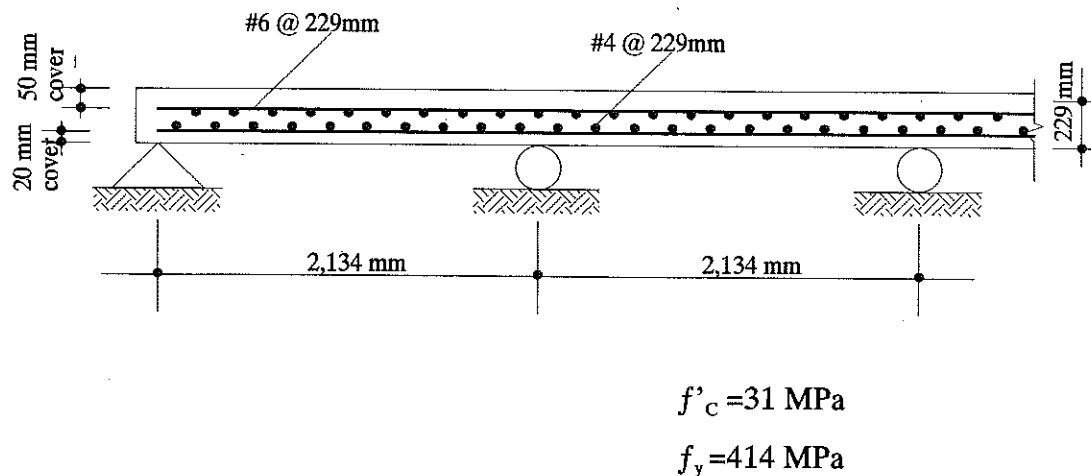
Figure 39. The Reinforced Concrete Bridge Deck.

Under an 80,000 N axle load applied as shown in Figure 40, the maximum bending moment in the deck slab is 34,678 N.m. One lane (about 3.5 m) of deck slab provides a nominal flexural strength of approximately 258,000 N.m. The factor of safety against flexural failure under this particular loading condition is thus 258,000/34,678 or 7.4.
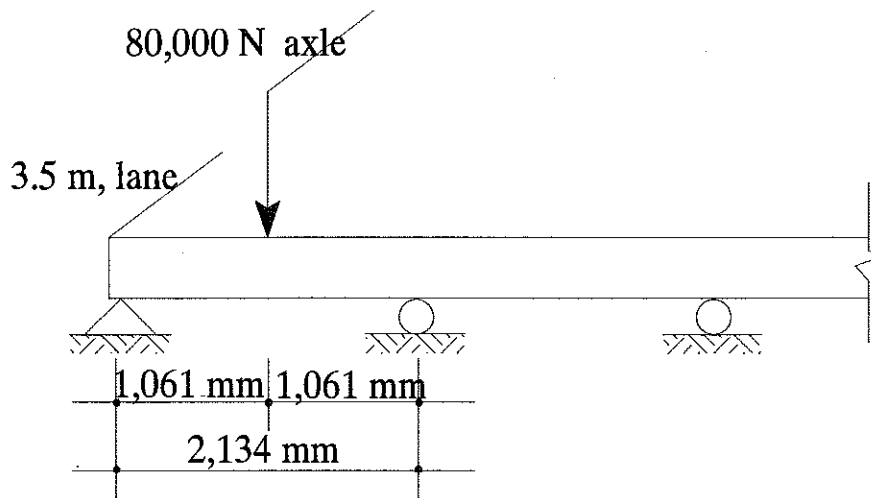
Figure 40. An Example Loading Condition of a Deck.

The ACI equation for nominal punching shear strength (V_C) is highly empirical and does not consider the reinforcement ratio as a factor. We considered a simplified tire contact area of 300X300 mm with a load of 40,000 N. The ACI equation for punching shear produced a nominal strength of 458,000 N, yielding a safety factor of 11.5. The British Standard [66] equation for punching shear strength (V_C) considers the effect of reinforcement ratio:

$$Vc = 3.16 * \sqrt[3]{100\rho} \sqrt[3]{f'c/25} \sqrt[4]{400/d} * (c+3d)*d \ -$$

Where, ρ is the reinforcement ratio (0.82% in this example), c is the side length of tire contact area (300 mm in this example) and d is the effective depth of slab (152 mm in this example). The nominal punching shear strength according to the British Standard would be 465,070 N, yielding a safety factor against punching shear failure of 11.6.

The above calculations suggest that safety factors against flexural failure (7.4) and shear failure (about 11.5) are quite high; this points at the conservative nature of bridge deck design practices. With the safety factor against flexure being smaller than that against punching shear, one would expect that flexure dominates the failure of this deck. However, it has been suggested that the restraining and arch actions within the deck slab increase safety against flexural failure to the point that punching shear dominates the failure process of deck slabs.

In an effort to develop a rational AFRP reinforcement configuration for the bridge deck considered here, we targeted a safety factor against punching shear failure of 5.5, and used the better developed Japanese (JSCE) design guides for FRP reinforced concrete to determine punching shear strength (V_C):

$$V_C = \beta_d \cdot \beta_p \cdot \beta_r \cdot f_{pcd} \cdot \mu_p \cdot d / \gamma_b$$

where,

$$\int_{pcd} = 0.2\sqrt{f'c} \leq 1.2 MPa$$

$$\beta_d = \sqrt[4]{1/d} \leq 1.5 \qquad \text{(d in meter)}$$

$$\beta_p = \sqrt[3]{100\rho * E_{AFRP} / E_{steel}}$$

$$\beta_r = 1+1/(1+0.25\ u/d)$$

u = periphery of contact area

μ_p = periphery of area at d/2 from contact area

$\gamma_b = 1.3$

An important consideration in the above equation is that it does not consider the tensile strength of FRP (as the British Standard did not consider the yield strength of steel). Instead,

the effectiveness of FRP versus steel in punching shear is defined in terms of the FRP-to-steel modular ratio. At a safety factor of 5.5, which requires a punching shear strength of 5.5X40,000=220,000 N in our example (over a simplified 300 mm square contact area), the above equation yields a required reinforcement ratio of 0.36% in this example. This reinforcement ratio is comparable to that of steel in Figure 39; however, due to the lower elastic modulus of AFRP, the safety factor against punching shear mode of failure is 5.5 with AFRP compared to 11.5 with steel reinforcement. For a 13 mm diameter AFRP rod (123 mm² nominal cross sectional area), a reinforcement spacing of 210 mm provides the required reinforcement ratio in each direction. The required reinforcement spacing with 7.4 mm diameter AFRP rods (42.4 mm² nominal cross sectional area) would be 75 mm.

5.2   DESIGN OF THE AFRP REINFORCED CONCRETE BRIDGE DECK

5.2.1 Design Load and Contact Area

Deck design is based on the control of punching shear failure under HS20-44 truck loading. The basic design equation is:

$$\eta \cdot \Sigma \gamma i \, Qi \leq \varphi Rn$$

Where $\eta = \eta_D \times \eta_R \times \eta_I > 0.95$

$=1.05 \times 0.95 \times 1.00$

$=1.0$

$\gamma i = 1.75$

$Qi = 1.33 \times 72.5$ KN (factor 1.33 accounts for impact)

$\varphi i = 1.0$

Hence,

$$1.0 \times 1.75 \times 1.33 \times 72.5 \leq 1.0 \, Rn$$

$$Rn \geq 169^{\,KN}$$

The total safety factor would thus be equal to 169/72.5 = 2.33.

The contact area on which the 169 KN load is applied should have a width of 510 mm. The length of the contact area is:

$$l = 2.28 \, \gamma \, (1 + {}^{IM}/_{100}) \times \rho$$

$$= 2.28 \times 1.75 \, (1.33) \times 72.5$$

$$= 385 \text{ mm}$$

5.2.2 Calculation of the AFRP Reinforcement Ratio

The reinforcement pattern is depicted in Figure 41; the objective of design is to calculate spacing of the 7.4mm diameter AFRP bars.
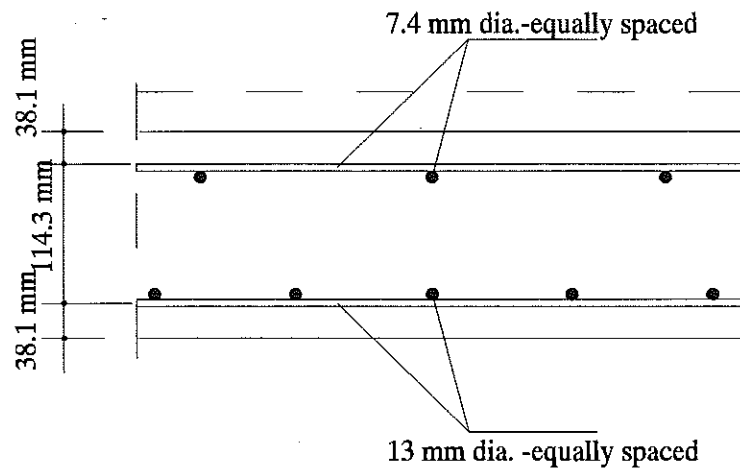
Figure 41. The Reinforcement Pattern.

Following the JSCE design procedures for punching shear (assuming 27.8 MPa concrete compressive strength):

$$V_C = \beta_d \cdot \beta_p \cdot \beta_r \cdot f_{pcd} \cdot u_p \cdot d / \gamma_b$$

$$= 1.5 * \sqrt[3]{100 \rho E_{fu} / E_o} * (1 + 1/1 + 0.25 * 1790/147) * (\sqrt{f'Cd}) * 2378 * 147 / 1.3$$

$$= 1.5 * 3 * \sqrt[3]{\rho} * 1.247 * 1.05 * 268,897$$

106

$$= 1,584,361 * \sqrt[3]{\rho} * N$$

V_C = Rn = 169,000 N

ρ = 0.0012 (0.12%) average of reinforcement ratio in both directions – total of top and bottom.

Given the relatively low elastic modulus of composites, the fact that the above reinforcement ratio is smaller than that required in isotropic steel reinforcement of bridge decks (about 0.5%) indicates that AASHTO's isotropic reinforcement provides a higher safety factors than the design presented above.

At a safety factor of 4.0 (compared to AASHTO's safty factor of 2.33), one arrives at a contact area of 510 mm x 779 mm. Repeating the above design procedure for the new safety factor (and loading condition), one arrives at 0.45% average reinforcement (average of the two directions - total of top and bottom). Following AASHTO's guide for isotropic reinforcement, using 1.5 times as much reinforcement in the bottom layers than at the top layers, the bottom and top reinforcement ratios (average of the two directions) would be 0.27% and 0.18%, respectively. Using 13mm diameter AFRP rods, bar spacings (in each direction) at bottom and top layers would be 104mm and 156mm, respectively. The final design is presented in Figure 42.
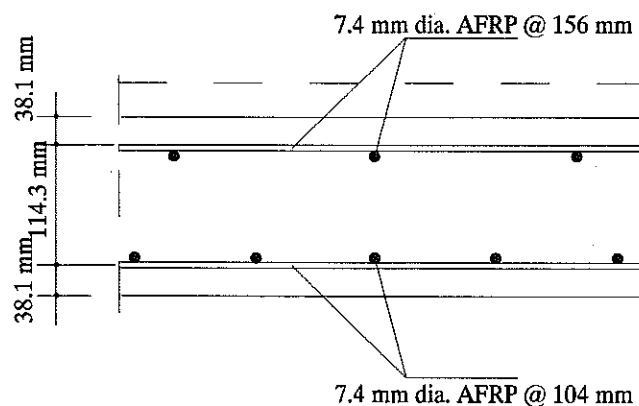
Figure 42. Final Design

5.2.3 Lap Splice Design

The JSCE equation for basic development length yields 1,494 mm and 850 mm for development lengths for the 13 mm and 7.4 mm diameter AFRP rods, respectively. JSCE does not provide sufficient information (available in English) for calculation of lap splice length. Following the logic of ACI lap splice design, noting that we have used a high safety factor, we can assume that our reinforcement ratio is more than twice that required; the lap splice lengths would thus be equal to the basic development lengths of 1,494 mm and 850 mm for 13 mm and 7.4 mm diameter AFRP rods, respectively.

5.3   EXPERIMENTAL PROGRAM FOR LABORATORY EVALUATION OF THE DECK SLAB

The effective span length for the selected bridge deck is 1,433 mm (Figure 43). We decided to use hinged supports in laboratory tests. This is because we did not recommend any special bracing of the beams; a hinged support providing no lateral restraint is thus a worst-case but plausible scenario.   Also, the span lengths presented here reflect on AASHTO's recommendations for modeling a deck supported on beams as a deck with hinged support. We have devised the experimental set-up of Figure 44 to simulate loading of HS20-44 truck on this bridge deck at a scale factor of 1.5.
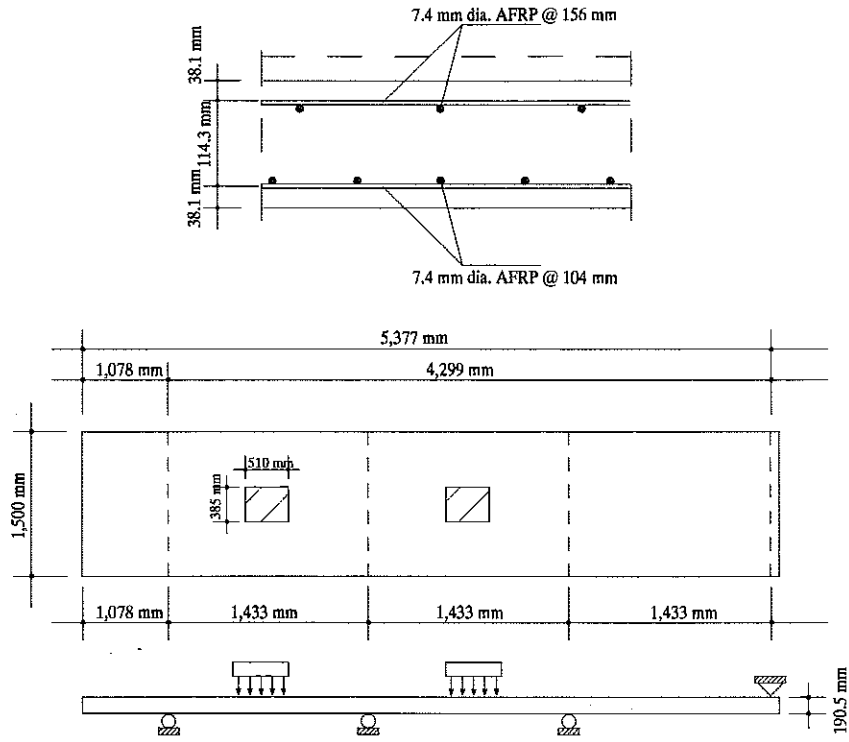
Figure 43. Prototype System.
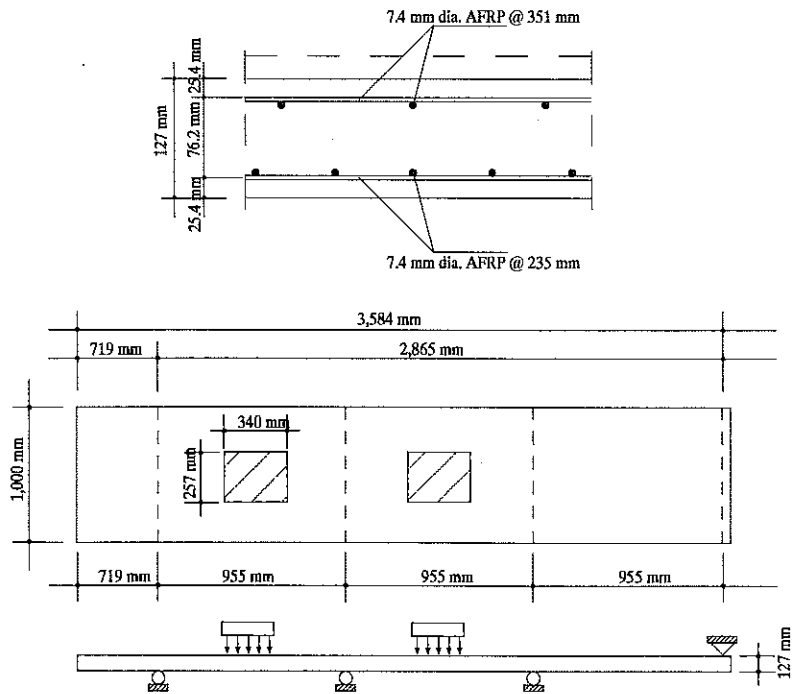
Figure 44. Experimental Set-Up.

109

The reinforcement configuration in scaled laboratory specimens is shown in Figure 45.
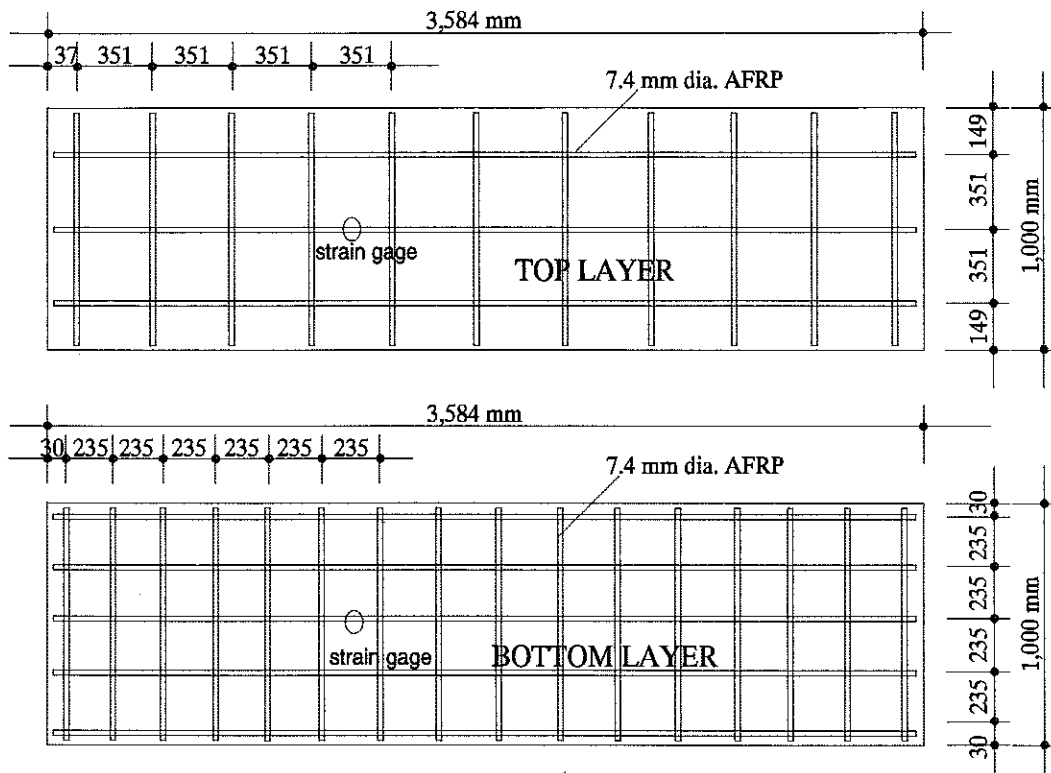
Figure 45. The Reinforcement Configuration in Scaled Laboratory Specimens.

The prototype steel reinforced concrete slab designed following AASHTO's isotropic reinforcement requirements is shown in Figure 46a; the scaled model of this slab is presented in Figure 46b. The test set-up for scaled model of steel reinforced concrete slab is shown in Figure 47.

10 mm dia. steel rebar @ 187 mm

38.1 mm

114.3 mm

38.1 mm

10 mm dia. steel rebar @ 226 mm

(a) Prototype

10 mm dia. steel rebar @ 421 mm

127 mm

25.4 mm

76.2 mm

25.4 mm

10 mm dia. steel rebar @ 285 mm
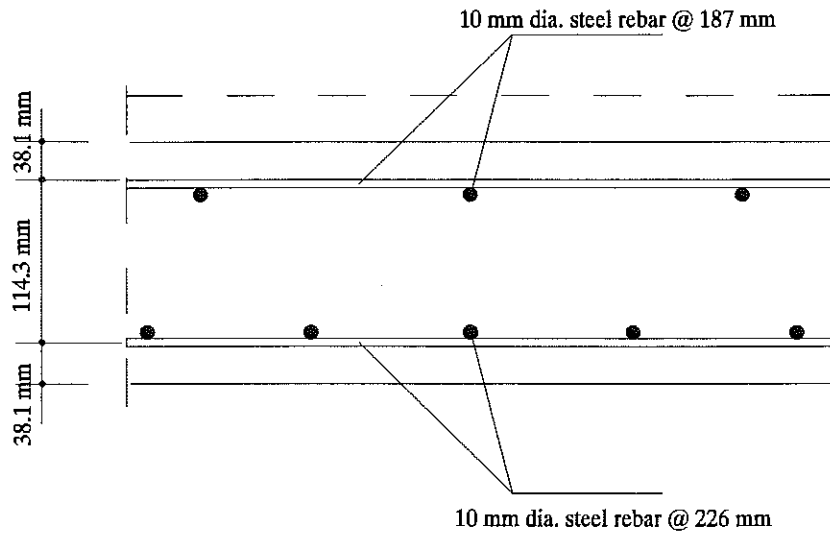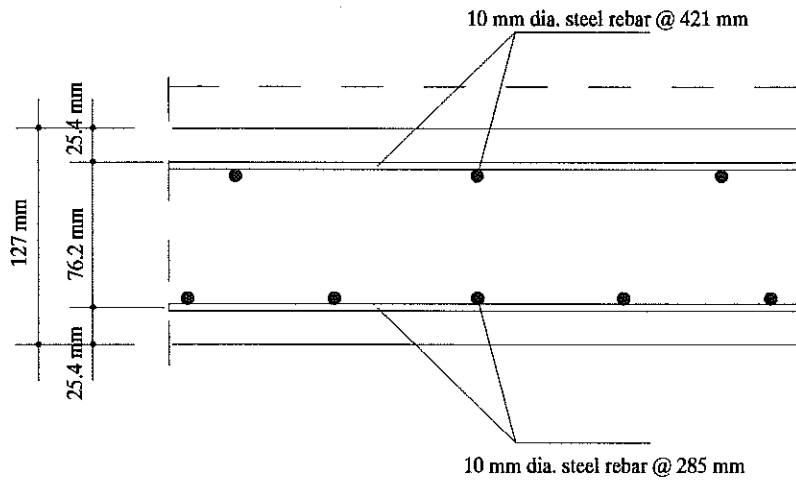
(b) Scaled Model

Figure 46. Steel Reinforced Concrete Slab Prototype and Scaled Model
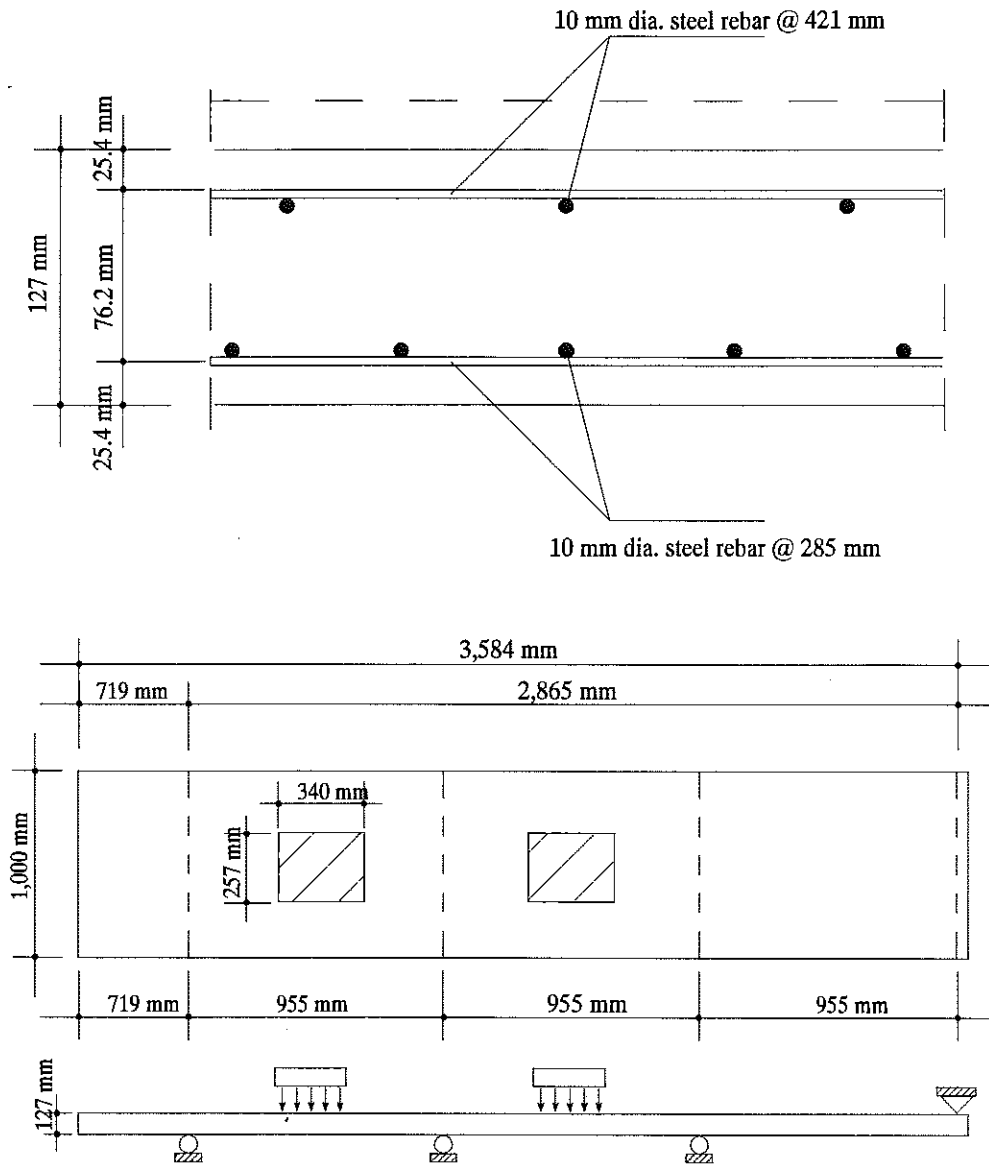
Figure 47. Test Set-Up for Scaled Model of Steel Reinforced Concrete Slab.

The quasi-static tests on the slab involve monotonic loading to failure. In the case of fatigue loading, following AASHTO's recommendations, a loading of 2 x (0.75 x 1.15 x 72.5) = 125 KN should be applied to prototype system repeatedly until failure occurred or the maximum of 2,000,000 load cycles is reached. Due to scaled modeling with same materials used in prototype, the loads applied to scaled model were 1.5^2 = 2.25 times smaller than their corresponding to prototype (this yields maximum fatigue load of 55.5 KN).

A total of 12 slabs were tested in this phase of the experimental program. The test plan is shown below.

	Technora AFRP	Steel
Static	3	3
Fatigue	3	3

Concrete mix proportions per cubic yard used in slab construction were as follows:

- ASTM Type I cement = 274.5 kg
- Coarse aggregate (max. particle size of ¾ in.) = 904.5 kg
- Fine aggregate = 488.5 kg
- Water-to-cement ratio = 0.40

Slump and air content of fresh concrete were measured prior to casting. Slump was measured in accordance with ASTM C 143-97, "Test Method for Slump of Hydraulic Cement Concrete," and air content was measured in accordance with ASTM C 231-92, "Test Method for Air Content of Freshly Mixed Concrete by Pressure Method." Slump was 114 mm and air content was 5.5%.

5.4   EXPERIMENTAL RESULTS

Figures 48, 49 and 50 show the forms with reinforcement cage, concrete placement, and surface finishing, respectively. Slab surfaces were sprayed with curing compound and cured at room temperature for seven days. At that time, the forms were removed. Three 15 x 30 cm. cylinders were prepared from the same concrete and were moist-cured and tested for compressive strength in accordance with ASTM C 39-96, "Compressive Strength of Cylindrical Concrete Specimens." Average compressive strength was 27.4 MPa at the age of 7 days, and 40.9 MPa at the test age of 28 days. Slabs were continuously kept indoors until tested.
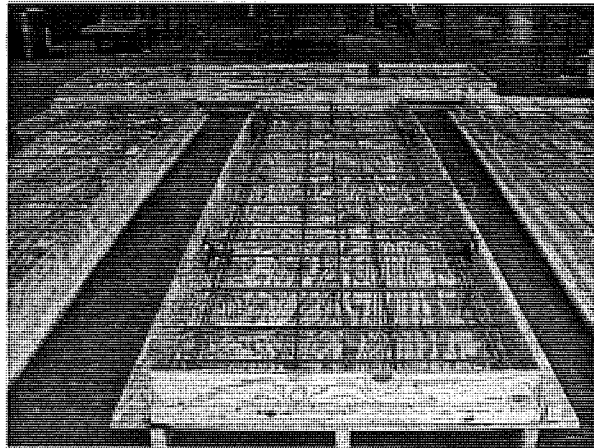
Figure 48. Slab Forms Prior to Casting.
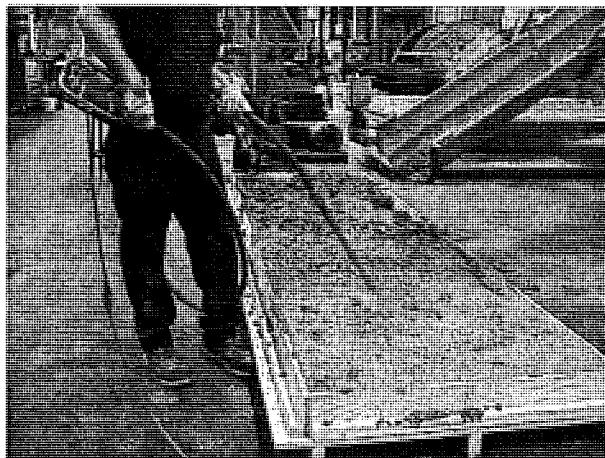
Figure 49. Concrete Placement.

114

Figure 50. Concrete Surface Finishing.

A schematic drawing of the test set-up and support system was shown in Figure 47. Figures 51 and 52 show photographs of the test set-up.
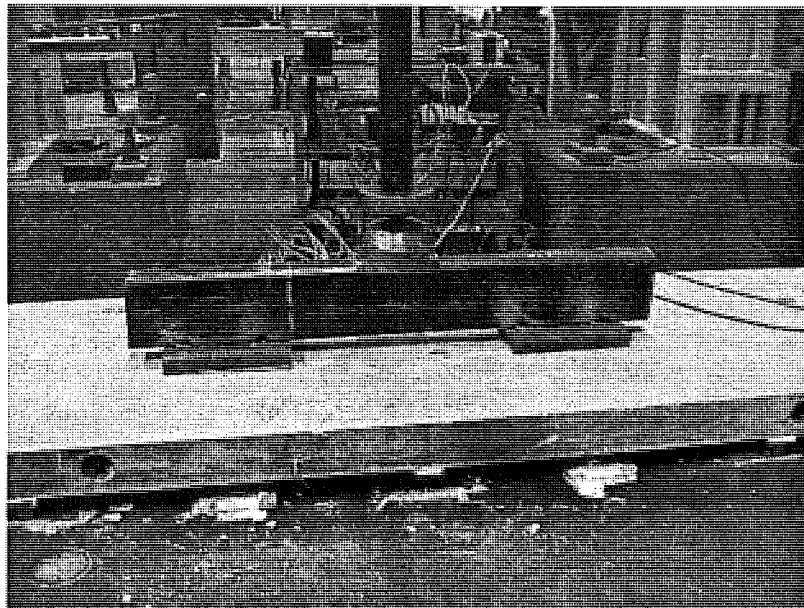
Figure 51. Test Set-Up.
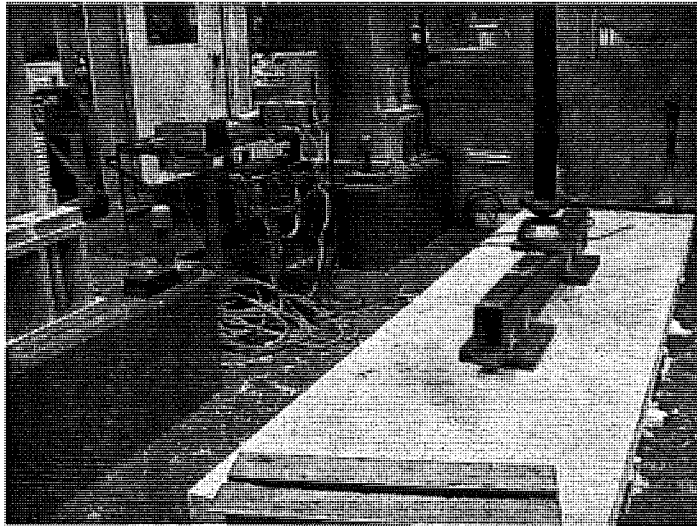
Figure 52. Test Set-Up.

Four electronic displacement transducers were attached to each slab prior to test. Two were placed near the restrained end of the slab (north side), and the other two were placed near the free end (south side). Displacement transducers on each side were placed on the transverse line passing through the center of the loading plates. Two strain gages were placed on the reinforcement in each slab. One gage was placed on the longitudinal bar and one on the transverse bar, both on the bottom layer of reinforcement (Figure 53). Both strain gages were located under the north side loading plate. The same setup was used for both fatigue and static tests. Maximum load in the fatigue test was 55,625 N. Slabs were subjected to 2,000,000 cycles at an average rate of 6 cycles per second. Testing was stopped periodically, and displacement and strain measurements in the static state were taken in static state. Measurements were taken at approximately 0 and 55,625 N.
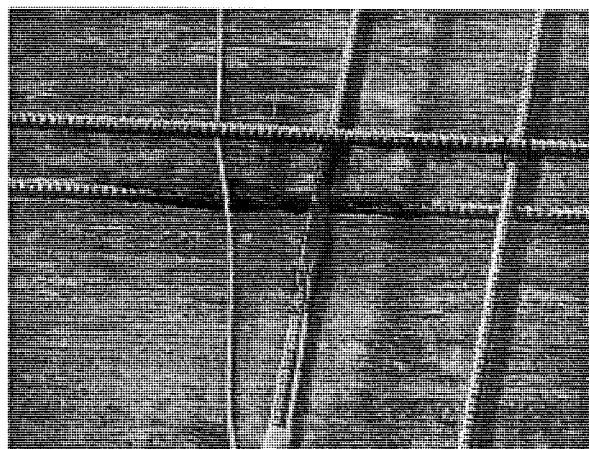
Figure 53. Strain Gage Locations.

In the static test, the slab was subjected to monotonic loading until failure. Displacement and strain were continuously measured using a digital data acquisition system. One of the steel reinforced slabs cracked during the set-up process prior to testing due to a malfunction of the testing machine, and was discarded.

5.4.2 Test Results

Fatigue test data are presented in tabular form. Tables 13 through 17 show the number of cycles, maximum and minimum loads, and deflection and strain measurements for each slab. Measurements were taken at predefined cycle intervals. The deflection reported is an average of two displacement transducer readings placed on each side of the slabs along a transverse line.

Table 13. Fatigue test data (SR Slab 1)

Cycles	Applied	North	South	Transverse	Longitudinal
Completed	Load, KN	Deflection, mm	Deflection, mm	Microstrain	Microstrain
0	0	-0.0254	0.0254	2	-18
0	55.720096	0.1016	0.127	21	21
150292	55.586656	0.1016	0.1524	20	27
150292	-0.06672	0.0254	0.0508	5	-12
540541	-0.02224	0.0254	0.4572	3	-17
540541	55.86688	0.1016	0.5842	18	23
655929	0	0.1778	0.7112	-4	-17
655929	55.817952	0.254	0.8636	11	21
1097011	0	1.2192	0.9652	-2	-16
1097011	55.7112	0.2794	1.0922	12	19
1265853	0	0.3556	1.016	-4	-18
1265853	55.973632	0.4318	1.143	11	20
1630571	-0.040032	0.381	1.016	-4	-17
1630571	55.631136	0.4318	1.143	10	19
2000000	0.182368	0.3556	0.9906	-13	-29
2000000	55.551072	0.4064	1.1176	2	7

Table 14. Fatigue test data (SR Slab 2)

Cycles Completed	Applied Load, KN	North Deflection, mm	South Deflection, mm	Transverse Microstrain	Longitudinal Microstrain
0	0.075616	0.0762	0.0254	-6	7
0	55.884672	0.4826	0.3302	1	90
31007	-0.102304	0.1524	0.2286	-11	27
31007	55.86688	0.2794	0.3302	-6	83
189986	0.204608	0.0254	1.1176	-14	30
189986	55.813504	0.2032	1.2446	-10	91
297134	0.142336	1.2954	1.5748	-15	33
297134	55.706752	1.4986	1.7272	-10	98
383117	0.262432	0.8636	1.524	-18	33
383117	55.893568	1.0668	1.7018	-13	104
505878	-0.048928	1.1684	2.3368	-21	39
505878	55.786816	1.3716	2.54	-20	113
833300	0.195712	-0.0254	0.6858	-23	36
833300	56.164896	0.2794	0.9398	-26	125
1163010	55.55552	0.2286	0.9144	-28	118
1163010	0.031136	0.0254	0.7112	-27	40
1561607	0	0.0254	0.762	-32	41
1561607	55.80016	0.2794	0.9652	-36	124
1738593	0.271328	-0.0254	0.6858	-38	29
1738593	55.475456	0.127	0.8128	-37	99
1842930	0.004448	0	0.7112	-39	34
1842930	55.849088	0.1524	0.8382	-38	107
2000000	0.217952	0.0254	0.7366	-37	36
2000000	55.506592	0.1778	0.8636	-40	109

118

Table 15. Fatigue test data (AFRP Slab 1)

Cycles Completed	Applied Load, KN	North Deflection, mm	South Deflection, mm	Transverse Microstrain	Longitudinal Microstrain
0	-0.013344	-0.0254	0	-1	-1
0	55.640032	0.0762	0.127	9	15
1144458	55.6	0.1524	0.1016	-16	-19
1144458	-0.102304	0.1524	0.1016	-16	-18
1606265	55.6	0.1778	0.127	-27	-34
1606265	0.20016	0.1778	0.127	-28	-34
2000000	0.120096	0.1778	0.127	-36	-43
2000000	55.586656	0.2794	0.254	-26	-25

Table 16. Fatigue test data (AFRP Slab 2)

Cycles Completed	Applied Load, KN	North Deflection, mm	South Deflection, mm	Transverse Microstrain	Longitudinal Microstrain
0	0.004448	-0.0254	-0.0254	0	-2
0	55.46656	0.1524	0.1016	10	40
539917	0.275776	0.0508	0.0508	-22	-27
539917	55.675616	0.2286	0.1524	-11	13
1185923	-0.057824	0.0762	0.0508	-1	-3
1185923	55.524384	0.254	0.1524	10	36
1864511	0.048928	0.0762	0.0508	-16	-15
1864511	55.871328	0.254	0.1778	-4	25
2000000	0.15568	0.1016	0.0508	-71	-80
2000000	56.262752	0.2794	0.1524	-59	-38
2000000	56.231616	0.2794	0.1524	-59	-38

Table 17. Fatigue test data (AFRP Slab 3)

Cycles Completed	Applied Load, KN	North Deflection, mm	South Deflection, mm	Transverse Microstrain	Longitudinal Microstrain
0	1.46784	-0.0254	-0.0254	0	-1
0	55.181888	0.127	0.1524	8	23
306053	1.463392	0.0254	0.0254	-15	-22
306065	55.3776	0.1778	0.1524	-10	15
720022	0.04448	0.0508	0.0762	-3	-5
720022	55.51104	0.2286	0.2032	10	39
1148472	0.2224	0.0762	0.0508	-5	-13
1148472	55.68896	0.254	0.2286	3	29
1508429	0.17792	0.0508	0.0254	-13	-22
1508429	55.46656	0.2286	0.2032	-9	32
2000000	0.062272	0.0508	0.0508	-11	-28
2000000	56.00032	0.254	0.2794	-23	42

Fatigue tests on both sets of slabs did not show any signs of failure or damage propagation. No cracks were observed on any of the slabs.

For the static tests, two AFRP and two steel reinforced (SR) slabs were tested on the same equipment that was used for fatigue test. The third slab of each set was tested on a different machine with a higher loading capacity and loaded until complete destruction. Figures 54 and 55 show the set-up used on this machine.

120
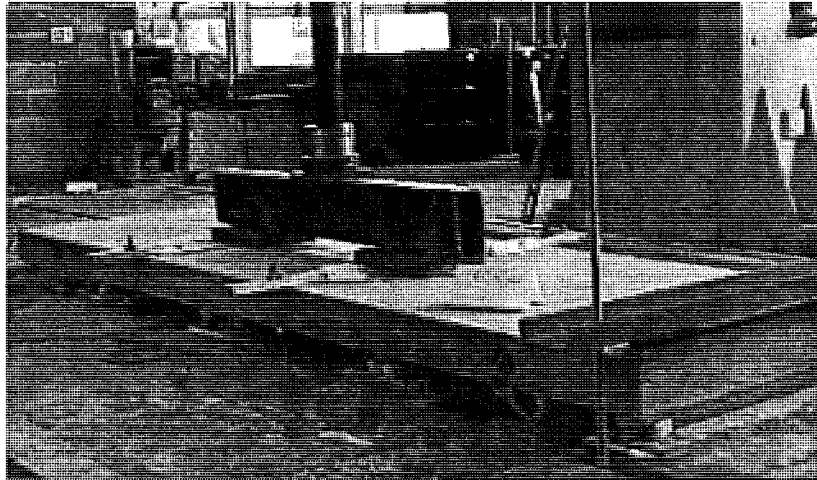
Figure 54. Test Set-Up (High Capacity Machine).
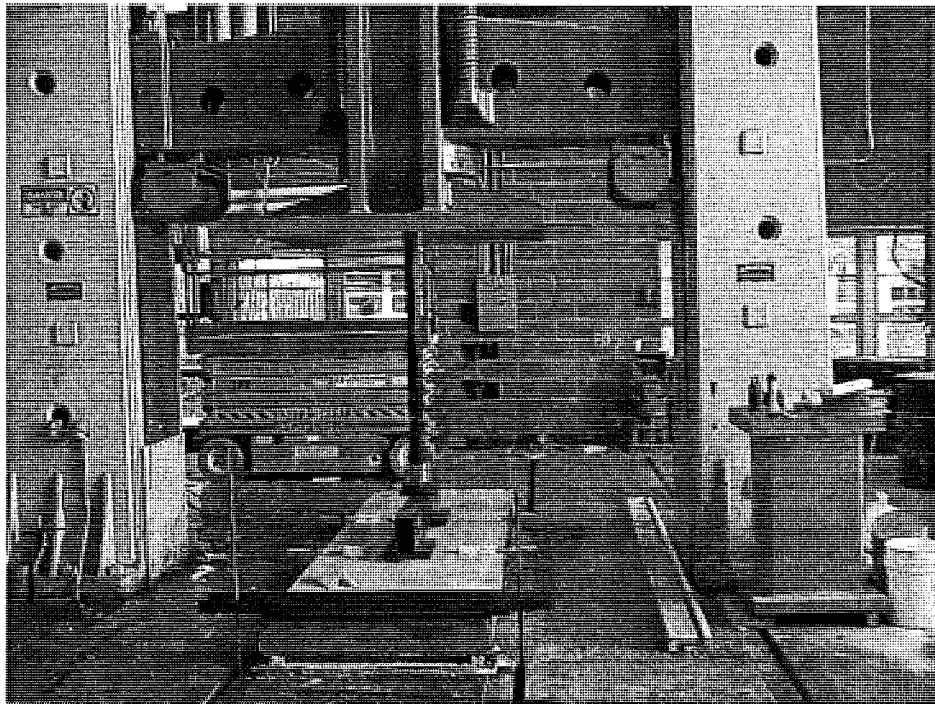
Figure 55. Test Set-Up (High Capacity Machine).

Load-deflection curves and load-strain curves of all slabs are shown in Figures 56 through 67. Figure 68 and 75 show results of tests on stronger frame where the slabs could be loaded to ultimate failure.
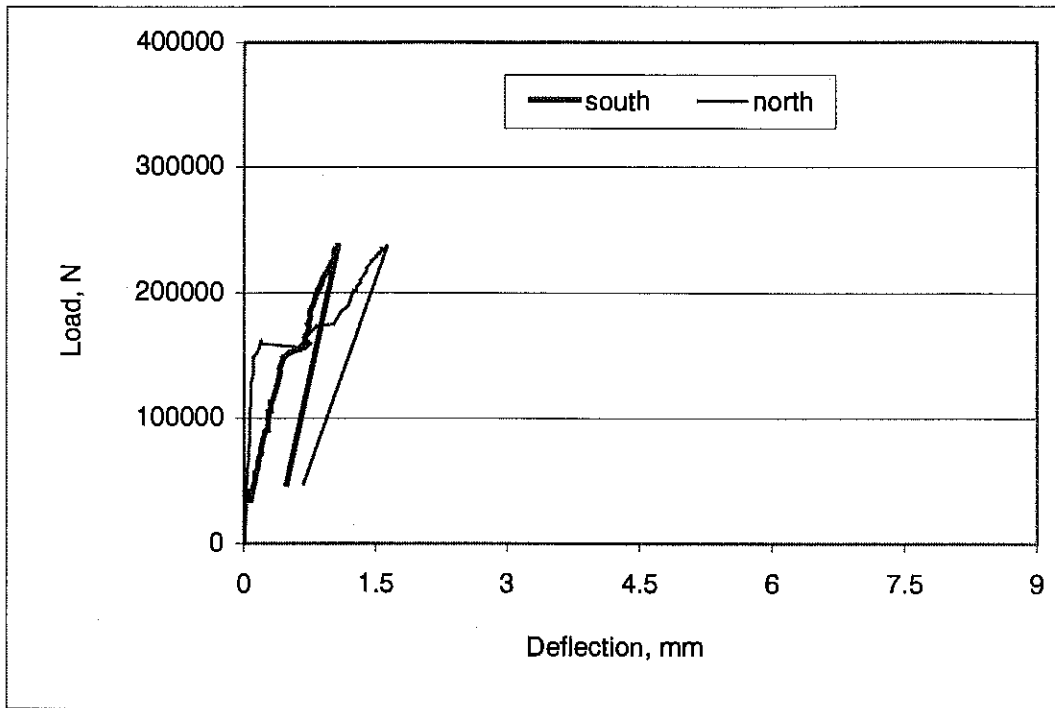
Figure 56. Load Vs Deflection for Steel Reinforced Slab
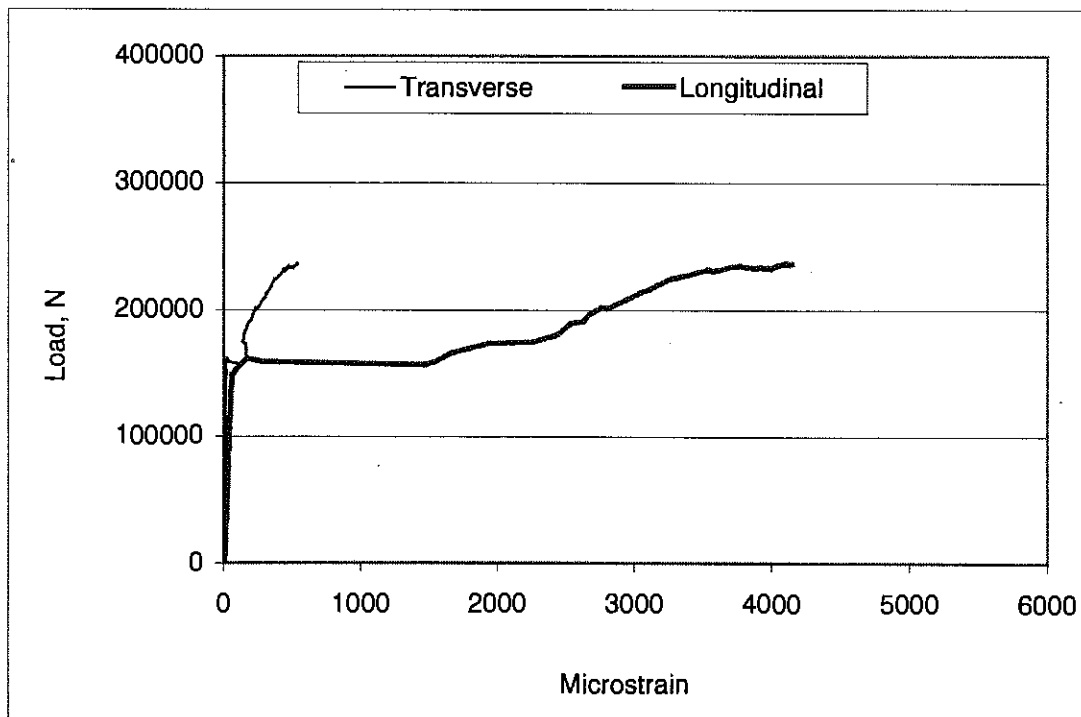
Figure 57. Load Vs Strain for Steel Reinforced Slab
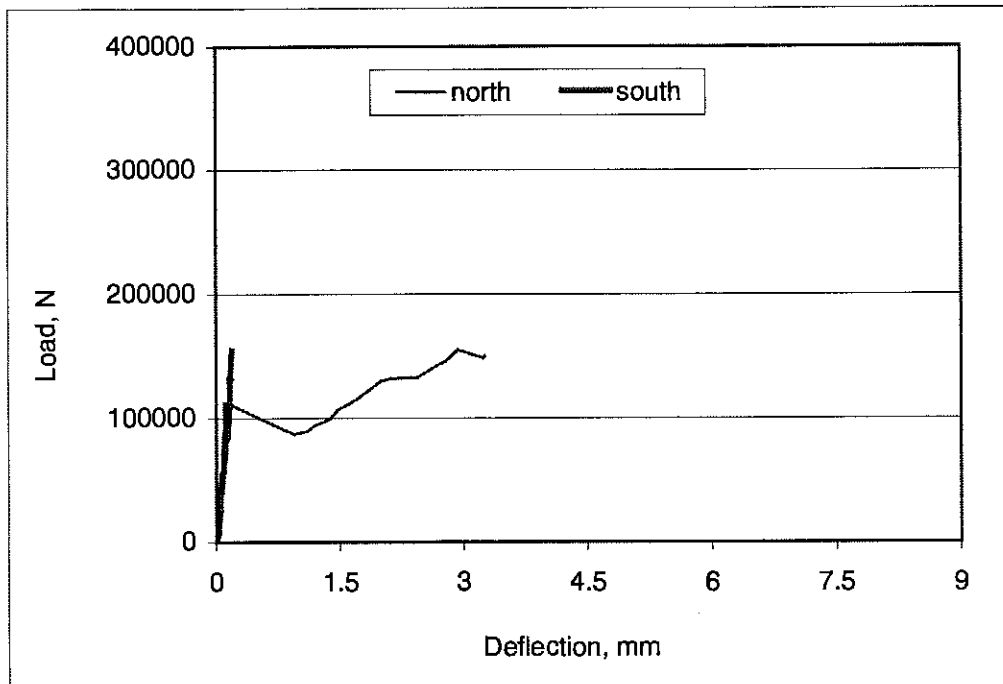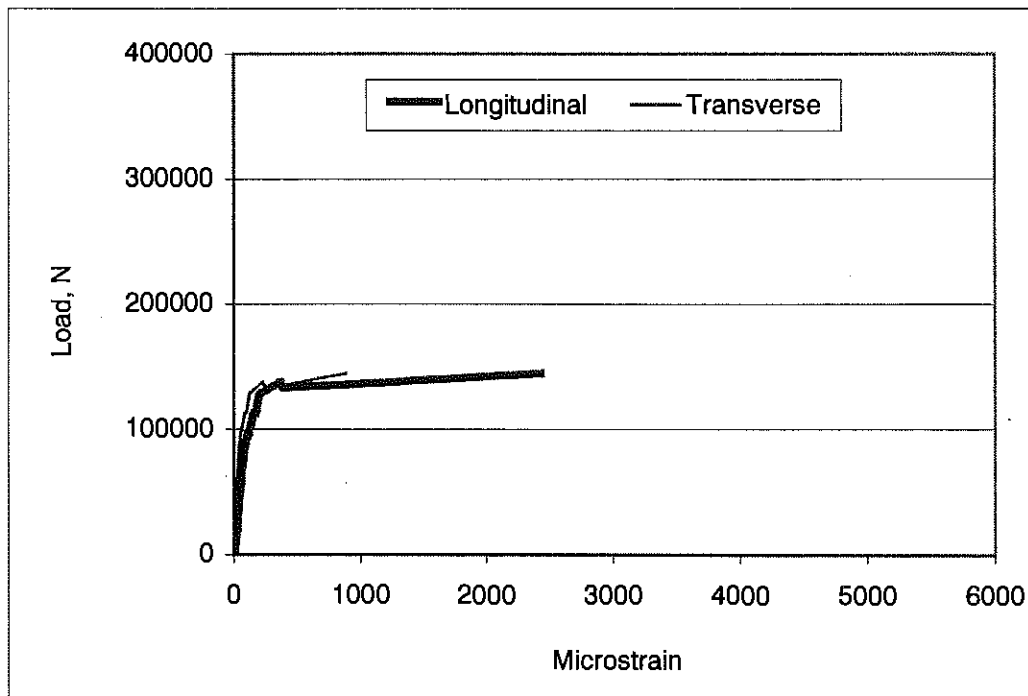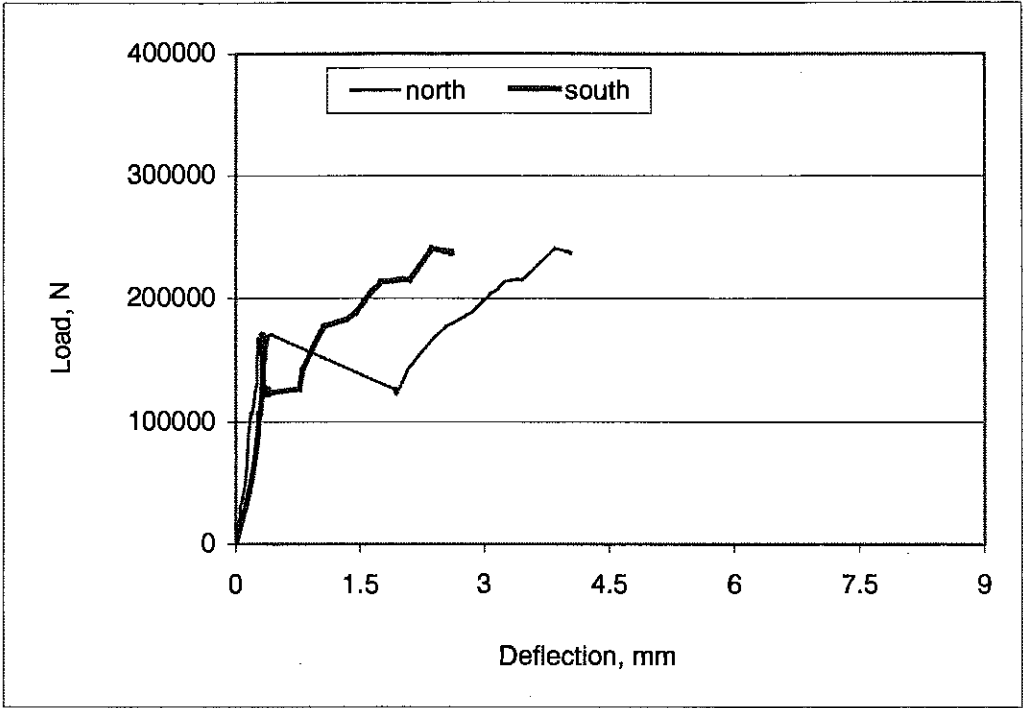
Figure 58. Load Vs Deflection for Steel Reinforced Slab
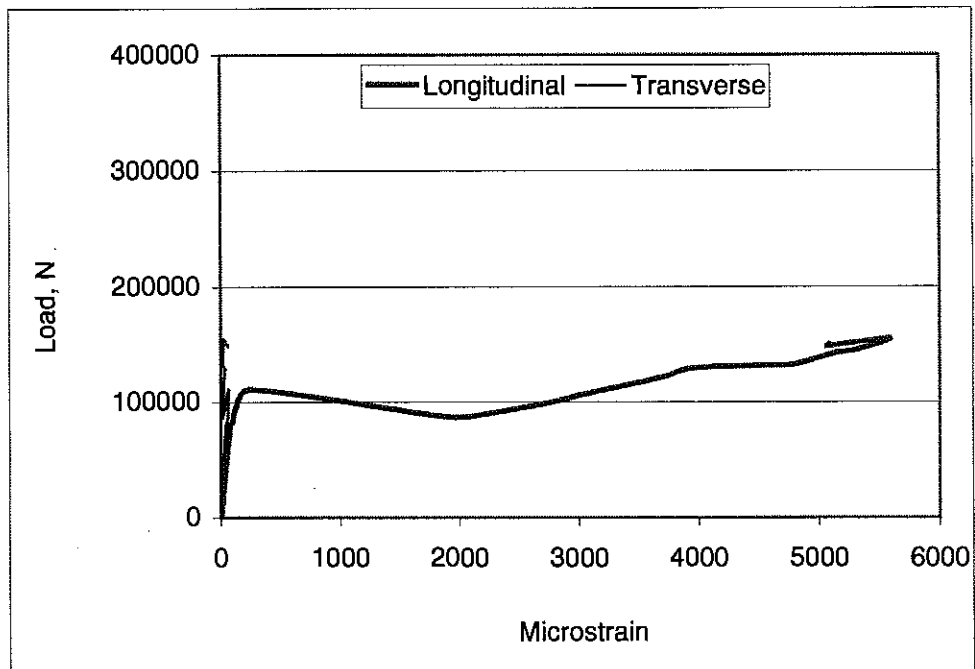
Figure 59. Load Vs Strain for Steel Reinforced Slab
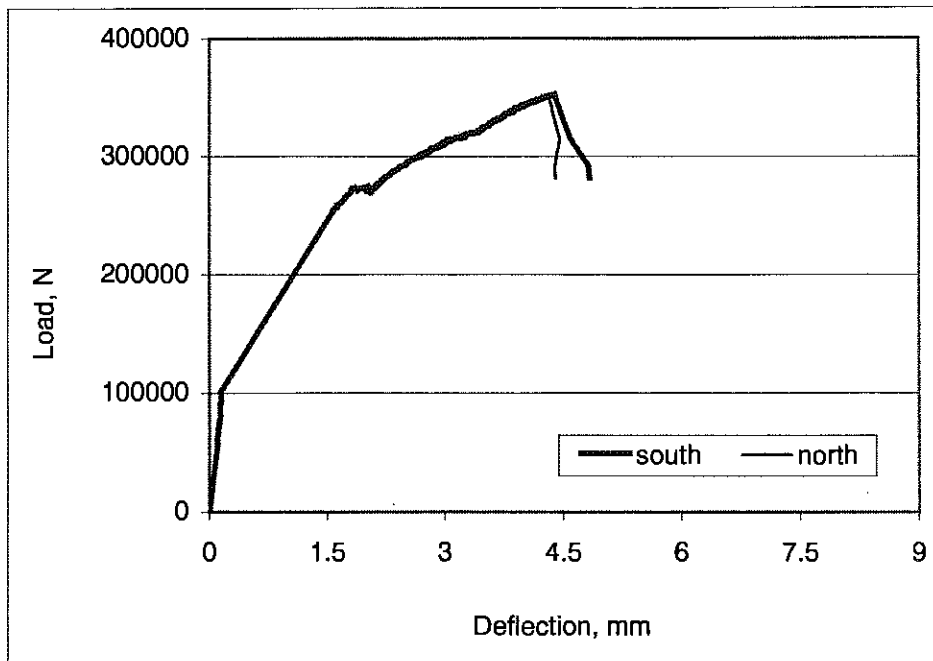
Figure 60. Load Vs Deflection for Steel Reinforced Slab
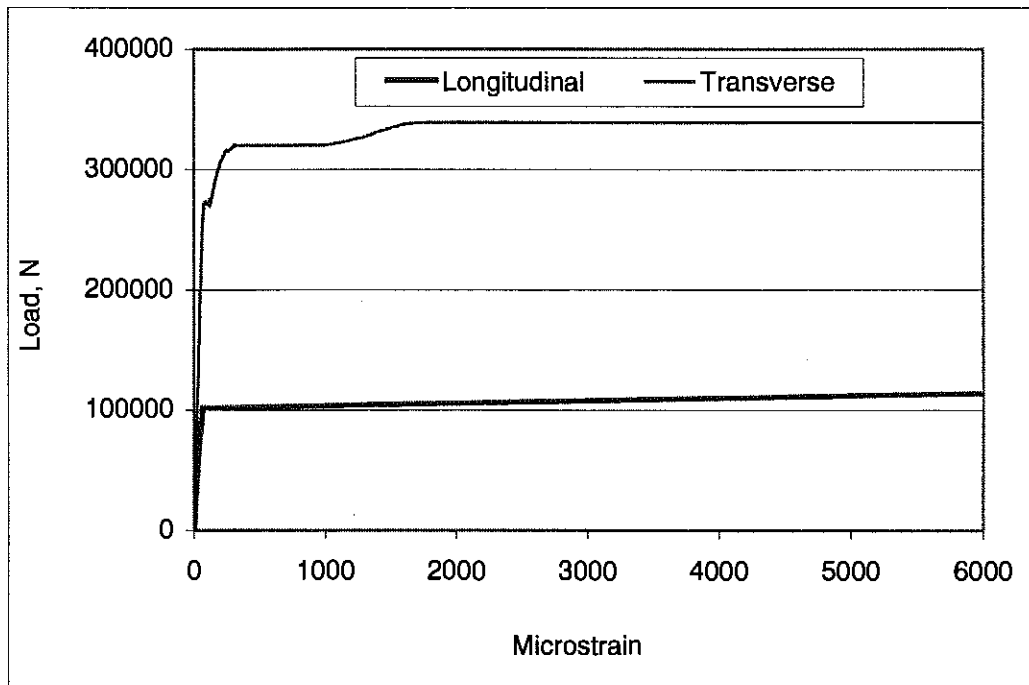
Figure 61. Load Vs Strain for Steel Reinforced Slab
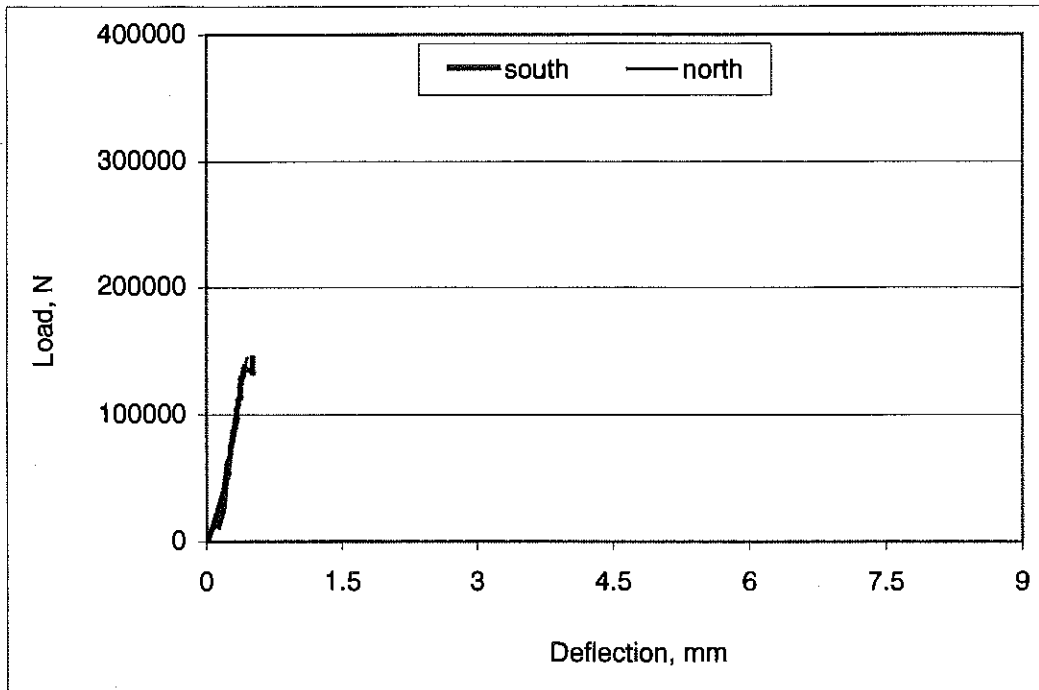
Figure 62. Load Vs Deflection for Technora AFRP Reinforced Slab

Figure 63. Load Vs Strain for Technora AFRP Reinforced Slab

Figure 64. Load Vs Deflection for Technora AFRP Reinforced Slab
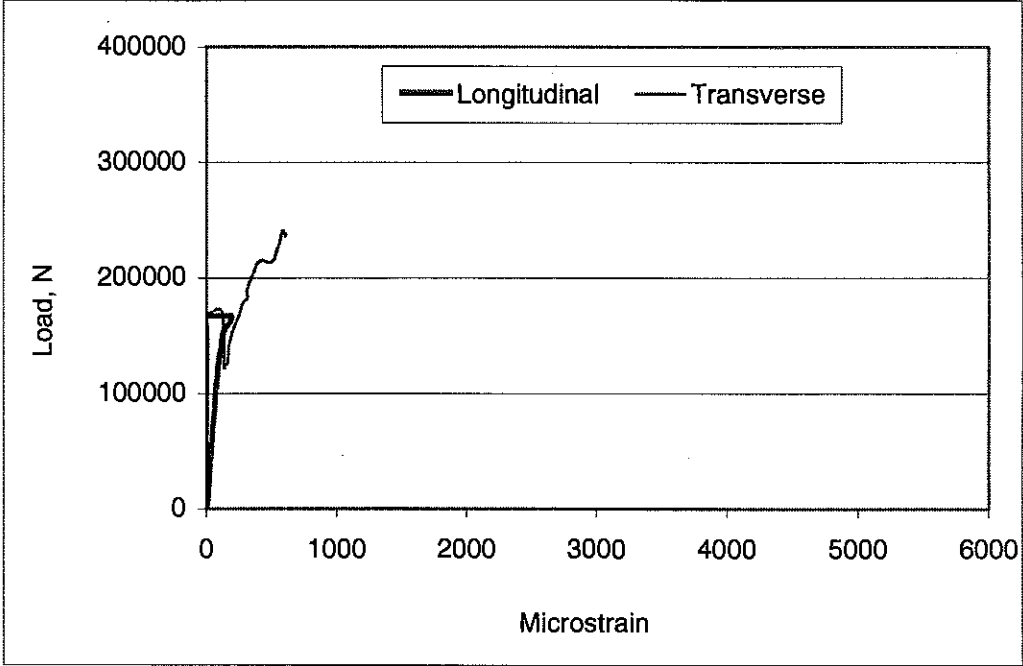
Figure 65. Load Vs Strain for Technora AFRP Reinforced Slab
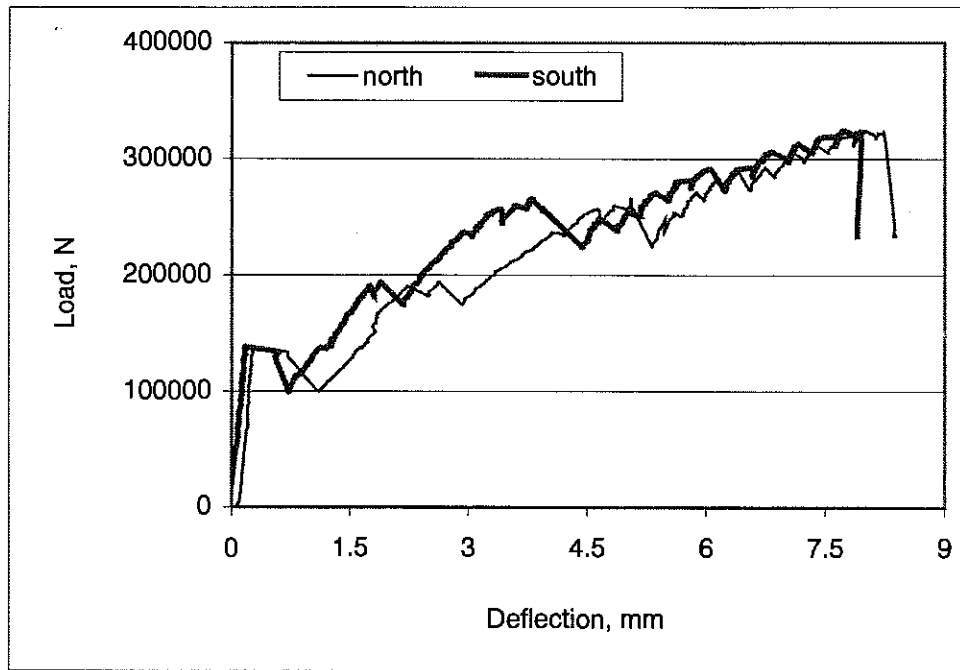
Figure 66. Load Vs Deflection for Technora AFRP Reinforced Slab
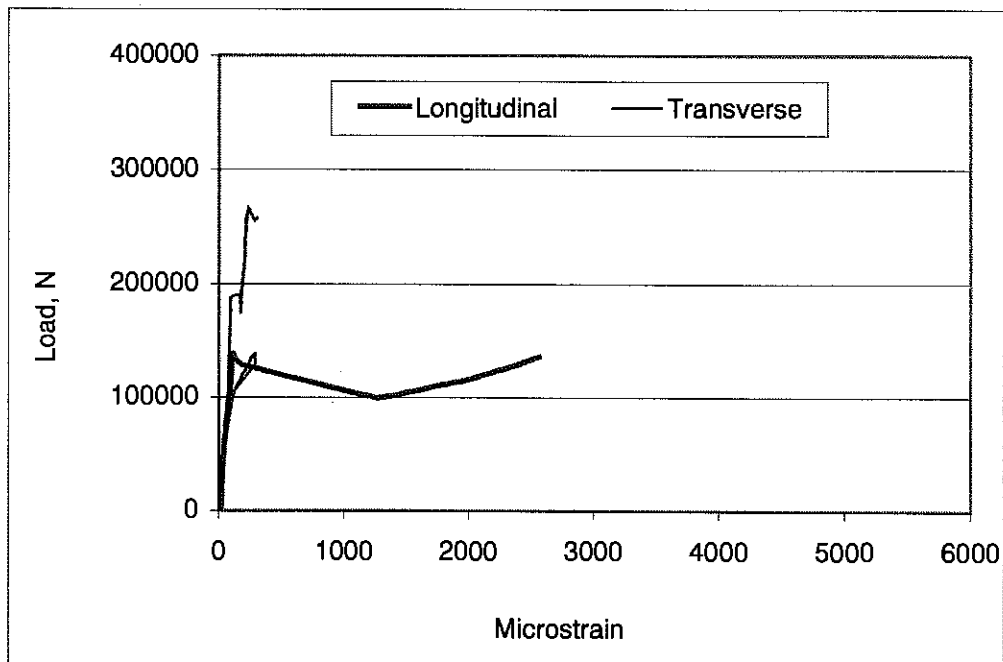
Figure 67. Load Vs Strain for Technora AFRP Reinforced Slab

Failure mechanisms for SR and AFRP slabs were similar. As the load approached 111,250, cracks started to appear over the support (negative moment) as shown in Figure 68. As load increased, cracks appeared in the mid-span (positive moment) as well (Figure 69). Crack width increased as load increased as shown in Figure 70. When the load exceeded 244,750 N (55,000 lbs), punching configuration around the loading plate (south side) near the free end of the slab started to appear (see Figures 71 and 72). An inclined crack also appeared on both sides of slabs as load increased (Figure 73). Figure 74 shows slab AFRP-6 after the test was completed. At the end of test, Slab AFRP-6 was taken apart in order to examine the AFRP bars. No bars which were ruptured or damage were found. Figures 75 shows the bars after the slab was examined.
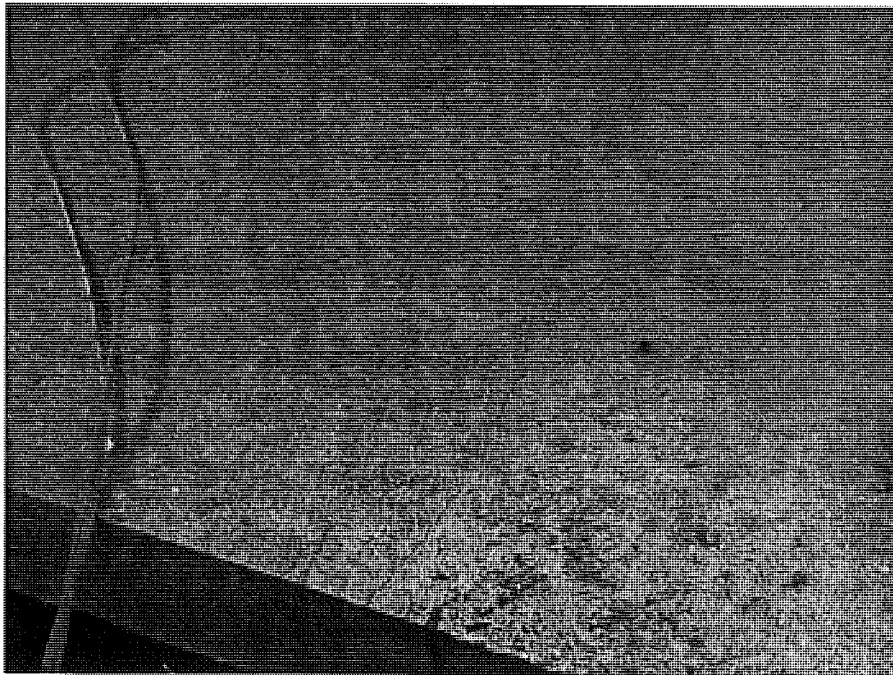
Figure 68. Starting of the Crack.
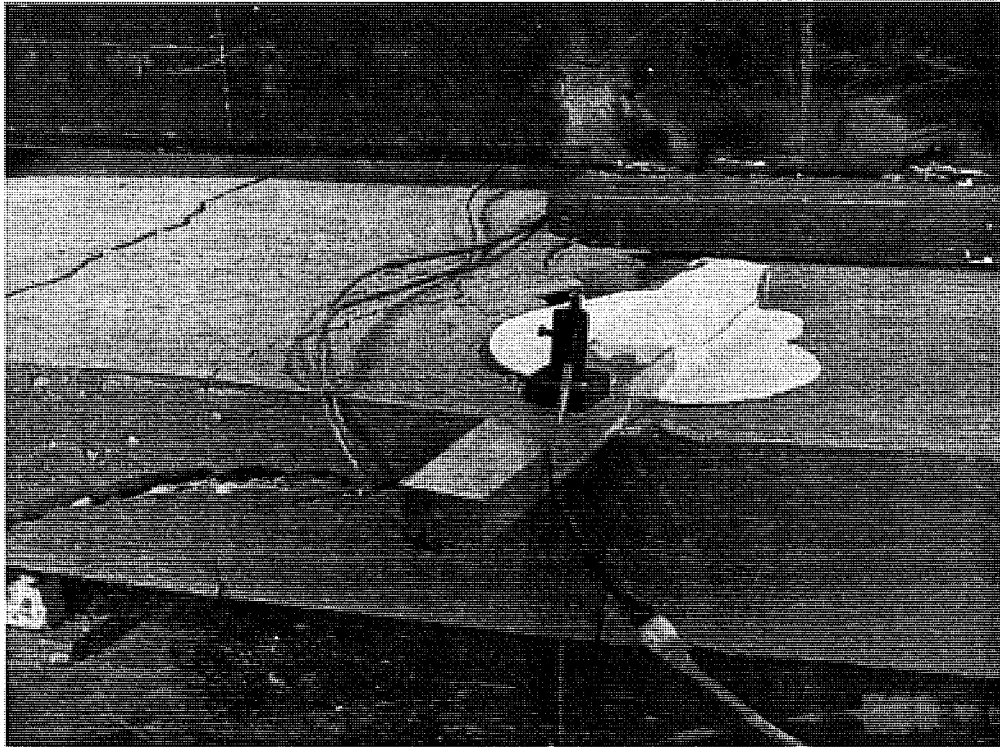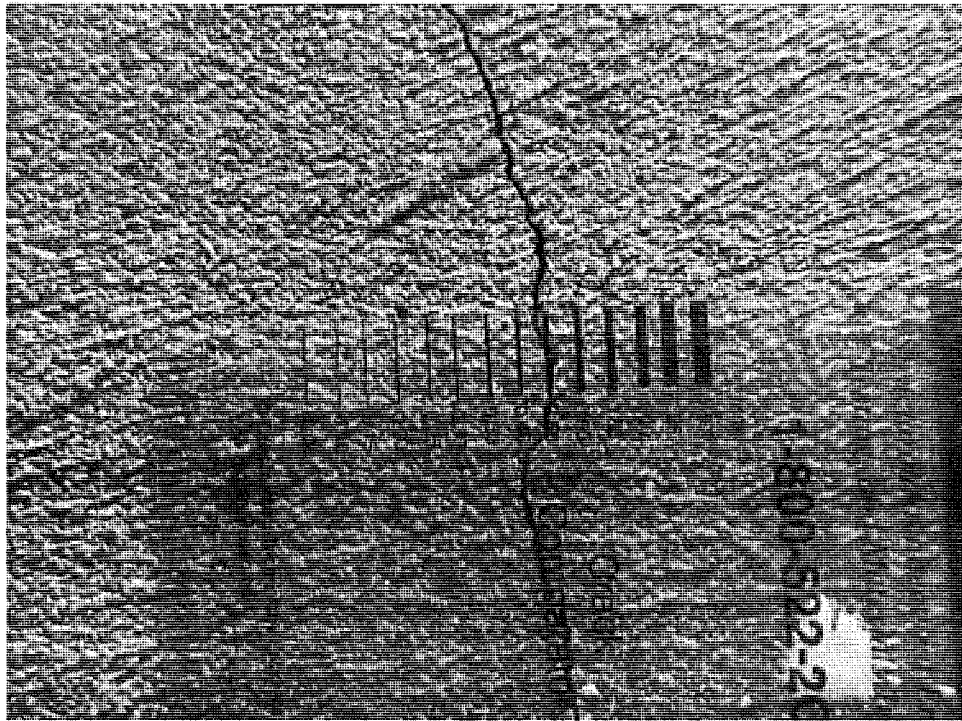
Figure 69. Crack Appears in the Mid-Span.

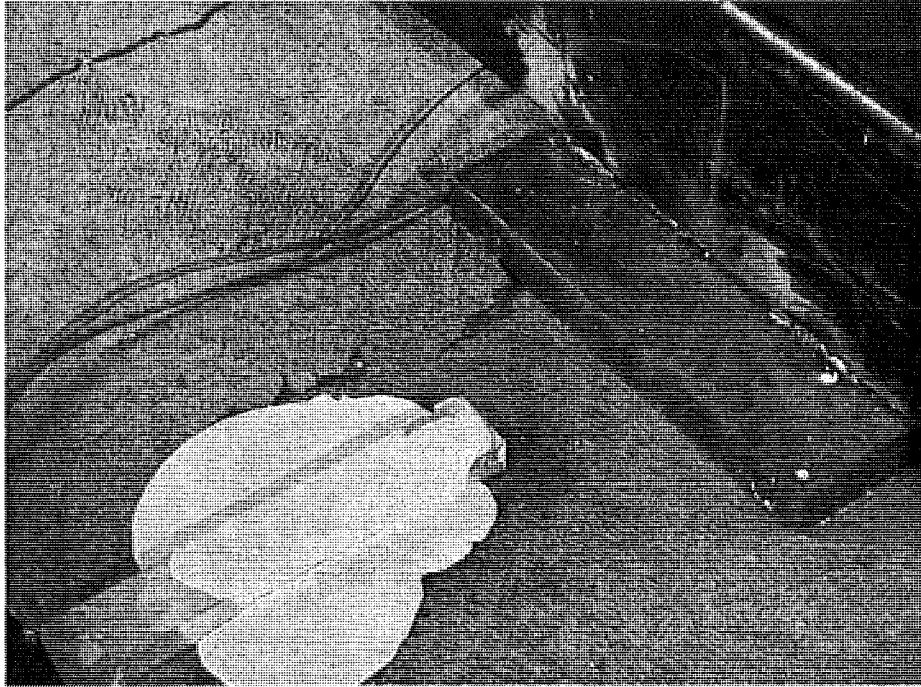Figure 70. Increased Crack Width with Load.

129

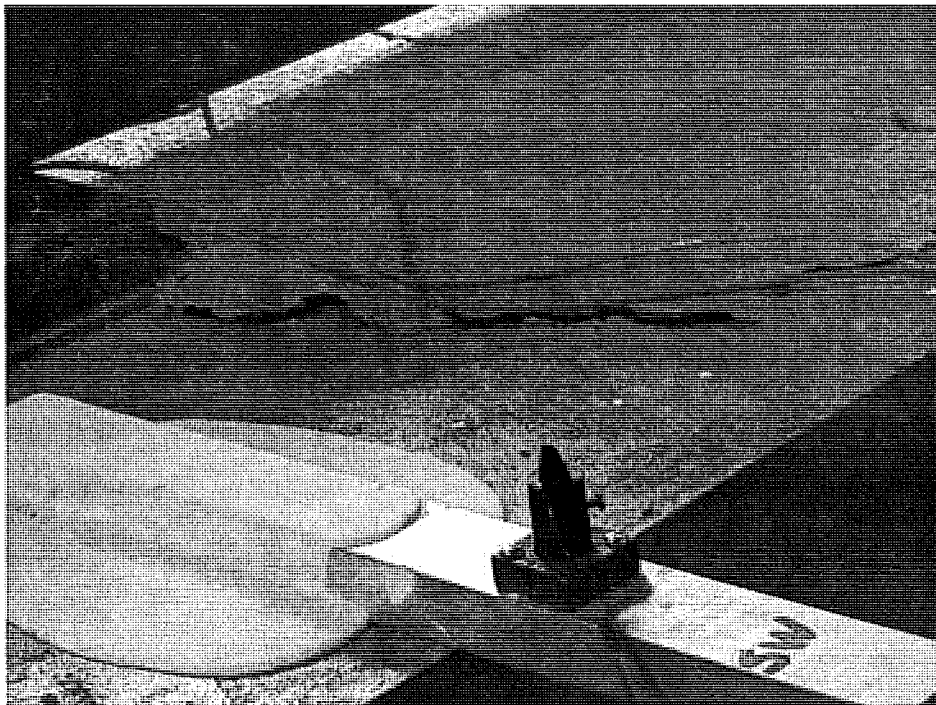Figure 71. Punching Shear Configuration.

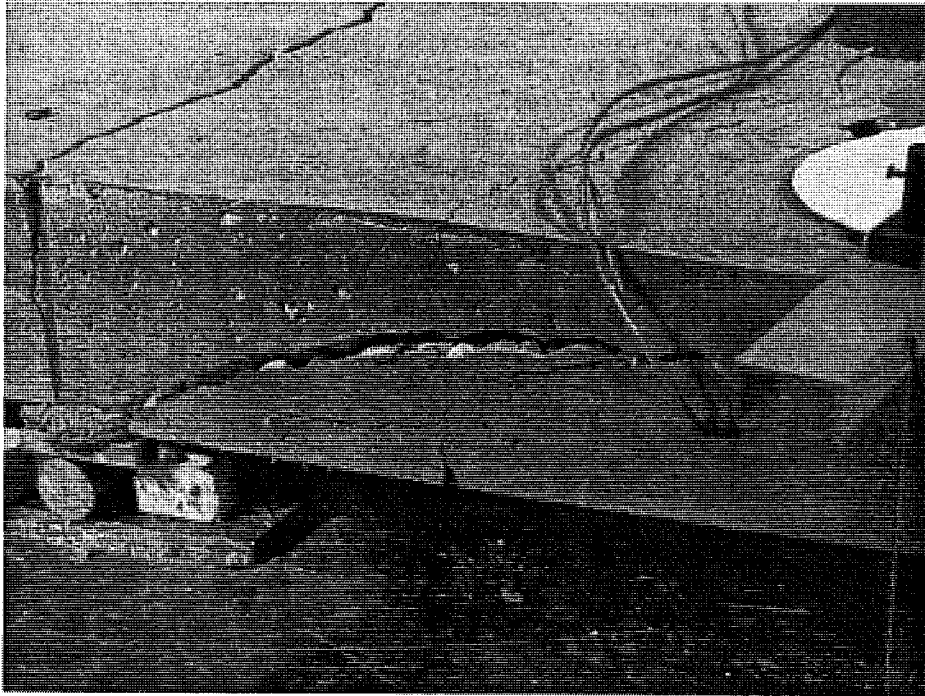

Figure 72. Punching Shear Cracks.
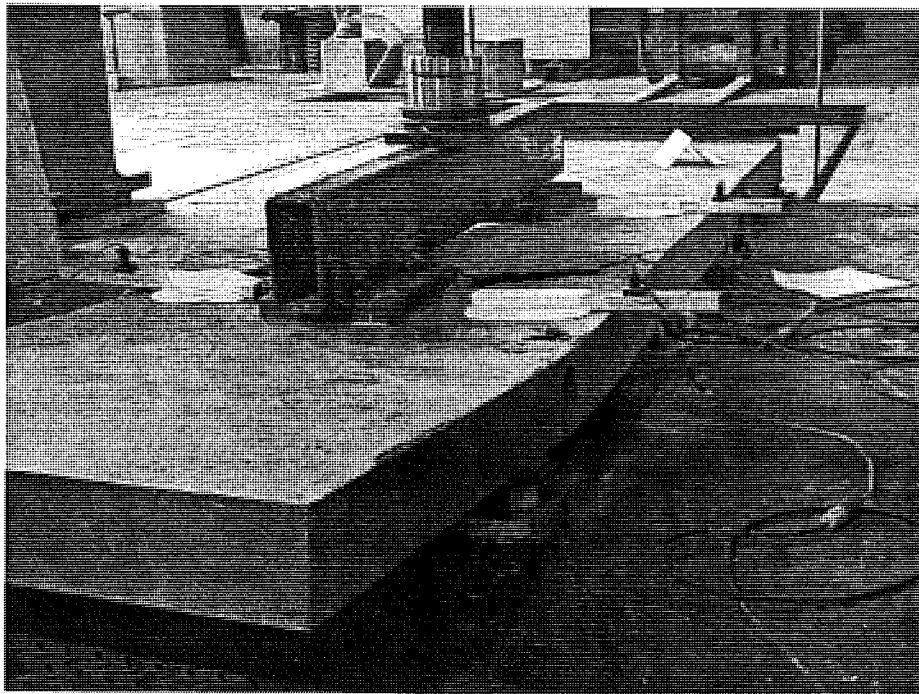
Figure 73. Inclined Cracks on the Slab Sides.

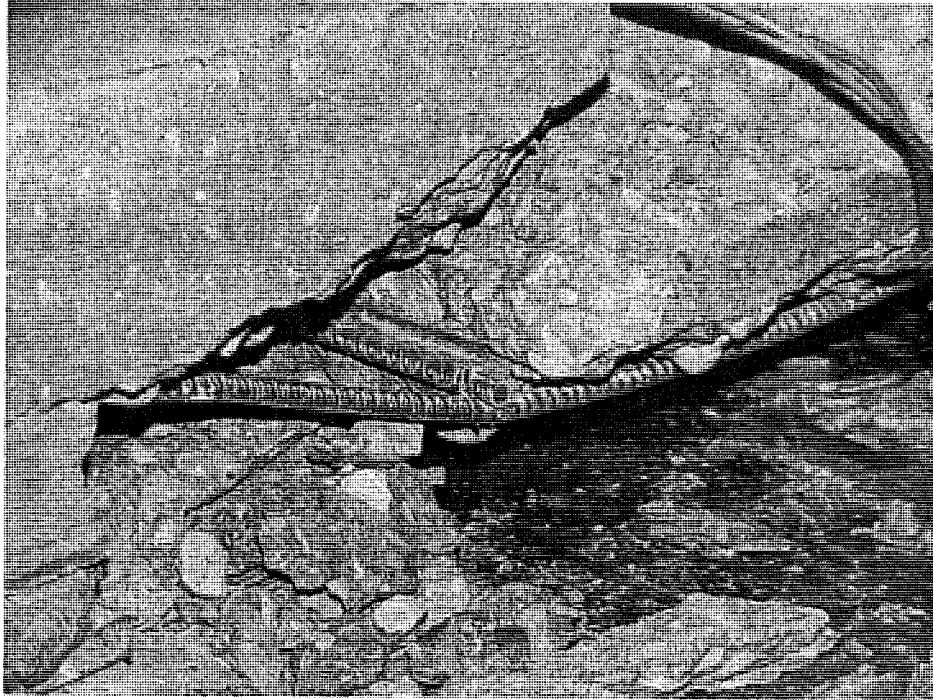Figure 74. Slab after Test was Completed.

Figure 75. Technora AFRP Positions after Test was Completed.

It can be concluded, based on the observed mechanism of failure, performance of AFRP bars is similar to that of reinforcing steel bars. Punching shear seems to play an important role in failure of the system. Technora AFRP and steel reinforced slabs provided similar capacities, which were close to levels they were designed.

6.0 FIELD DEMONSTRATION PROJECT

6.1 INTRODUCTION

The Michigan Department of Transportation (MDOT) built a demonstration project using AFRP reinforcement in a reinforced concrete bridge deck. The project received funding from the FHWA's Innovative Bridge Research and Construction Program. The bridge deck is located on M-15 in Vassar Township, Tuscola County, Michigan (see Figure 76). Figures 77a and b show the elevation and typical deck section, respectively, for this bridge. The existing steel bar reinforced concrete deck for this bridge was replaced with an aramid (Technora®) fiber composite bar reinforced concrete deck. The design for this new deck was presented in the previous chapter.

The deck section and plan view are presented in Figures 78a and 78b, respectively. Some reinforcement details for Section marked in Figure 78b are presented in Figure 78c. Bar designations AA indicate straight AFRP bars.
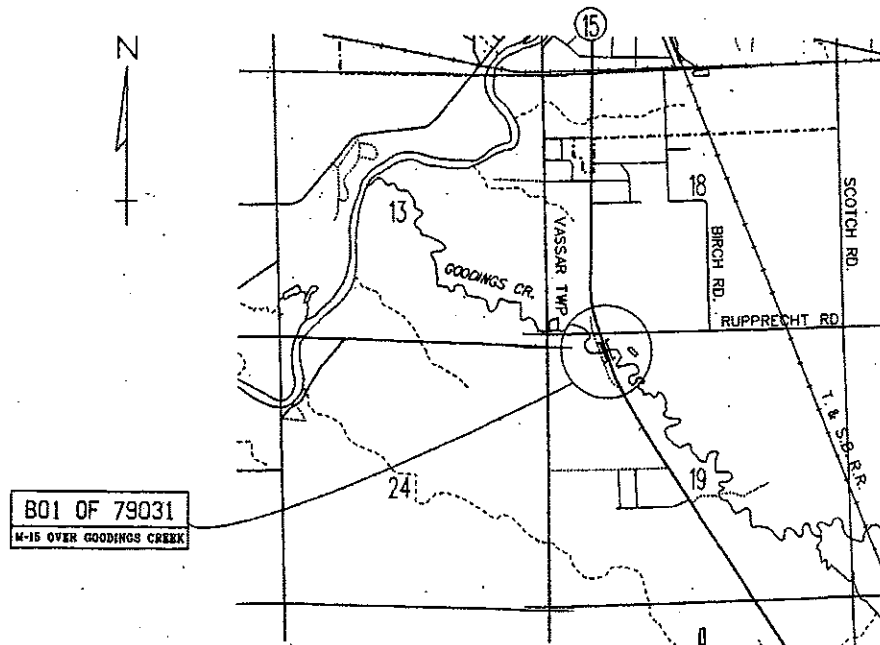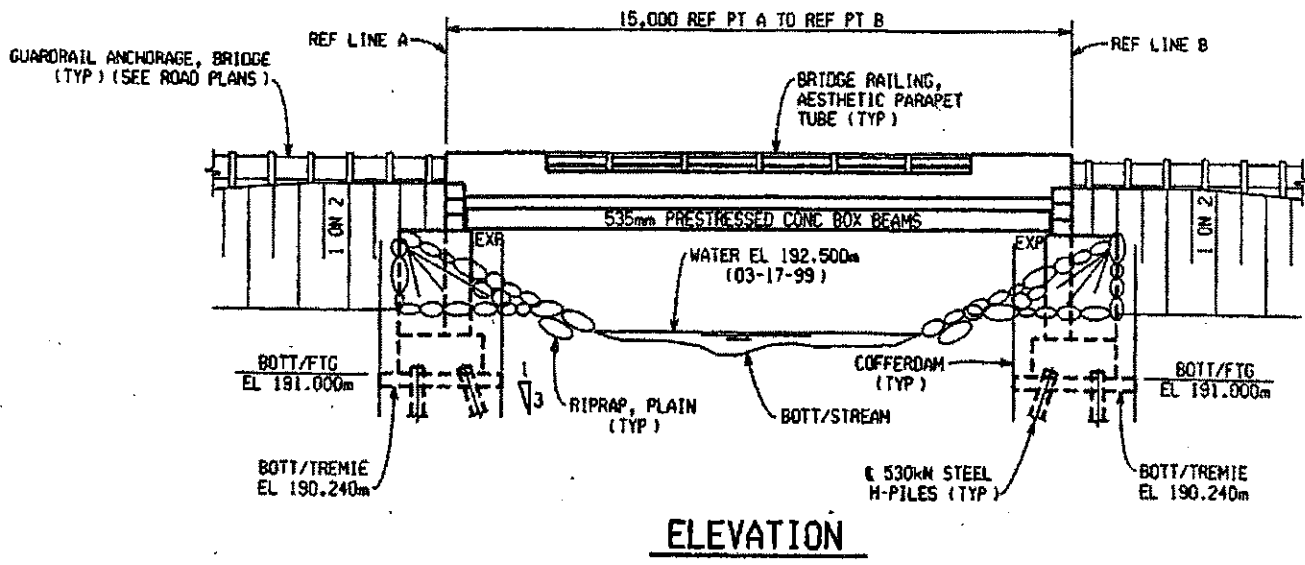

Figure 76. Location of The Bridge.

ELEVATION

(a) Elevation.

TYPICAL DECK SECTION
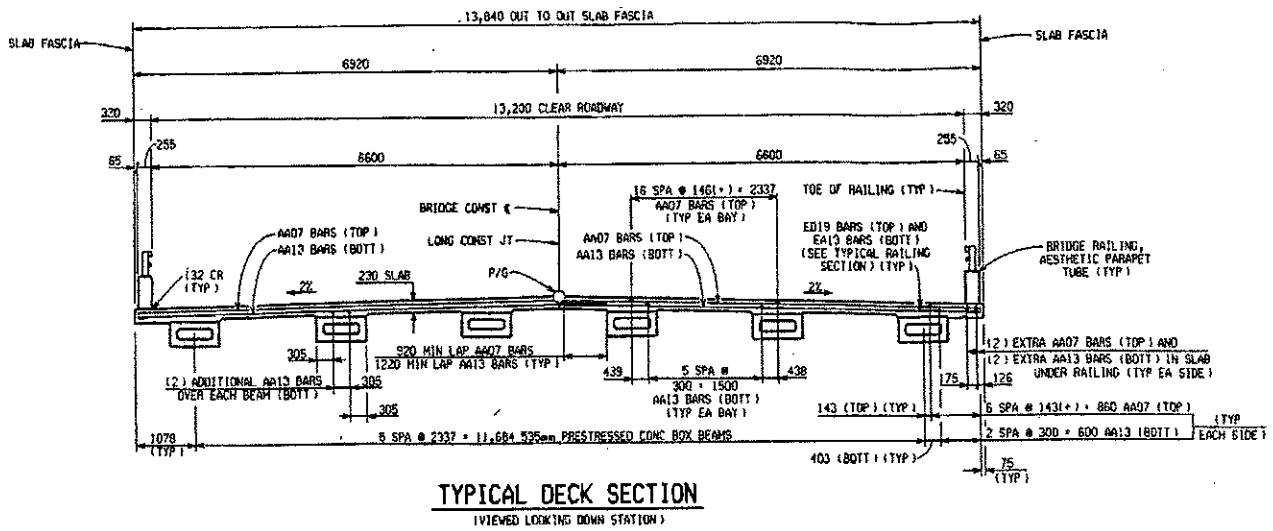### (LOOKING UPSTATION)
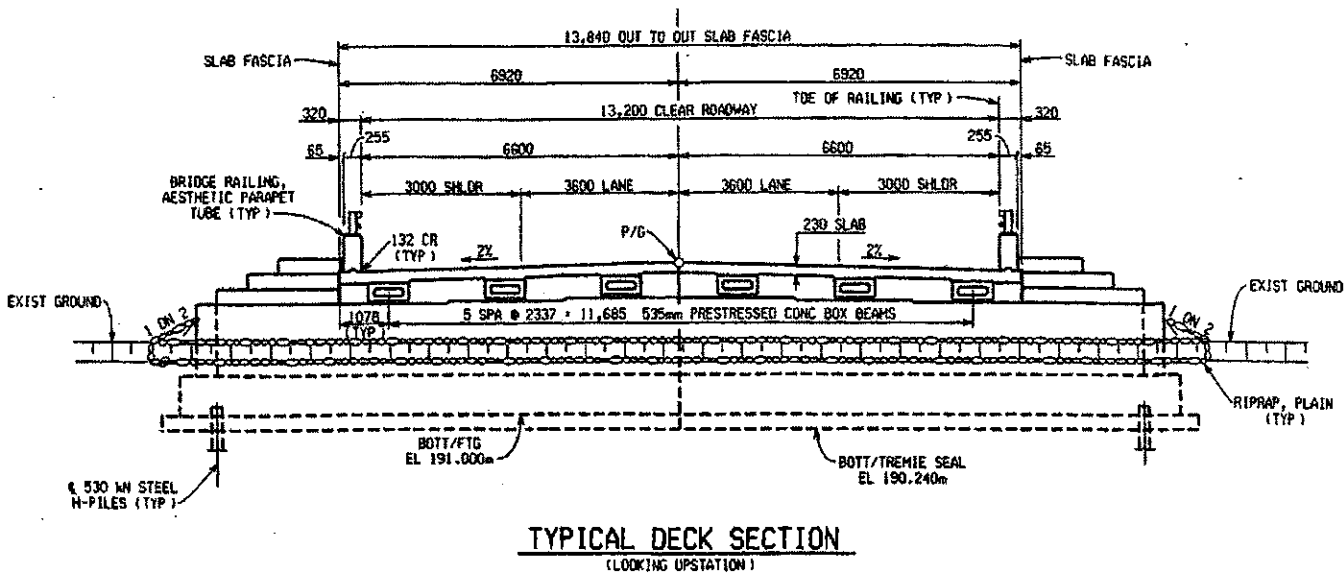
(b) Overall View of Typical Deck Section.

Figure 77. Elevation and Overall View of Typical Deck Section.

134

(a) Deck Section.

(b) Plan View.

Figure 78. Deck Section, Plan View and Reinforcement Details.

135

SECTION A-A

NOTE: WHERE OPTIONAL CONSTRUCTION JOINTS ARE USED, THERE
WILL BE NO PAYMENT FOR THE REQUIRED JOINT WATERPROOFING.

SECTION B-B

NOTE: WHERE OPTIONAL CONSTRUCTION JOINTS ARE USED, THERE
WILL BE NO PAYMENT FOR THE REQUIRED JOINT WATERPROOFING.
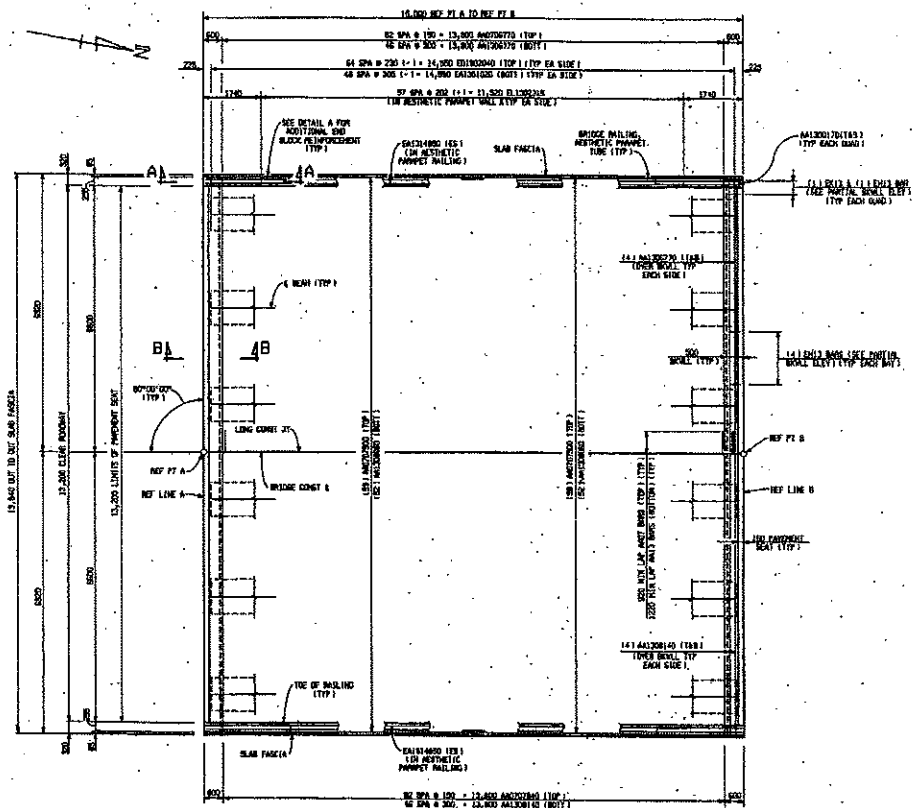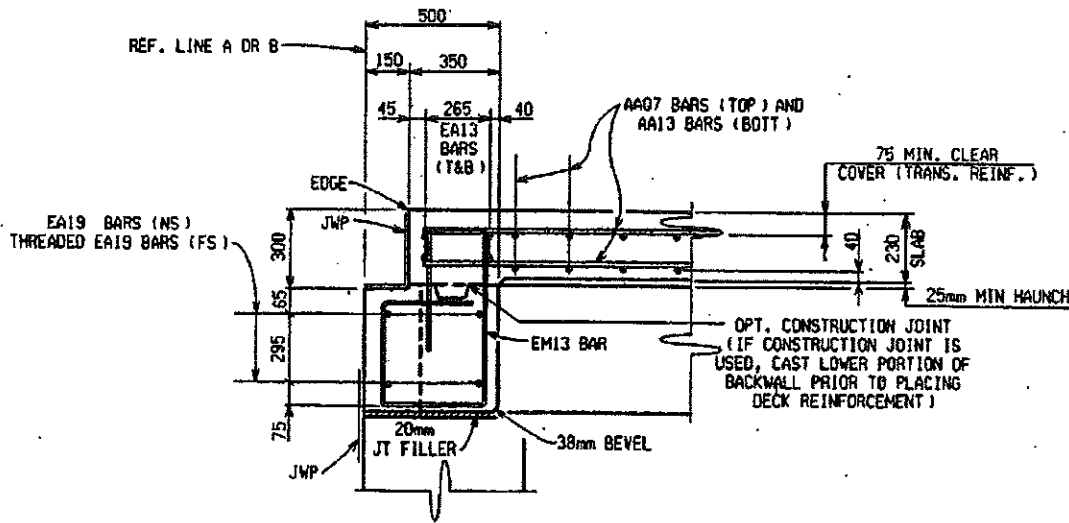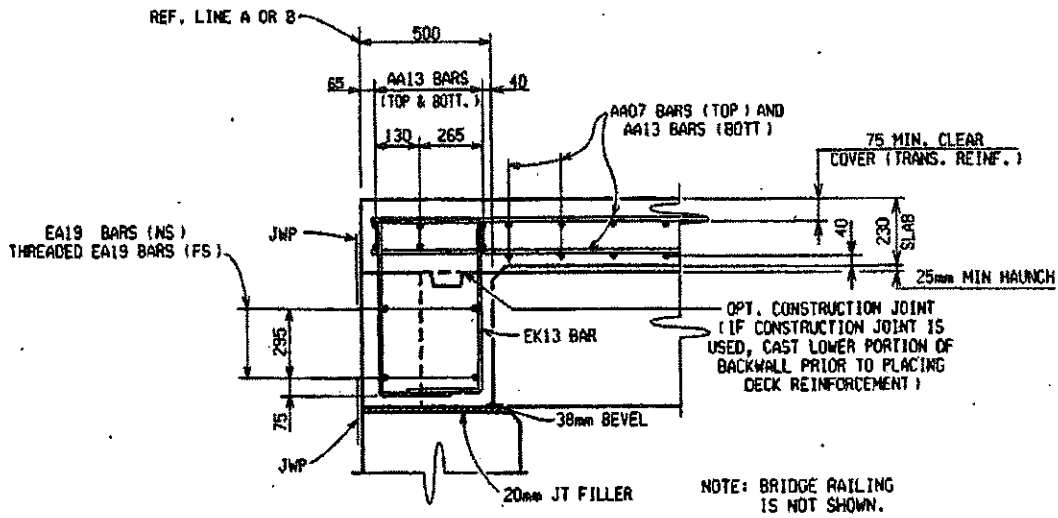
(c) Reinforcement Details

Figure 78. Deck Section, Plan View and Reinforcement Details continued).

136

6.2 CONSTRUCTION OF THE DECK AND PRELIMINARY COST ANALYSIS

The bridge deck was constructed in Summer and Fall of year 2000. The Special Provisions for construction of this deck are presented below. Some key issues covered in these provisions address cutting of AFRP rebars and repair of cut ends, supporting on chairs, and general protection of AFRP rebars during storage and construction.

MICHIGAN

DEPARTMENT OF TRANSPORTATION

SPECIAL PROVISION

FOR

ARAMID FIBER REINFORCED POLYMER (AFRP)

C&T:DAJ

07-16-99
C&T:APPR:RDT:JTL 09-03-99

a. **Description.**-This work shall consist of furnishing and installing Aramid Fiber Reinforced Polymer (AFRP) reinforcement in structural concrete. This work shall be done in accordance with Subsection 706.03.E of the 1996 Standard Specifications for Construction, except as modified herein; i.e. - in the referenced subsection, "AFRP reinforcement" shall be substituted for "steel reinforcement."

b. **Materials.-**

1. AFRP reinforcement shall be Technora Deformed Shaped Rod distributed by:

TEIJIN SHOJI (U.S.A.), INCORPORATED.

42 West 39th Street,

6th Floor, New York,

NY 10018, U.S.A.

Tel: 212-840-6900

Fax: 212-719-9656

E-Mail : tyoshimura@teijinshoji.com

Att : Mr.T.YoShiMura

2. The delivery time for the AFRP Reinforcement is approximately 80 calendar days.

c. **Construction Methods**

1. The AFRP reinforcement shall be stored away from heat and direct sunlight under waterproof sheeting.

2. The AFRP reinforcement placed in the deck shall be covered to prevent exposure to the sun's ultraviolet rays and to moisture when the concrete for the deck has not been cast within one week from the time of placing the reinforcement.

138

3. The AFRP reinforcement shall be cut using a high-speed grinder. Cut ends shall be repaired using an epoxy as recommended by the manufacturer.

4. Bending.- The AFRP reinforcement shall not be bent.

5. For bridge decks, spacing of bar chairs for AFRP reinforcement shall be one half of that required for steel reinforcement.

6. For bridge decks, the upper layer of AFRP reinforcement shall be securely tied to the structural steel, stud shear developers, slab ties, or other structural components at no greater than 750 mm intervals along each beam or girder.

7. Mechanical splicing of AFRP reinforcement is not permitted.

8. Nicks and gouges in the AFRP reinforcement is cause for rejection and replacement.

9. For bridge decks, plywood (12 mm minimum thickness) walkways shall be placed on installed AFRP reinforcement. Foot traffic on exposed AFRP reinforcement is not permitted.

d. Measurement and Payment-The completed work as measured for Aramid Fiber Reinforced Polymer (AFRP) Reinforcement will be paid for at the contract unit price for the following pay items:

Contract Item (Pay Item)   **Pay Unit**

Reinforcement, AFRP 7.4 mm Diameter... ... ...meter

Reinforcement, AFRP 13 mm Diameter... ... ...meter

The item of Reinforcement, AFRP, will be paid for by the meter for the specified diameter of the-bar, and consists of furnishing and installing all component materials as specified in the Special Provision and on the plans.

Figure 79 presents overall views and some details of the bridge deck reinforcement. Figure 80 shows an overall view of the formwork for the bridge deck. Placement and consolidation of concrete for the deck followed conventional concrete construction practices except where modified by the Special Provisions. The AFRP reinforcement suffered some damage during preparation and construction, which highlights the need for careful handling of composite reinforcement. As shown in Figure 81a, the ends of some AFRP bars become frayed if not protected by an epoxy as specified. The contractor sometimes did not place plywood over the reinforcement before walking on the reinforcement cage. However, this did not appear to damage the bars. Another practical issue with aramid FRP was lack of compact splices; the 1.22 meter lap splice lengths presented a problem for the contractor at the longitudinal construction between the staged construction. The long lay lengths interfered with placement of temporary sheet piling between construction stages. The long lay lengths also interfered with placement of foundation piles at the abutments.

Unlike with conventional steel reinforcement, the AFRP bars could not be bent to allow clearance (and then straightened later). Because of the interference with temporary sheet piling and foundation piles, the contractor was tempted to bend the AFRP bars. This action resulted in 13 of the top 7.4 mm diameter bars, and 7 of the bottom 13 mm diameter bars being damaged. The damage ranged from mild (i.e. breaking of a few of the outside aramid strands) to more severe (i.e. breaking of many of the strands resulting in a frayed look to the bar). To account for the damaged bars, the contractor was instructed to drill holes in the stage 1 bridge deck, each side of the damaged bar, and set the same size AFRP rebar into the hole with a structural epoxy. The retrofit is shown in Figure 81c.
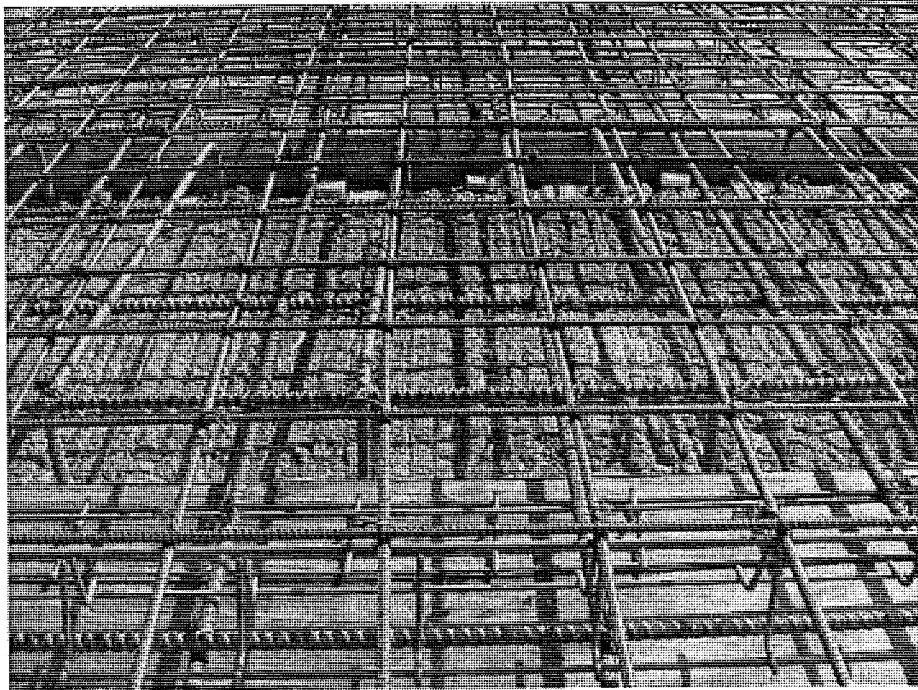
(a)
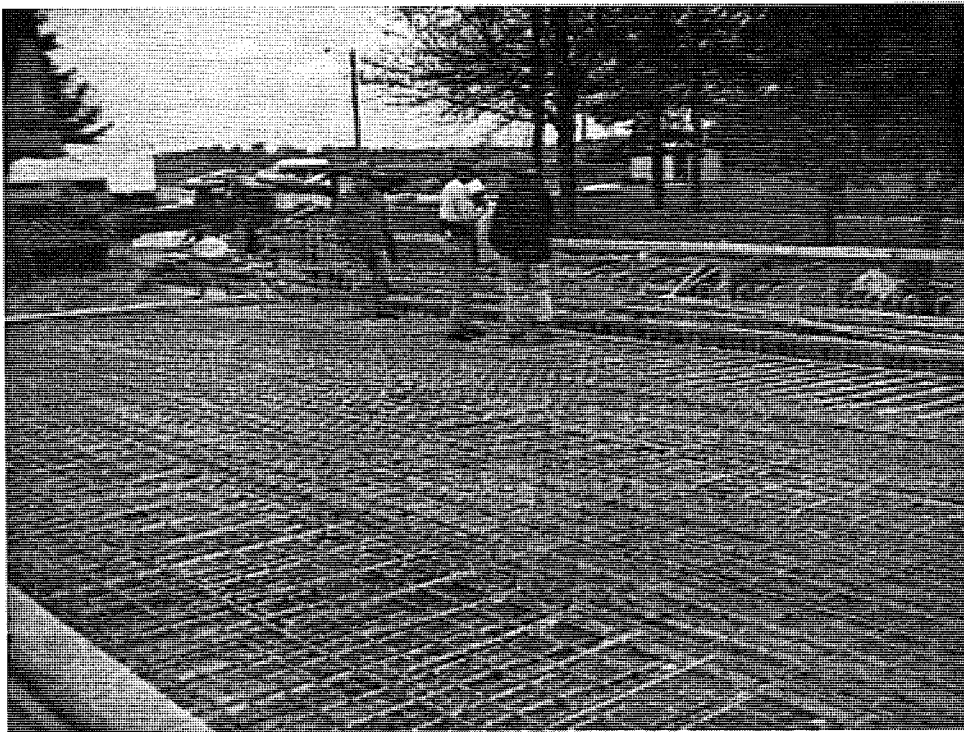
(b)

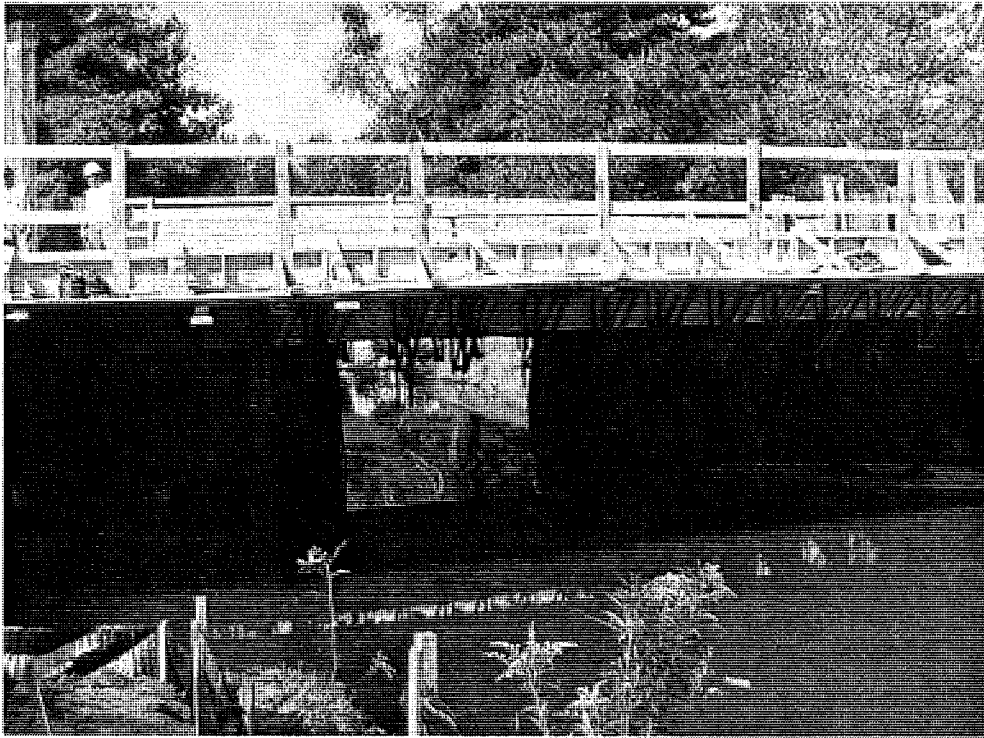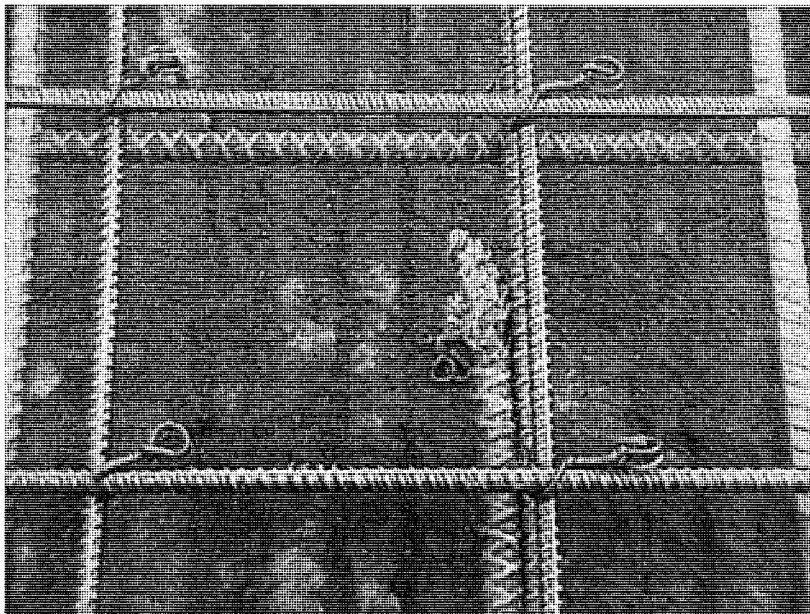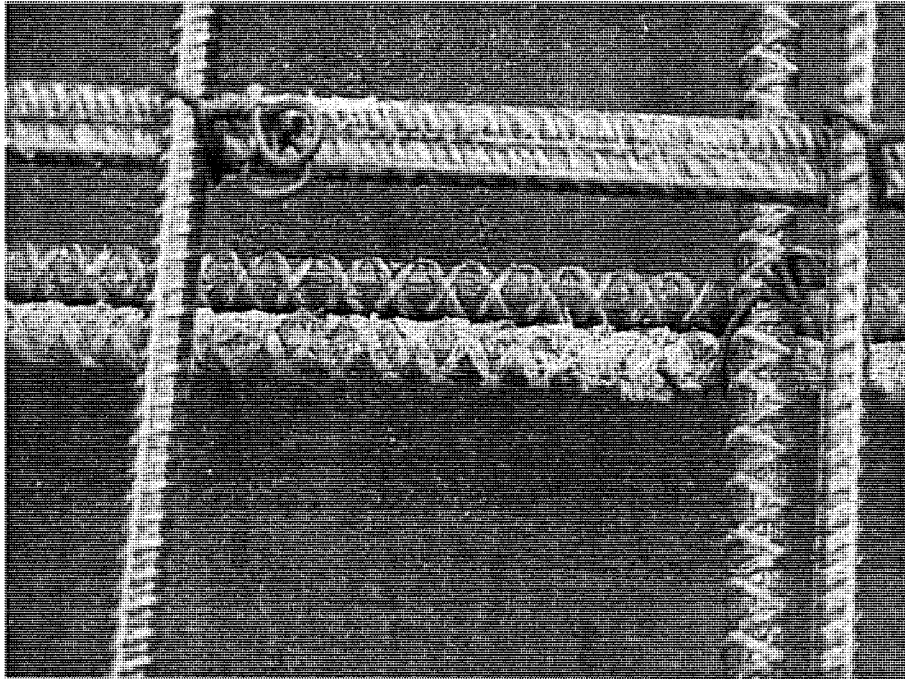Figure 79. Overall Views of The Bridge Deck Reinforcement Cage.

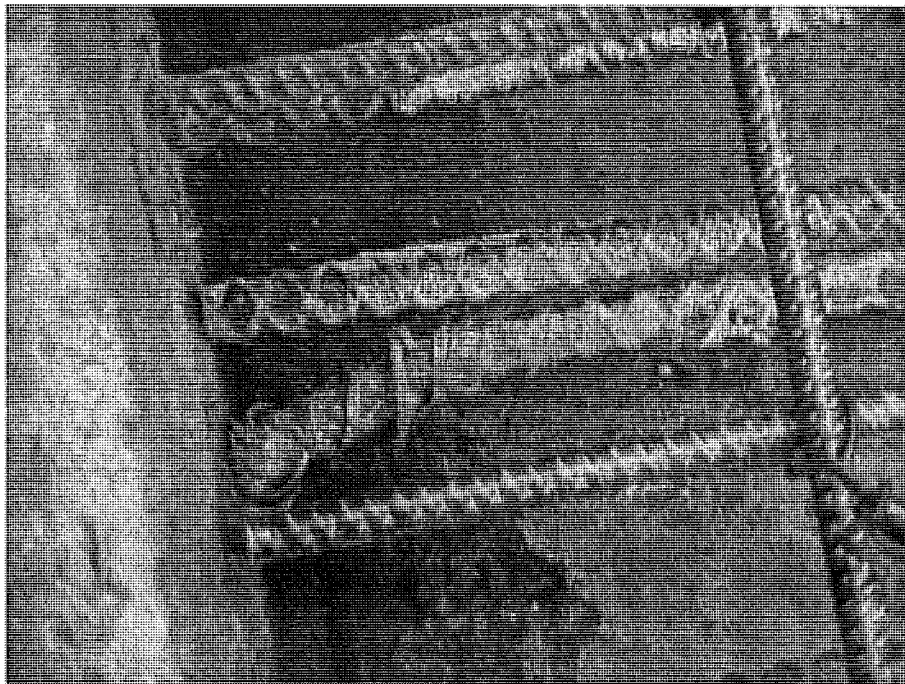Figure 80. Overall View of The Bridge Deck Formwork.

(a)

Figure 81. Damage of AFRP Reinforcement During Preparation and Construction.

(b)

(c)

Figure 81. Damage of AFRP Reinforcement During Preparation and Construction.

Aramid FRP rebars were selected in lieu of glass FRP rebars based on their alkaline resistance and durability in concrete environment. However, from the economic point of view, one should consider the cost implications of this selection. Conventional steel rebars (with about 420 MPa yield strength) cost close to $0.39/m at 9.5 mm diameter. Comparable prices for glass FRP (with about 850 MPa tensile strength and 9.5 mm diameter) and aramid FRP (with about 1,600 MPa tensile strength and 7.4 mm diameter) are about $1.35/m and $8.2/m, respectively. Normalization of these costs by expressing them in dollar/(meter. Kilo Newton) yields 0.0131, 0.0224 and 0.155 $/(m.KN), respectively, for steel, glass FRP and aramid FRP rebars. Hence, the costs of providing comparable levels of reinforcement with glass and aramid FRP are, respectively, 1.71 and 11.8 times higher than that of conventional reinforcing steel.

In the field project, where epoxy coated steel was compared with aramid FRP, the total cost of epoxy coated steel reinforcement for the deck would have been about $11,000 compared to the actual aramid FRP cost of about $68,000. While this represents 6 times increase in deck reinforcement cost, with the total expense of deck replacement at about $650,000, replacement of epoxy coated steel with aramid FRP represents less than 10% increase in total project expenses.

6.3   PLANS FOR LONG-TERM MONITORING OF THE DECK

Long-term monitoring of the bridge deck will be done by MDOT's Structural Research Unit. Inspections will provide valuable information on the actual field performance of aramid FRP reinforcement. The approach to monitoring of the deck will involve visual inspection and crack mapping approximately one month after construction, and then one year and five years after the deck experiences traffic. Reports will be issued by MDOT showing the performance of the AFRP reinforced bridge deck.

The monitoring effort at each of these time steps may also involve tests conventionally used to determine internally spalled areas of bridge decks for the purpose of local concrete removal and patching.

144

7.0 CONCLUSIONS

Glass and aramid (Technora) fiber reinforced composite bars were evaluated at materials and structural levels for use as reinforcement in concrete bridge decks. The research effort led to the following conclusions.

1.   Glass and aramid (Technora) fiber reinforced composites, when compared with steel bars, provide relatively high levels of tensile strength, but relatively low values of elastic modulus and shear strength.

2.   The coefficient of thermal expansion of glass fiber composites is comparable to that of concrete. Aramid (Technora) fiber reinforced composites provide a relatively small coefficient of thermal expansion, which varies with temperature and can even assume negative values at lower temperatures.

3.   Saturation of glass fiber composites does not alter their tensile performance. In the case of aramid (Technora) fiber reinforced composites, there is a relatively small (less than 10%) and reversible loss of tensile performance upon saturation.

4.   Extensive accelerated aging tests were conducted on glass and aramid fiber composites, covering effects of the following exposure conditions on tensile performance: sustained loading in salt solution, extended immersion in alkali solution at room temperature and 60°C, extended immersion in salt solution, repeated wetting-drying in salt solution, repeated freezing-thawing, extended immersion in neutral water at room temperature and 80°C, extended exposure to ultraviolet radiation, fatigue loading, extended exposure to cold temperature, and repeated temperature cycling. Major adverse effects on tensile strength of glass fiber composites were caused by extended immersion in alkali solution at 60°C and in hot water at 80°C. The tensile strength of aramid (Technora) fiber composites, on the other hand, was relatively stable under accelerated aging effects.

5.   Aramid (Technora) fiber composite bars with surface deformations provide about 20% higher bond strength per unit area to concrete. The fact that the tensile strength of aramid fiber composites is about twice that of steel, however, implies that the required development

length is longer for aramid fiber composites when compared with steel reinforcement bars of similar diameter.

6.   Failure of the bond between aramid fiber composite bars and concrete is more brittle than bond failure of steel reinforcing bars in concrete.

7.   Concrete slabs reinforced with aramid (Technora) fiber composite and steel reinforcement were designed based on flexural criteria. These slabs were fabricated and tested in unaged condition and also after the following accelerated aging effects: repeated freezing-thawing in salt solution, repeated wetting-drying, and repeated temperature cycling. A tendency towards shear modes of failure was observed in both aramid fiber composite and steel reinforced slabs. Accelerated aging effects were relatively small for both steel and aramid fiber composite slabs.

8.   The tendency towards shear modes of failure in concrete bridge decks has led to the development of bridge deck design methodologies which focus on preventing the punching shear mode of failure. The elastic modulus of reinforcement is a key design criterion in such methodologies. The relatively low elastic modulus of aramid fiber composites, in spite of their relatively high tensile strength, raises the required reinforcement ratio in aramid fiber composite reinforced bridge decks.

9.   Typical bridge decks reinforced with steel and aramid fiber composite bars were designed, and were fabricated at 1.5 scale factor. These slabs were subjected to static and fatigue tests simulating truck loading effects on bridge decks. Steel and aramid fiber composite has both exhibited satisfactory fatigue performance. The static behavior to failure of steel and aramid fiber composite reinforced decks were comparable, with both exhibiting a tendency towards punching shear mode of failure. The test results successfully verified the design methodology developed for aramid fiber composite reinforced bridge decks.

10.   A field demonstration project involving aramid FRP reinforced bridge deck replacement was implemented successfully. Valuable experience was gained in construction with aramid FRP. The field project will be subjected to long-term monitoring in order to evaluate the performance of the aramid FRP reinforced deck under actual traffic and exposure conditions.

11.   Introduction of FRP reinforcement to the mainstream of concrete construction requires design and construction guides tailored specially for FRP reinforcement, accounting for the differences between proprietary products supplied by different manufacturers.

8.0   REFERENCES

1. Owens-Corning Fiberglass Corporation, "S-2 Glass Fiber," Publication 15PL-16154-A, 1993.

2. Gerritse, A. and Schurhoff, H.J., "Prestressing with Aramid Tendons," Proceedings, Tenth FIP Congress, New Delhi, India, 1986, 7 pp.

3. Mallick, P.K., "Fiber Reinforced Composites - materials, Manufacturing and Design," Marcel Dekker, Inc., New York, 1988, p. 21.

4. Metter, D.G., "Handbook of fibergflass and Advanced Plastic Composites," edited by G. Lubin, Van Nostrand Reinhold Company, New York, 1969, p. 176.

5. Creative Pultrusion Process Inc., "Design Guide," Alum Bank, PA, 1994, pp. 1-3.

6. Schwartz, M.M., "Composite Materials Handbook," McGraw-Hill, Inc., New York, 1992, p. 2.122.

7. Faza. S/. "Behavior of Concrete Members Reinforced with Fiber Reinforced Plastic Rebars," Ph.D. Dissertation, West Virginia university, Morgantown, WV, 1991, pp. 148-1154.

8. Ehsani, M.R., Saadatmanesh, H., Abdelghany, I.H. and Elkafrawy, W., "Flexural Behavior of masonry Walls Strengthened with Composite Fabrics," Proceedings, ACI International Symposium of Non-Metallic Continuous Reinforcement, Vancouver, Canada, 1993, pp. 495-507.

9. Iyer, S.L. and Anigol, M., "Testing and Evaluating Fiber Glass, Graphite and Steel Cables for Pretensioned Beams," Advanced Composite Materials in Civil Engineering Structures, Proceedings of the Specialty Conference, ASCE, Las Vegas, February 1991, pp. 44-56.

10. Wu, W.P., "Thermomechanical Properties of Fiber Rienforced Plastic (FRP) Bars," Ph.D. Dissertation, West Virgina University, Morgantown, W.V., 1990, pp. 87-98.

11. Bedard, C., "Composite Reinforcing Bars: Assessing their Use in Construction," Concrete International, january 1992, pp. 55-59.

12. Porter, M.L., Hughes, B.W., Barnes, B.A., Viswanath, K.P., "Non-Corrosive Tie Reinforcing and Dowel Bars for Highway Pavement Slabs," Departmetn of Civil and Construction Engineering, Engineering Research Institute, Iowa State University, Ames, IA, 1993.

13. Budelmann, H. and Rostary, F.S., "Creep Rupture Behavior of FRP Elements for Prestressed Concrete - Phenomenon, Results and Forecast Models," Proceedings, ACl International Symposium on FRP Reinforcement for Concrete Structures, Vancouver, Canada, March 1993, pp. 87-100.

14. Anigol, M.U., "Testing and Evaluating Fiberglass, Graphite and Steel Prestressing Cables for Pretensioned Beams," M.S. Thesis, South Dakota School of Mines & Technology, Rapid City, SD, 1991, 112 pp.

15. Khubchandani, A., "Evaluation of Graphite Compostie Cables for Prestressing Concrete," M.S. Thesis, South Dacota School of Mines & Technology, Rapid City, SD, 1991, 127 pp.

16. Franke, L., "Behavior and Design of High-Quality Glass Fiber Composite Rods as Reinforcement for Prestressed Concrete Members," Report, International Symposium, CP/Ricem/iBk, Prague, 1981, 52 pp.

17. Gorty, S.S., "Mechanical Properteis of Composite Cables," M.S. Thesis, South Dakota School of Mines & Technology, Rapid City, SD, 1994, pp. 21-23.

18. Sen, R., Mariscal, D. and Shahawy, M., "Durability of Fiberglass Pretensioned Beams," ACI Structural Journal, Vol. 90, No. 5, 1993, pp. 525-533.

19. Rostary, F.S., Hankers, C. and Ranisch, E.H., "Strengthening R/C and P/C Structures with Bonded FRP Plates," Proceedings, First International Conference on Advanced Composite Materials in Bridges and Structures, Sherbrooke, canada, 1992, pp. 253-263.

20. Proctor, B.A., Oakley, D.R. and Ligherland, K.L., "Developments in the Assessment of Performance of GRC Over 10 Years," Composites, Vol. 13, No. 2, 1992, pp. 173-179.

21. Porter, M.L., Lorenz, E.A., Barnes, B.A. and Viswanath, K.P., "Thermoset Composite Concrete Reinforcement," Department of Civil and Construction Engineering, Iowa State University, Ames, IA, October 1992, 119 pp.

22. Lorenz, E.A., "Accelerated Aging of Fiber Composite Bars and Dowel," M.S. Thesis, Iowa State University, Ames, IA, 1992, 161 pp.

23. GangaRao, H.V.S., "Bending and Bond Behavior of Concrete Beams Reinforced with Plastic Rebars," WVDOH-RP-83 Phase I Report, West Virginia University, Morgantown, WV, 1992, 158 pp.

24. Chen, H.L., Sami, Z. and GangaRao, H., "Acoustic Emission Measurements of FRP Bars, Debonding Behavior and FRP Reinforced Concrete Beam," Vibroacoustic Characterization of Materials and Structures, NCA-Vol. 14, ASME, Nov. 1992, pp. 93-100.

25. Chen, H.L., Sami, Z. and GangaRao, H., "Acoustic Emission Characteristics of FRP Bars and FRP Reinforced Concrete Beams," The Fourth International Symposium on Acoustic Emission From Composite Materials, Seattle, WA, AECM-4, ASNT, July 1992, pp. 147-156.

26. Chen, H.L., Sami, Z. and GangaRao, H., "Identifying Damage in Stressed Aramid FRP Bars Using Acoustic Emission," Dynamic Characterization of Advanced Materials, NCA-Vol. 16, November 1993, pp. 171-178.

27. Beal, D.B., "Load Capacity of Concrete Bridge Decks," ASCE Journal of the Structural Division, No. ST4, April 1982, pp. 814-832

28. Burgoyne, C.J., "Laboratory Testing of Parafil Ropes," Les Materiaux Nouveaux Pour la Precontrainte et la Renforcement Douvrages Dart, Paris, October 1988.

29. Mast, R.F., "Unified Design Provisions for Reinforced and Prestressed Flexural and Compression Members," ACI Structural Journal, Vol. 89, No. 2, march/April 1992.

30. Mutsubyoshi, H., Vehara, K. and Machida, A., "Mechanical Properties and Design Methods of Concrete Beams Reinforced with Carbon Fiber Reinforced Plastics," Transactions of the Japan Concrete Institute, Vol. 12, 1990, pp. 231-238.

31. Meisseler, H.J. and Wolff, R., "Experience with Fiber Composite Materials and Monitoring with Optical Fiber sensors," Proceedings, Advanced Composite Materials in Civil Engineering Structures, ASCE, 1991, pp. 167-181.

32. Gerritse, A. and Werner, J., "Arapree, A Non-Metallic Tendon - Performance and Design Requirements," Advanced Composite Materials in Civil Engineering Structures, Proceedings of the Specialty Conference, ASCE, las Vegas, February 1991, pp. 143-154.

33. Dolan, C.W., "Kevlar Reinforced Prestressing for Bridge Decks," Third Bridge Converence, Transportation Research Board, Washington, D.C., 1991.

34. Nanni, A., "Flexural Behavior and Design of RC Members Using FRP Reinforcement," Journal of Structural Engineering, ASCE, Vol. 119, No. 11, 1993, pp. 3344-3359.

35. Faza, S., "Behavior of Concrete Members Reinforced with Fiber Reinforced Plastic Rebars," Ph.D. Dissertation, West Virginia university, Morgantown, WV, 1991, pp. 148-154.

36. Brown, V.L. and Bartholomew, C.L., "FRP Reinforcing Bars in Reinforced Concrete Members," ACI Materials Journal, Vol. 90, No. 1, Han.-Feb. 1993, pp. 34-39.

37. GangaRao, V.S. and Faza, S.S., "Bending and Bond Behavior and Design of Concrete Beams Reinforced with Reinforced Plastic Rebars," Technical Report, Construction Facilities Center, West Virginia university, Morgantown, WV, 1991, pp. 47-154.

38. Mutsuyoshi, H., Machida, A. and Shiratori, N., "Application of Carbon Fiber Reinforced Cables to Concrete Structures," Proceedings, IABSE Symposium, Vrussels, Belgium, 1990, pp. 623-628.

39. Kakihara, R., et al.,, "A New Aramid Rod for the Reinforcement of Prestressed Concrete Structures," Proceedings, Advanced Composite Materials in Civil Engineering Structures, AQSCE, New Yourk, 1991, pp. 132-141.

40. Rizkalla, S.H. and Tadros, G., "A Smart Highway Bridge in Canada," ACI Concrete International, June 1994, pp. 42-44.

41. Jeong, S.M., Naaman, A.E. and Tan, K.H., "Investing of Beams Partially Prestressed with Carbon Fiber Reinforced Composite Tendons," Proceedings of the Fip CII International Congress, may 1994, pp. B56-B61.

42. Nawy, E.G. and Neuwerth, "Behavior of Fiber Glass Reinforced Concrete Beams," Journal of the Structural Division, ASCE, Sept. 1971, pp. 2203-2215.

43. Nawy, E.G. and Neuwerth, G.E., "Fiberglass reinforced Concrete Slabs and Beams," Journal of the Structural Division, ASCE, Feb. 1977, pp. 421-440.

44. Larralde, J., Renbaum, L. and Morsi, A., "Fiberglass Reinforced Plastic Rebars in Lieu of steel Rebars," TRB Annual Meeting, Task Force A2C51 - Structural Applications of Fiber Reinforced Plastics, August 1988.

45. Saadatmanesh, H. and ehsani, M.R., "Fiber Composite Bar for Reinforced Concrete Construction," Journal of Composite Materials, Vol. 25, Feb. 1991, pp. 188-203.

46. Satoh, K., Kodama, K. and Ohki, H., "A Study on the Bending Behavior of Repaired reinforced Concrete Beams using Fiber Reinforced Plastic (FRP) and Polymer Mortar,"

Evaluation and Rehabilitation of Concrete Structures and innovations in Design, Proceedings, ACI international Conference, Hong Kong, 1991, pp. 1017-1031.

47. Goodspeed, C., Schmeckpeper, E., Gross, T., Henry, R., Yost, J., and Zang, M. (1991). Cyclic Testing of Concrete Beams Reinforced With Fiber Reinforced Plastic (FRP) Grids., Advanced Composites Materials in Civil Engineering Structures, Proceedings of the Specialty Conference, Las Vegas, Nevada, February 1991, pp. 278-287.

48. Bank, L., Xi, Z., and Mosallam, A. (1991). Experimental Study of FRP Grating Reinforced Concrete Slabs., Advanced Composites Materials in Civil Engineering Structures, Proceedings of the Specialty Conference, Las Vegas, Nevada, February 1991, pp. 111-122.

49. Faza, S.S., end GangaRao, H.V.S. (1992a). Bending and Bond Behavior of Concrete Beams Reinforced with Fiber Reinforced Plastic Rebars., WVDOH-RP-83 Phase I Report, West Virginia University, Morgantown, WV, pp. 128-173.

50. Zia, P., Ahmad, S., Garg, R., and Hanes, K. (1992). "Flexural and Shear Behavior of Concrete Beams Reinforced With #-D Continuous Carbon Fiber Fabric., Concrete International, December, pp. 48-52.

51. Bank, L. and Xi, Z. (1992). Performance of Doubly-Reinforced Pultruded Grating/Concrete Slabs.", Advanced Composite Materials in Bridges and Structures, Proceedings of The 1st International Conference, Sherbrooke, Canada, 1992, pp. 351-360.

52. Decks-, Materials Performance And Prevention of Deficiencies and Failures, Proceedings of The Materials Engineering Congress, Atlanta, Georgia, August 1992, pp. 618-631.

53. Nanni, A.(1993). "Flexural Behavior and Design of R.C. members FRP Reinforcement," Journal of Structural Engineering, ASCE, 119 (11), pp. 3344-3359.

54. Larralde, J. (1992). Feasibility of FRP Molded Grating-Concrete Composite For One-Way Slab Systems., Materials Performance and Prevention of Deficiencies and Falures, Proceedings of the Materials Engineering Congress, Atlanta, Georgia, August 1992, pp. 645-654.

55. GangaRao, V.S., and Faza, S.S. (1991). Bending and Bond Behavior and Design of Concrete Beams Reinforced with Reinforced Plastic Rebars,. Technical Report, Construction Facilities Center, West Virginia University, Morgantown, WV, pp. 47-154.

56. Pleimann, L. G. (1991). "Strength, Modulus of Elasticity, and Bond of Deformed FRP Rods," Advanced Composite Materials in Civil Engineering Structures, Proceedings of the Specialty Conference, ASCE, Las Vegas, Feb., pp. 99-110.

57. Chaallal, O., Benmokrane, B., and Masmoudi, R. (1992). "An Innovative Glass-Fibre Composite Rebars for Concrete Struemres," Advanced Composite Materials in Bridges and Structures, Proceedings of the 1st International Conference, Sherbrooke, pp. 169-177.

58. Daniali, S. (1992). "Development Length for Fiber Reinforced Plastic bars," Advanced Composite Materials in Bridges and Structures, Proceedings of the 1st International Conference, Sherbrooke, 1992, pp. 179-188

59. Tao, S. (1994). "Bond of Glass-Fiber-Reinforced-Plastic Reinforcing Bars to Concrete," Ph.D. Dissertation, Department-of Civil Engineering, University of Arizona, Tucson, pp. 197.

60. Rahman, A.H., Taylor, D.A., and Kingsley, C.Y., (1993), "Evaluation of FRP as Reinforcement for Concrete Structures," International Symposium, ACI SP-138, American Concrete Institute, pp. 71-86.

61. Porter, M.L., Hughes, B.W., Barnes, B.A., Viswanath, K.P. (1993) Non-Corrosive Tic Reinforcing ant Dowel Bars for Highway Pavement Slabs,. Department of Civil and Construction Engineering, Engineering Research Institute, Iowa State University, Ames, LA.

62. Ferguson, P.M. (1966), Bond Stress - The State of the Art,. Journal of the American Concrete Institute, Proceedings 63, No. 11, pp. 1161-1190.

63. Mathey, R.C., and Watstein, D. (1961) reinvestigation of Bond Strength in Beam and Pullout Specimens with High-Yield-Strength Deformed Bars,. Journal of the American Concrete Institute Proceedings 57, No. 9, March, pp. 1071-1090.

64. Nawy E.G. and Neuwerth, G.E. (1971). "Behavior of Fiber Glass Reinforced Concrete Beams.," Joumal of the Structural Division, ASCE, September, pp. 2203-2215.

65. Benmokrane, B., Tighiouart, B., and Chaallal, O. (1994). "Investigation on Bond Performance of FRP Rebars," Summary papers for projects presented during the Technical Session on Bond of FRP Rebars ant Tendons, ACI Spring Convention, San Francisco, CA, March 21, pp. 1 4.

66. "Code of Practice for the Structural Use of Concrete (CP 110)," British Standards Institution, London, 1972, Part 1, 155 pp.